APPLICATION OF FRACTIONAL CALCULUS TO POLARIZATION DYNAMICS IN SOLID DIELECTRIC MATERIALS

by

Gary William Bohannan

A dissertation submitted in partial fulfillment
of the requirements for the degree

of

Doctor of Philosophy

in

Physics

MONTANA STATE UNIVERSITY
Bozeman, Montana

November 2000

APPROVAL

of a dissertation submitted by

Gary William Bohannan

This dissertation has been read by each member of the dissertation committee and has been found to be satisfactory regarding content, English usage, format, citations, bibliographic style, and consistency, and is ready for submission to the College of Graduate Studies.

George F. Tuthill _____ _____
(Signature) Date

Approved for the Department of Physics

John C. Hermanson _____ _____
(Signature) Date

Approved for the College of Graduate Studies

Bruce R. McLeod _____ _____
(Signature) Date

STATEMENT OF PERMISSION TO USE

In presenting this dissertation in partial fulfillment of the requirements for a doctoral degree at Montana State University, I agree that the Library shall make it available to borrowers under rules of the Library. I further agree that copying of this dissertation is allowable only for scholarly purposes, consistent with "fair use" as prescribed in the U. S. Copyright Law. Requests for extensive copying or reproduction of this dissertation should be referred to Bell & Howell Information and Learning, 300 North Zeeb Road, Ann Arbor, Michigan 48106, to whom I have granted "the exclusive right to reproduce and distribute my dissertation in and from microform along with the non-exclusive right to reproduce and distribute my abstract in any format in whole or in part."

Signature _____

Date _____

ACKNOWLEDGEMENTS

With great appreciation for the assistance from fellow graduate and undergraduate students who participated in the development and execution of the experiments crucial to this work: Darin Arbogast, Michael Chase, Jil Hallenberg, Michelle Lindmier, Erica McKenzie, and Delphine Medicine Horse.

I am especially grateful to Recep Avci and Sara Maccagnano for allowing me to participate in their study of anomalous diffusion.

This work was supported by a Montana Space Grant Fellowship, NASA EPSCoR Grant NCC5-240, and NSF Grant DMR-9805272.

TABLE OF CONTENTS

LIST OF TABLES

LIST OF FIGURES

ABSTRACT

The fractional calculus has been suggested as an appropriate mathematical tool for the description of a wide variety of physical, chemical and biological processes, in particular non-Debye relaxation in dielectrics. While there have been substantial improvements in our understanding of the physical interpretation of the results of fractional differential equations, there is still much unknown. There is, as yet, not even complete agreement over the notation to be used, let alone the underlying definition of the fractional derivative.

This dissertation explores the hypothesis that there must be an intimate relation between the *ac* and *dc* response in any given material represented by a dynamical equation of motion. That at least one of the forms of the fractional calculus does, in fact, provide a useful and practical tool for describing some of the dynamics of immediate interest is demonstrated. The process investigated is that of polarization dynamics in condensed matter dielectric materials. The dielectric material studied in detail is poly(vinylidine fluoride) (PVDF) which finds use in piezoelectric sensor and actuator applications. A dynamical model, based on the fractional calculus, is shown to reproduce both the *ac* and *dc* responses to an applied electric field.

Many of the results are directly applicable a wide range of other dynamics including mechanical relaxation processes.

CHAPTER 1

INTRODUCTION

This dissertation focuses on the application of the fractional calculus to the problem of describing polarization dynamics in dielectric materials. The use of fractional calculus for this purpose has been suggested in the literature but not thoroughly investigated. In particular, the investigation focuses on the requirement that there must be an intimate relation between the *ac* and *dc* response in any given material represented by a dynamical equation of motion.

In order to appreciate the statistical interpretation of the results, a discussion of the problem of anomalous surface diffusion has been included as an appendix. This will allow comparison and contrast between the study of bulk behavior and individual particle behavior.

Polarization dynamics in ferroelectric materials, as in all dielectrics, pose a very complicated problem. Among the complications is the fact that the relaxation response is rarely, if ever, a simple exponential function as described by Debye. [1] Instead a fractional power exponential decay (the "stretched exponential") of the form

$$\phi(t) = \phi_0 \exp\left(-\left(\frac{t}{t_0}\right)^{\alpha}\right), \tag{1.1}$$

with $0 < \alpha < 1$, or power law of the form

$$\phi(t) \approx \left(\frac{t}{t_0}\right)^{-\alpha}, \tag{1.2}$$

at long times, again with $0 < \alpha < 1$, are far more common, to the point of being referred to as universal responses.

Additionally, at very "low" frequencies, or "long" times, the relaxation current flowing after application of an external field, the "charging current," follows a power law of the form

$$i(t) \approx \left(\frac{t}{t_0}\right)^{-n}, \tag{1.3}$$

with $0 < n < 1$. Although many articles in the literature are ambiguous on this point, it appears to be "universally" true that the "discharging" current follows a different power-law relation than the "charging" current. What is common is that there are power-law relations involved in both cases.

Dielectric materials share these non-Debye relaxation responses with mechanical systems that exhibit non-exponential strain relaxation after removal of an external stress and power-law creep under continuous stress. Fractional power-law behavior is the norm in condensed matter dynamics. To quote Ngai:

> The relaxation phenomena ... include relaxation, a.c. conductivity, creep, stress relaxation, internal friction, relaxation observed through photon correlation spectroscopy, nuclear magnetic resonance relaxation, spin-echo measurements, transient capacitance (i.e. time resolved) electrical transport, transient optical luminescence, volume and enthalpy relaxation and recovery, differential scanning calorimetry, steady flow viscosity, stress-strain relationship and its dependence on strain-rate, ultrasonic attenuation, noise, diffusion, diffusion controlled chemical reactions and electronic recombination, etc. Materials involved include liquids, supercooled

> liquids, inorganic glasses, electrolytes, ionic conductors, dielectrics, gate insulators of electronic devices, amorphous semiconductors, xerographic materials, polymer melts and solutions, amorphous polymers, rubbers, plastics, epoxies, metals, ... ceramics, piezoelectrics, pyroelectrics, ferroelectrics, biopolymers, ... etc. The wealth of physics, the number of interesting physical phenomena are staggering. [2]

By focusing on non-exponential response functions, this work gains a broad applicability to many problems in condensed matter physics. The intent is to improve our understanding of this universal behavior in order to better understand complex dynamics in a wide variety of condensed matter systems.

Traditionally, the broad relaxation spectra, i.e. relaxation rates encompassing nine or more decades of frequency, have been described as resulting from a linear combination of exponential responses with an extremely large distribution of time constants (e.g. see [3]). This "distribution of exponential time constants" description has been used extensively as it relies on traditional concepts of weakly interacting systems with a wide range of simple exponential relaxation mechanisms.

The debate between the distribution of relaxation times (DRT) and power-law points of view has abated with the two views now being virtually complementary, at least for the frequency regime around the dielectric loss peak. The fact of power-law behavior has been incorporated into texts such as Reference [4], which extensively cites early works on power-law behavior, e.g. References [5, 6, 7, 8], while still using the DRT description to flesh out physical models when appropriate. The DRT approach was incorporated into a simulation model in Reference [9], and has been recently been

posed in terms of multifractals in Reference [10], for example.

Hill and Jonscher [11] suggested that the power-law behavior is a result of the many-body interactions within bulk condensed matter. Funke [12] offered a reasonable model for the interactions. Funke's model can be generalized to cover a broad range of behaviors, even those that Funke discarded in his paper. It is somewhat ironical that an argument based on distributions of relaxation times may provide the most direct route to power-law behavior.

What has been missing is a coherent dynamical model, even a phenomenological one, that allows both the steady state *ac* response and the transient *dc* response to be included in one composite whole over all relevant frequency and time scales. Such a model would be a great boon to both the basic characterization of materials and to the problem of developing control systems to apply materials to applications. The thrust of this dissertation is to examine the hypothesis that the power-law description is fundamental and covers a broad range of measured phenomena. The hypothesis includes the statement that the fractional calculus is appropriate and tractable for use in describing power-law dynamics.

The problem of anomalous diffusion is related to that of relaxation dynamics in a very deep sense. The motion of individual charge carriers making up an electronic or ionic current is, after all, a diffusive process. There are some substantial differences, however, in the underlying causes of power-law dynamics in super-diffusive versus sub-diffusive processes. Sorting out these similarities and differences is crucial to

understanding dynamics in materials.

As will be discussed in subsequent chapters, power-law processes are fundamentally non-Markovian and pose a number of very substantial theoretical and computational difficulties. Approaches for dealing with several of these difficulties are presented in the context of solid state dielectric materials, but the results could be applied to a wide range of problems in mechanical and biological systems as well. A computational method for simulating power-law dynamics through the use of fractional difference equations is presented in detail in this thesis.

A major difficulty remains, however. The language of physics is ill-equipped to deal with non-Markovian processes. The term "initial conditions" is moot; these conditions incorporate all of history. Also, processes which produce power-law-like behavior are often assumed to be nonlinear. The dynamical equations derived in subsequent chapters are first order in the dynamical variables and the fractional derivative is a linear operator. So, in what sense are these systems linear or nonlinear?

Chapter 2 describes the dielectric relaxation problem in more detail and formally states the hypothesis that the fractional calculus provides a workable description of the dynamics. Chapter 3 develops the generalized micro- and macroscopic model of many-body interactions leading to non-Debye behavior.

Chapter 4 provides an overview of the fractional calculus and its application to the problem of non-exponential response. In Chapter 5 time domain fractional differential equations are derived from *ac* response measurements. Two methods for integrating

the differential equation are derived in Chapter 6, and verification testing results are presented. Chapters 5 and 6 represent the major theoretical and computational contribution to the field of non-Debye relaxation dynamics.

In Chapter 7, experimental methods for characterizing the polarization response under varying external field conditions are discussed. Permittivity measurements are used to predict transient currents. This connection between the *ac* and *dc* measurements demonstrates the validity of the hypothesis.

Chapter 8 outlines possible extensions of the research into other areas of interest as well as discussing several open questions related to the understanding of fractional dynamics. Chapter 9 provides a summary of the results and conclusions.

Appendix A provides details of the generalized central limit theorem and a brief discussion of the statistics of anomalous drift and diffusion.

Appendix B explores the use of the fractional calculus to the description of anomalous diffusion. A simulation model is developed which reproduces both "normal" and extremely anomalous surface diffusion. One of the objectives of including this appendix is to clarify the differences between the coarse grained modeling used in the earlier chapters for description of polarization dynamics and detailed modeling of individual particle behavior.

CHAPTER 2

PROBLEM STATEMENT AND HYPOTHESIS

A direct consequence of the Kramers-Kronig relations is that the ideal dielectric, i.e. lossless over all frequencies, violates causality and cannot exist. If the ideal capacitor model with impedance $Z = 1/i\omega C$ is not physical, what description should we use? In general, we are looking for constitutive equations of the form $\mathbf{D} = \epsilon\mathbf{E}$. If the ideal capacitor model isn't physically possible, then ϵ cannot be independent of frequency. A number of models dating back to Debye [1] have been proposed, but we should evaluate the models on their ability to reproduce the measured dynamics of materials and devices. This issue arises in mechanical systems as well, in fact, in any system capable of storing energy.

This work will be focused on the dynamical response of solid dielectric materials to an external electric field, using the methods of impedance spectroscopy. The problem originates in the need to characterize the dynamic response of materials that may ultimately be used in devices and systems, as well as in the desire to understand fundamental properties of condensed matter. This chapter provides background on traditional attempts to develop permittivity models and proposes a hypothesis for development of future models.

Example Application

Of specific interest is the problem of obtaining effective, efficient control of piezoelectric materials for applications such as actuators and sensors. [13, 14, 15] Piezoelectric properties are usually addressed in terms of displacement, or strain, per unit voltage, or electric field, applied [16]. In the particular application of interest, vibration isolation in space applications, operating high voltage amplifiers in the linear mode is unacceptably wasteful of power due to losses in the amplifiers themselves.

Since the poly(vinylidine fluoride) (PVDF) used as the piezoelectric material has an exceedingly small rated *dc* conductivity, as do most popular piezoelectrics, it would be much more efficient to operate the devices with pulsed charge-pump type circuits and use the PVDF actuator material itself as a capacitor in the charging system. Here the problem becomes one of refining the linear approximation between charge and voltage, $Q = CV$. The direct, linear relation between the electric field, $\mathbf{E}$, and the electric displacement, $\mathbf{D}$, no longer holds if the capacitance changes with time and frequency. [17]

The problem will only become more difficult with the advent of high-strain piezoelectric materials such as those reported in Reference [18]. These exhibit a definite nonlinear response in strain versus field. We must expect that the strain and dielectric properties of these materials will show time and frequency dependence as well as nonlinearity with respect to applied field.

The Permittivity

Impedance spectroscopy is a method of characterizing many of the electrical properties of materials and their interfaces with electrically conducting electrodes. It can be used to investigate the dynamics of bound or mobile charges in the bulk or interfacial regions of solid or liquid material. Of principal interest is the complex permittivity function $\epsilon^*(\omega) = \epsilon'(\omega) - i\epsilon''(\omega)$, which is the *steady state ac* response of the polarization to an applied external field. We will consistently be referring to the relative permittivity as the permittivity. In MKSA units, the polarization and electric displacement are related to the electric field through the constitutive equations

$$\mathbf{P} = \chi_e \epsilon_0 \mathbf{E}, \tag{2.1}$$

and

$$\mathbf{D} = (1 + \chi_e)\epsilon_0 \mathbf{E} = \epsilon\epsilon_0 \mathbf{E}, \tag{2.2}$$

where χ_e is the *electric susceptibility*. In this notation $\epsilon\epsilon_0$ represents the *absolute permittivity*.

The permittivity is related to other response functions, such the impedance, according to Table 1 via the current to displacement relation

$$i = \frac{\mathrm{d}}{\mathrm{dt}} D(t). \tag{2.3}$$

These functions are also referred to as "spectral" functions.

To be precise, the displacement, as defined in Equation 2.3, is actually proportional to the total integrated current through the material, rather than the charge

Table 1. Relations Between the Four Basic Immitance Functions.

	Modulus (M)	Impedance (Z)	Admittance (Y)	Permittivity (ϵ)
M	M	μZ	μY^{-1}	ϵ^{-1}
Z	μ^{-1}M	Z	Y^{-1}	$\mu^{-1}\epsilon^{-1}$
Y	μM	Z^{-1}	Y	$\mu\epsilon$
ϵ	M^{-1}	μ^{-1}Z^{-1}	μ^{-1}Y	ϵ

$\mu = i\omega \mathrm{C}_C$, where C_C is the capacitance of the empty cell.

accumulated across the material. There is much interest in removing the *dc* conductivity, σ, from the permittivity function in order to write the static contribution to the current as $i = \sigma\mathbf{E}$. This would allow one to determine the charge stored across the dielectric versus that lost to conductivity. One of the objectives of dielectric spectroscopy is to determine the bound charge density, ρ_b, and the free charge density, ρ_f. As will be seen, this is not as straightforward a process as one would desire.

Given that $\mathbf{P}$ and $\mathbf{D}$ differ by the ratio $\chi/(\chi+1)$, with $\chi \geq 10$ for many dielectrics of interest, there is a tendency to use the term "polarization" when "displacement" would be more precise. This difference is washed out even more when considering the fact that materials and measurements can vary by 10% or more. In what follows, we will follow this convention that the term polarization refers to the total integrated current unless specifically noted otherwise. Additionally, in scaling for numerical modeling, the MKSA scale factor ϵ_0 will be set to unity.

Permittivity of Dilute Dipolar Liquids

Debye [1] developed the theory of dielectric relaxation of polar molecules in a

viscous medium. In the materials he studied, the concentrations were low enough to appropriately approximate the molecules as non-interacting dipoles. Equation 2.4 expresses the relation in terms of ϵ_s, the low frequency limiting value, and ϵ_∞, the high frequency limiting value, and τ, a characteristic reorientation time for a single dipole.

$$\epsilon^* - \epsilon_\infty = \frac{\epsilon_s - \epsilon_\infty}{1 + i\omega\tau} \quad \text{(Debye)} \tag{2.4}$$

The real, ϵ', and imaginary, ϵ'', are shown in Figure 1. A plot of ϵ'' versus ϵ' is shown in Figure 2 and is used as a standard display of the same information.

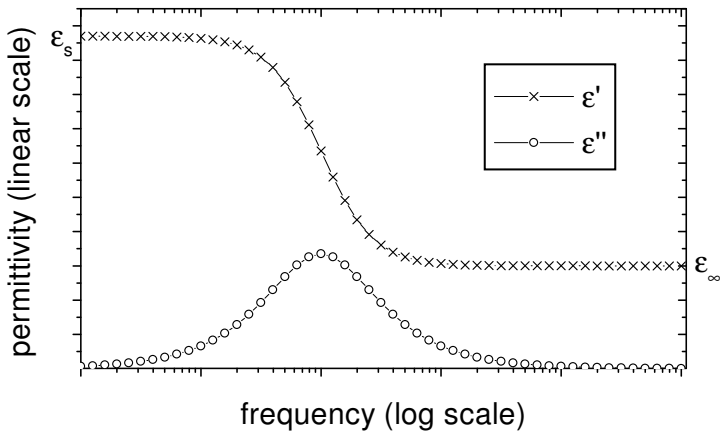

Figure 1. A schematic representation of the real, ϵ', and imaginary, ϵ'', parts of the complex permittivity as predicted by the Debye model.

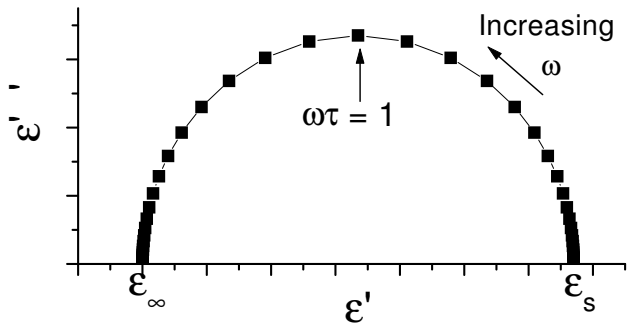

Figure 2. A schematic representation of ϵ'' versus ϵ' as predicted by the Debye model.

Permittivity of Solid Dielectrics

In dielectric solids, the assumption of non-interacting dipoles breaks down and the simple relaxation function of the Debye model is no longer adequate. Cole and Cole [3] found that, at least for a range of frequencies around the loss peak, the permittivity data for non-dilute materials looked more like that shown in Figure 3. When plotted as ϵ'' versus ϵ', they noted that the result was a circular arc with the center below the real axis as depicted in Figure 4.

By appeal to purely geometric arguments they developed the following form for the permittivity function:

$$\epsilon^* - \epsilon_\infty = \frac{\epsilon_s - \epsilon_\infty}{1 + (i\omega\tau)^{1-\alpha}} \quad \text{(Cole-Cole)} \tag{2.5}$$

where the exponent parameter α is determined from the depression of the center of the circular arc below the real axis. In fact, $\alpha\pi/2$ is the angle of offset of the center of the arc with respect to the real axis. The meaning of ϵ_s and ϵ_∞ remain as for the Debye case, but the time constant τ and the exponent parameter α need additional

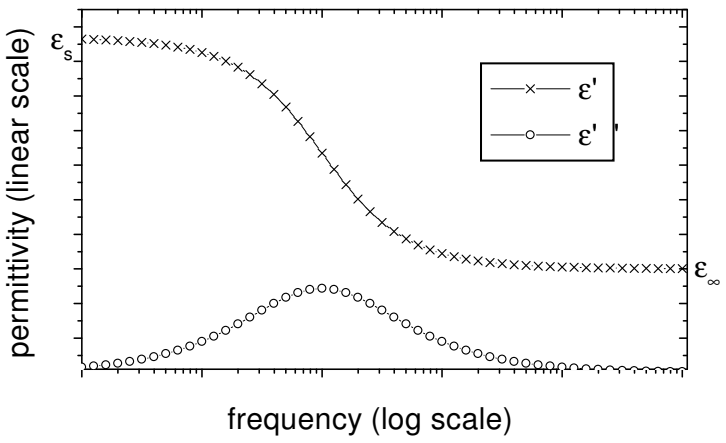

Figure 3. A schematic representation of the real, ϵ', and imaginary, ϵ'', parts of the complex permittivity as predicted by the Cole-Cole model.

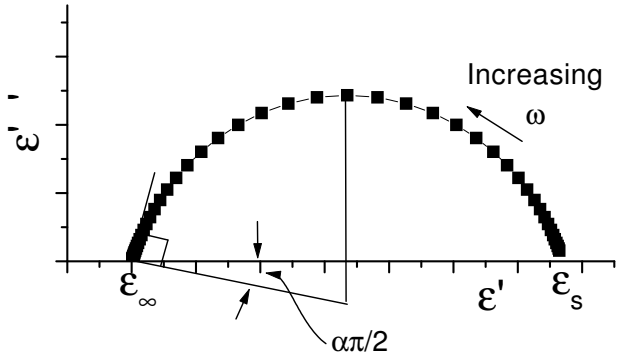

Figure 4. A schematic representation of ϵ'' versus ϵ' as predicted by the Cole-Cole model.

physical interpretation. Since Cole and Cole made the plot of ϵ'' versus ϵ' popular, it is now often referred to as a "Cole-Cole" plot regardless of whether or not the data fit Equation 2.5.

The differences between the Debye and Cole-Cole models become more dramatic when displayed together in a log-log scale as in Figures 5 and 6. The loss peak for the Cole-Cole model is broader than that predicted by the Debye model.

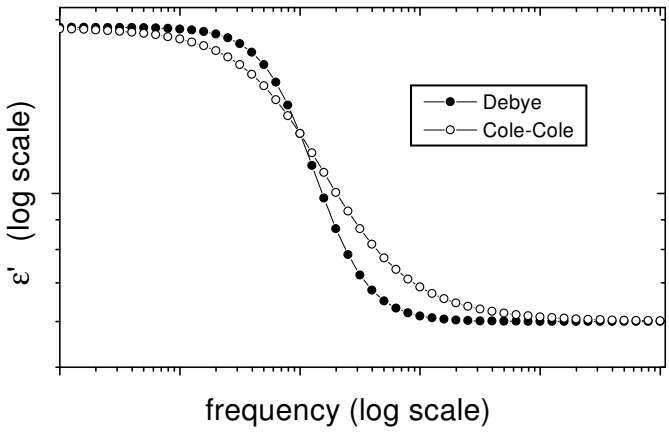

Figure 5. A comparison of the real, ϵ', parts of the complex permittivity as predicted by the Debye and Cole-Cole models.

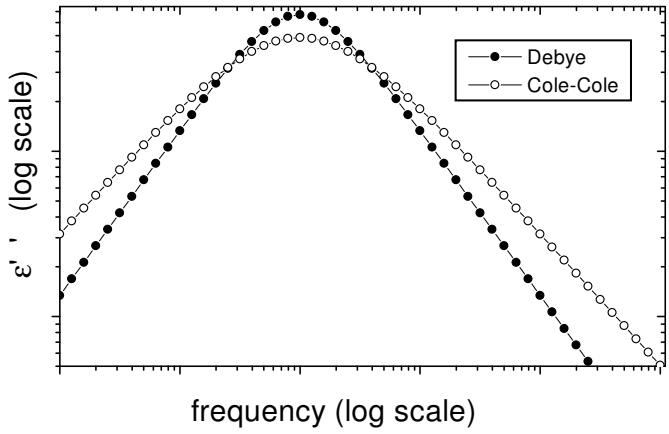

Figure 6. A comparison of the imaginary, ϵ'', parts of the complex permittivity as predicted by the Debye and Cole-Cole models.

The distribution of time constants idea is based on the assumption of a superposition of many linear relaxation processes contributing to the permittivity. In general:

$$\epsilon^* - \epsilon_\infty = \int_0^\infty \frac{(\epsilon_s - \epsilon_\infty)G(\tau)\mathrm{d}\tau}{1 + i\omega\tau} \tag{2.6}$$

where $G(\tau)$ represents a normalized distribution of relaxation times. For the Cole-Cole model:

$$G(\tau) = \frac{1}{2\pi\tau} \frac{\sin \alpha\tau}{\cosh(1-\alpha)\log(\tau/\tau_0) - \cos \alpha\tau} \tag{2.7}$$

The distribution is even with respect to a central frequency, but other distributions need not be. A more detailed analysis of distribution functions for non-Debye relaxation processes can be found in Reference [10].

In the time domain, Cole-Cole relaxation is best fit with a "stretched exponential" function at short to intermediate times (compared to τ) and asymptotically with a power law at very long times. The difficulty in making consistent decay measurements is that materials generally exhibit memory of past polarization. [19] This effect will be addressed in detail in Chapters 6 and 7.

Equivalent Circuits

An equivalent circuit for the Debye model is shown in Figure 7a. The circuit parameters are related to the measured ϵ values as follows:

$$\mathrm{C}_\infty = \epsilon_\infty \mathrm{C_c}, \quad \mathrm{C_s} = (\epsilon_s - \epsilon_\infty)\mathrm{C_c}, \quad R_\mathrm{s} = \frac{\tau}{\mathrm{C_s}} \tag{2.8}$$

where τ is the reciprocal of the angular frequency of the loss peak and $\mathrm{C_c}$ is the capacitance of the empty test cell.

Cole and Cole proposed the equivalent circuit shown in Figure 7b and introduced the concept of the "constant phase element" (CPE). This label was given to the new

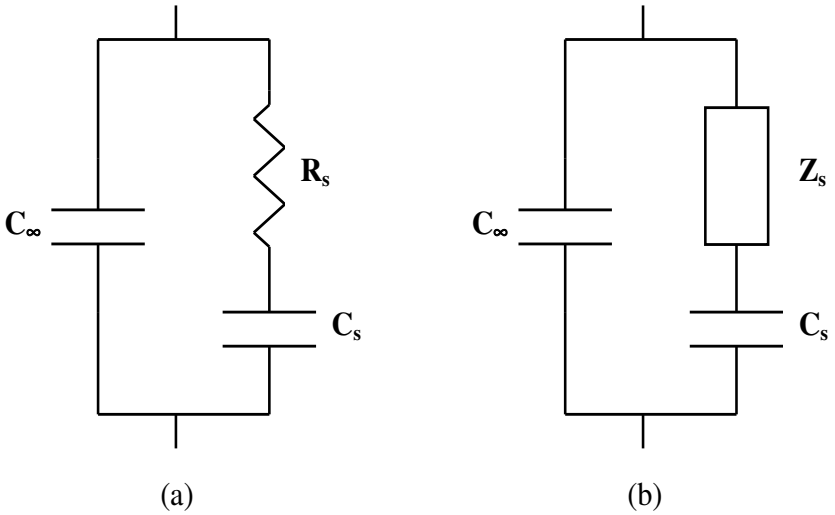

Figure 7. Equivalent circuits for (a) the Debye model and (b) the Cole-Cole model.

frequency dependent "lossy" element, Z_s, because it produced a nearly constant phase shift, and a nearly constant loss tangent ($\tan\delta = \epsilon''/\epsilon'$), over a large frequency range. The energy lost per cycle is nearly independent of frequency. The loss tangent is not strictly constant. The term originated from the fact that the variation in ϵ'' is dramatically less than that predicted by the Debye model as is evident in Figure 6. A comparison of the loss tangents for the two models is shown in Figure 8. Why the variation in the loss tangent should be suppressed was left as an open question by Cole and Cole.

The element Z_s is related to the measured values by:

$$Z_s = \frac{\tau(i\omega\tau)^{-\alpha}}{C_s}. \tag{2.9}$$

It is evident that, for $0 < \alpha < 1$, the element Z_s is neither a resistor nor a capacitor, but some mixture of the two. Distributed arrays of conventional ideal resistors and

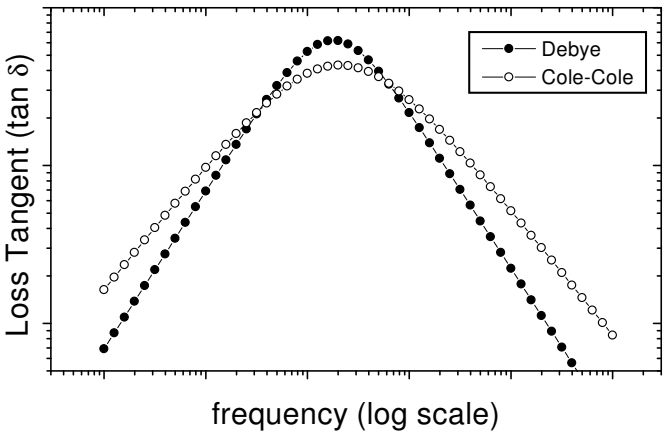

Figure 8. Comparison of the loss tangent for the Debye and Cole-Cole Models.

capacitors that produce the CPE properties have been proposed, e.g. Reference [4] and Reference [9].

Other Proposed Symmetric and Asymmetric Permittivity Functions

Not all dielectric loss peaks display the symmetry of the Cole-Cole equation in the log-log plot of ϵ'' versus ϵ'. A number of variations on Equation 2.5 have been proposed to provide better parametric fit to the data obtained from experiment.

These functions generally include terms of the form $\epsilon^* - \epsilon_\infty$ and $\epsilon_s - \epsilon_\infty$, in which the assumption is made that there is a polarization response in the material at the highest frequencies of interest,

$$\epsilon_\infty - 1 = \mathbf{P}_\infty / \epsilon_0 \mathbf{E}. \tag{2.10}$$

The "infinite" frequency is typically in the microwave region or below.

In Table 2, taken from Reference [11], Hill and Jonscher redefine the constitutive equation (2.1) along these lines with

$$\chi(\omega) = \epsilon(\omega) - \epsilon_\infty \tag{2.11}$$

where $\omega_p = 1/\tau$ and $\chi(\omega) = \chi(0)F(\omega/\omega_p)$. $F(\omega/\omega_p)$ is referred to as a spectral function and the exponents $\alpha, \beta, \Delta, \gamma$, m and, n as spectral parameters. The functions $F(\omega/\omega_p)$ are displayed in the second column of Table 2.

Galiyarova reviewed many of these various forms in Reference [20] but used the notation $e^* = (\epsilon^* - \epsilon_\infty)/(\epsilon_s - \epsilon_\infty)$, so that $e^* = F(\omega/\omega_p)$. Using this convenient form, the Cole-Cole form, Equation 2.5, can be written

$$e^* = \left(1 + (i\omega\tau)^{1-\alpha}\right)^{-1}. \tag{2.12}$$

The other spectral functions in Table 2 follow. This notation avoids the confusion induced in redefining the constitutive equation.

The assumptions that both the high and low frequency responses are purely capacitive are difficult, if not impossible, to verify in practice. At the high frequency end, phonon and other interactions can mask the polarization response and ϵ_∞ becomes a parameter estimated from graphical analysis of the Cole-Cole plot or through numerical Kramers-Kronig transform calculations. At the low end ϵ_s is more often than not mixed with conductivity.

Table 2. Spectral Functions and Their Power-Law Exponents.

		exponent $\omega << \omega_p$		exponent $\omega >> \omega_p$	
Model	Function*	$\Delta\chi'(\omega)$	$\chi''(\omega)$	$\chi'(\omega)$	$\chi''(\omega)$
One parameter					
Debye	$(1+i\omega/\omega_p)^{-1}$	2.0	1.0	-2.0	-1.0
Cole-Cole	$(1+\{i\omega/\omega_p\}^{1-\alpha})^{-1}$	$1-\alpha$	$1-\alpha$	$\alpha-1$	$\alpha-1$
Fuoss-Kirkwood†	$2(\omega/\omega_p)^{\gamma}(1+\{\omega/\omega_p\}^{2\gamma})^{-1}$	γ	γ	$-\gamma$	$-\gamma$
Davidson-Cole	$(1+i\omega/\omega_p)^{-\beta}$	2.0	2.0	$-\beta$	$-\beta$
Williams-Watts	$\sum_{s=1}^{\infty}\frac{\Gamma(\Delta s)}{(s-1)!}\left\lvert\frac{\exp(-i\Delta\pi/2)}{\omega^{\Delta}\omega_p^{-\Delta}}\right\rvert^s$	2.0	1.0	$-\Delta$	$-\Delta$
Two parameter					
Havriliak-Negami	$\{1+(i\omega/\omega_p)^{(1-\alpha)}\}^{-\beta}$	$1-\alpha$	$1-\alpha$	$-\beta(1-\alpha)$	$-\beta(1-\alpha)$
Jonscher	$\{(\omega/\omega_1)^{-m}+(\omega/\omega_2)^{1-n}\}^{-1}$	m	m	$n-1$	$n-1$
Hill	$\omega^m(\omega_p^{2s}+\omega^{2s})^{-(m+1-n)/2s}$	m	m	$n-1$	$n-1$
Dissado-Hill	$\{\omega_p/(\omega_p+i\omega)\}^{(1-n)}\,{}_2F_1\left(1-n,1-m;2-n;\frac{\omega_p}{\omega_p+i\omega}\right)$	m	m	$n-1$	$n-1$

*All the spectral parameters are fractional and positive.

†The Fuoss-Kirkwood relationship gives only the imaginary component $\chi''(\omega)$.

Taken from Reference [11]

Low-Frequency, Long-Time Anomalies

Overwhelming experimental evidence indicates that at low enough frequency, or long enough times, all materials, even the best insulators, appear to be conductive to some extent. True, linear resistor-like, conductivity would show up on the Cole-Cole type plots as a vertical line at the lowest frequencies. This represents an ideal limiting case and is often only approximated in nature. The slope of the low-frequency tail varies with composition, temperature and other conditions. Some authors suggest that the low frequency tail could be due to electrode interface effects, although this is still controversial. [4]

Typical permittivity measurements result in a plot such as shown in Figure 9.

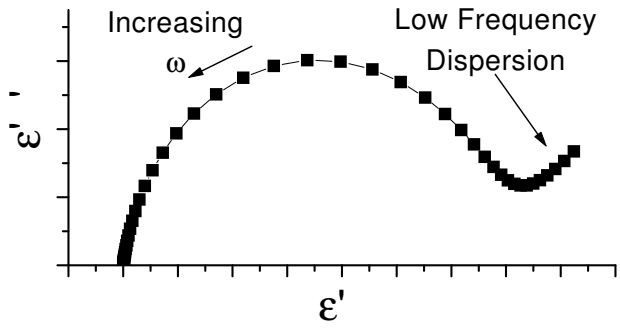

Figure 9. A schematic representation of a typical data set from measurements of a ferroelectric material.

Extensive studies of the very low-frequency, long-time, permittivity behavior of a wide variety of dielectric materials follows the form

$$\epsilon(\omega) \sim \omega^{\eta-1}, \tag{2.13}$$

where $0 < \eta < 1$. For solid-like materials $\eta \gtrsim 0.6$ and $\eta \sim 0.3 - 0.5$ for liquid-like materials. [2] The cause of this low-frequency dispersion is still an open question (see e.g. [21, 22]).

In the Debye model, the charging and discharging currents are simply opposite in sign but have the same time dependence. This is controversial. In Reference [23], Kumar states that there is a depolarizing current $i_d(t) \sim t^{-\eta}$ after removal of the the polarizing field. This would imply an infinite polarizability of matter if the relation held for all t. In Reference [19], Westerlund states that the current $i_d \sim t^{-\eta}$ is the relaxation response current at long times after the polarizing field is applied. He models the response as a time varying capacitance and attributes long-time dielectric breakdown to the material exceeding some limiting charge capacity. Many articles addressing this low frequency response fail to distinguish between the relaxation after application of the field versus after removal of the field.

The differences between the charging and discharging currents upon application of a pulse of finite duration were predicted by Jonscher in Reference [8] according to the following argument. Experimentally, for the vast majority of dielectric materials, the charging current asymptotically follows a power-law of the form $i \propto t^{-\eta}$. If superposition applies, then a square pulse of duration T could be considered to be a field of +A being turned on at time $t = -T$ and staying on forever with another field of -A being turned on at $t = 0$. The asymptotic current should then be the sum of

the two response currents for $t > 0$:

$$i(t) \propto (T + t)^{-\eta} - t^{-\eta} \tag{2.14}$$

and in the limit of short times, $t \ll T$

$$i(t) \propto t^{-\eta} \tag{2.15}$$

since the first term is negligible in comparison with the second in Equation 2.14. In the limit of long times, $t \gg T$,

$$i(t) \propto t^{-\eta} \left\{ \left(1 + \frac{T}{t} \right)^{-\eta} - 1 \right\} \simeq \eta T t^{-\eta-1}. \tag{2.16}$$

Jonscher was worried that the discharge currents after a pulse of finite duration would only follow the "genuine" characteristics of the material in question for a very short time. He predicted the cross over time for the discharge current to change from $-\eta$ to $-1 - \eta$, which would allow the measurement of η from discharge currents.

Polarization versus Conductivity

According to the relations in Table 1, the permittivity function ϵ includes all of the integrated current through the material, due to conductivity as well as the charge stored due to internal polarization. As discussed above it is desirable to "subtract out" the conductivity in order to model the "actual" polarization, i.e. charge stored across the dielectric. Unfortunately, the conductivity is not readily determined from the low-frequency tail of the permittivity, so it is not at all certain what should be

subtracted, especially when different authors refer to the low-frequency response as a time varying conduction and others as a time varying capacitance.

It bears remembering that the plots shown above are for fixed electrical boundary conditions. This leads to a substantial question: with the anomalous conductivity evident in the typical case, how does the voltage across the device behave in the open circuit case? In other words, can we discern the internal leakage from the standard permittivity measurements? This question applies equally to any of the other immitance functions as well.

In line with the thrust of this investigation: does the open circuit relaxation bear any relation to the parameters in the fixed field case? Does it show power-law decay as well? Exploring this question will probably require significant finesse in experimental technique. See chapter 8 for additional discussion.

From Whence the Power-law?

Numerous models for the causes of the memory effect have been postulated. For example, in Reference [24], Ngai and Rajagopal postulated that the time dependent transition rates giving rise to non-Debye relaxation are due to the interaction with the heat bath. In this theory, the low-energy level spacings of the heat bath determine the long-time relaxation process. It is difficult to see how the concentration of a dipolar liquid would cause variation in the long-time response if the rate were determined by interaction with the environment as opposed to internal interactions. Additionally,

this model predicts stretched exponential response, not power-law. Other models, mostly based on some fixed distribution of defects within the material, predict power-law behavior over only a limited frequency range.

Given the universal nature of the power-law forms of the observed relaxation processes in solids and non-dilute liquids, it may be reasonable to suspect that it is a natural consequence of a many body problem. The polarization can be viewed as being due to bound charge carriers hopping to between states with different charge symmetries than their ground states. In addition to the possibility that the charged particles might undergo relaxation back to the original states, it may be possible for the local environments to relax around the new states, reducing the likelihood of the return to the ground states. These metastable states may have lifetimes many orders of magnitude greater than that which would occur if the environments had not been modified. These metastable states may again interact with one another and form new relaxation conditions leading to the observed "distribution of decay times."

One major new possibility comes into play: the distribution of the trapping times may be such that the second moments diverge. In this case, the canonical central limit theorem no longer holds. That is, the statistics are not necessarily Gaussian. Instead, a Lévy, or α-Stable, distribution can result. The Lévy distribution is noted for its long power-law tails. These divergent tailed distributions percolate their way up to the macroscopic scale as a long-time power-law memory. A similar argument for conductive response can be made. These models will be discussed in some detail in

Chapter 3. The natural mathematics of power-law relations is the fractional calculus, which will be discussed in Chapter 4.

If the power-law relations represent true memory effects and are not just convenient curve fitting parameters, then there must be an intimate relation between the *ac* and *dc* response in any given material represented by a dynamical equation of motion. It should be possible to associate variation of parameters in a power-law model with variation in composition and boundary conditions.

Hypothesis

Hypothesis: *Dielectric dynamics can be accurately modeled using the fractional calculus.*

- Included in the hypothesis is that the low-frequency, long-time tails in the permittivity must also be accounted for via a memory function in the fractional calculus model.
- The testing of the hypothesis will begin with development of numerical techniques for dealing with non-Markovian differential equations represented in the fractional calculus. This will then allow for comparison of predictions of time domain response generated from modeling, using data obtained in the frequency domain, with measured time domain response for a variety of materials under a variety of conditions.

- For the hypothesis to be falsified, either the *ac* measurements should substantially deviate from power-law behavior or the time domain response should deviate from that predicted by the model developed from the *ac* response.
- For the hypothesis to be rendered non-applicable, the exponents and coefficients should show no discernible pattern of variation as a result of incremental changes in composition or boundary conditions.

CHAPTER 3

THE MODEL

The composite model for dielectric relaxation to be discussed in this Chapter is based on ideas by Hill and Jonscher [11], Funke [12] and Bouchaud and Georges [25]. In each of these cited references, the assumption is made that the bound or mobile charge carriers hop or move about in an environment that interacts with the charge carrier. That is, the local energy potential landscape is not independent of the motion of the charge carriers.

Stated more precisely, these models consistently drop the assumption that there is some defect structure inherent in the material with some fixed distribution of trapping times or energies. Rather, the defect structure is seen to be a direct result of the dynamics of the polarization or conduction. The result is an "annealed" as opposed to "quenched" disorder in the material.

Polarization and Conduction as Statistical Quantities

Polarization and conduction in bulk materials are statistical quantities representing the sum of a large number of contributions from the motion of bound or mobile charge carriers. Viewing ideal conductivity as a friction limited drift under an external force (the applied field), the current should depend linearly on the field and therefore

be constant under constant field. Viewing polarization as purely bound charge, the current should fall to zero exponentially after application of a field. As pointed out in the previous chapter, neither of these ideal behaviors are seen. Instead, power-law relations in time and frequency are the norm. Indeed, Westerlund [17] reported that after measuring "tens of thousands of capacitors of all types and makes," every unit exhibited "anomalous" behavior.

As limits of sums of statistical distributions, the bulk quantities of polarization and conductivity should have statistics which obey the law of large numbers, and the central limit theorem (CLT), at first glance, should require that the sum of independent random variables converges to a Gaussian distribution. Linear systems are expected to exhibit exponential relaxation dynamics. Why then are non-Gaussian and non-exponential behaviors so ubiquitous even in the small signal, linear response regime?

A Statistical Digression

To adequately address the question raised above, it will be necessary to review the law of large numbers and the central limit theorem to see when they apply and when they break down. In what follows, we assume that the material is homogeneous so that a single statistical distribution can be used to describe the behavior of a given process throughout the sample. One material may exhibit a number of different processes, but, this number of distinctly different processes is assumed to be small.

The competition among these processes will be discussed later. For now, we discuss one process at a time.

The law of large numbers states that average of a set of measurements will converge to the mean of a distribution if the mean exists. This law does not depend on the existence of a variance or second moment of the distribution. It is the law of large numbers that allows us to treat fundamentally statistical processes such as the flow of current as deterministic events at the macroscopic scale. The canonical central limit theorem, however, does depend on the existence of a second moment.

As discussed in more detail in Appendix A, the canonical central limit theorem depends on two fundamental assumptions; first that the distributions of the contributing events have a convergent second moment, and, second, that the events contributing to the the sum are adequately independent. We are most concerned with the failure of the first assumption here. Failure of the second assumption will be discussed in Appendix B.

There is a generalized central limit theorem which states that if the events are adequately independent, but have tails to the probability distribution that fall off slower than $t^{-1-\alpha}$, where $2 < \alpha < 0$, then the limit (sum) distribution will have the form of a Lévy, or α-stable, distribution with its characteristic power-law tails. The implication here is that the power-law tails show up in a macroscopic way in the sum distribution. In the case of divergent waiting times to be discussed here, it means that the polarization and current dynamics will exhibit power-law behavior. Further, we

expect that the exponents for the response under an applied field and the relaxation response in the absence of a field will be different.

Polarization

Hill and Jonscher suggested that the power-law behavior in dielectrics should be considered a consequence of the many-body interactions making up bulk condensed matter. A model formalizing this idea and reproducing the Cole-Cole plot (Figure 4) over a broad range of frequencies was proposed by Funke [12]. The basic premise is that the potential energy landscape creating the double- or multi-well potential of a bound charge is not independent of the motion of the charge.

Figure 10 provides a schematic of the hop processes proposed by Funke. In addition to the possibility that an excited particle could relax by returning to the ground state directly, there is the possibility that the local environment could relax. In Figure 10 this is represented by the energy profile relaxing from curve (a) to curve (b) and the particle undergoing the "transition" indicated by process (3). In this case, the time to return to the ground state, process (2), can be many orders of magnitude greater than that predicted by the Debye theory, which accounts for only this possibility. Funke's result is independent of any specific model of relaxation of the environment and will not be reproduced here. All that is needed is that the distribution of waiting times for return to the ground state, i.e. jump process (2), fall off slower than t^{-3}.

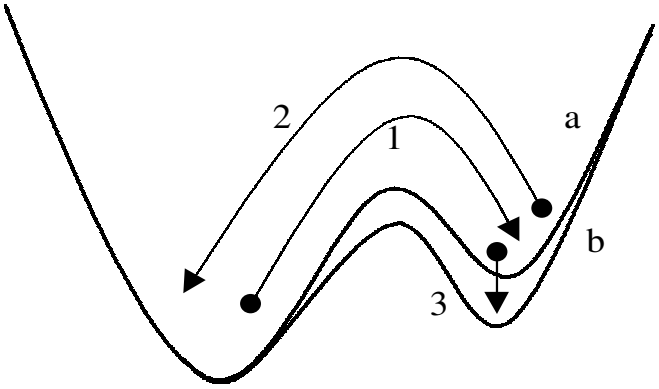

Figure 10. A schematic representation of the bound charge hopping model. The initial potential landscape is represented by curve (a). After a hop to the right (1), the particle can relax back to the initial state (2), or the environment can relax to curve (b) reducing the energy (3) resulting in reduced likelihood of return to the ground state.

Funke places several limitations on the theory, which now appear to be unnecessary. First, there is the assumption that the Cole-Cole curve must make a vertical approach to the real axis on the ϵ'' vs. ϵ' plot at both the highest and lowest frequencies. Second, the low-frequency dispersion is out-of-hand relegated to a surface effect and unrelated to the bulk response. Neither of these assumptions were justified in Reference [12].

Conductivity

A model for frequency dependent conductivity, the "universal dielectric response," was proposed by Bouchaud and Georges [25]. This model is in many ways an extension of that of Funke. Mobile charge carriers interact with defects formed by the creation of carriers in the first place. This is necessarily a dynamic effect. Again, the trapping

of the mobile charges by these defects is a dynamic process and the local environment is given the opportunity to relax around the defect and a charge carrier can be trapped in the defect. Again there is the possibility of a divergent waiting time for escape from the trap. In this model the mobility follows a power law $m(\omega) \sim (i\omega)^{\alpha}$. This power law is the source of the memory. The longer a trapping site lasts, the longer it is likely to last. In addition, it is more likely to affect sites in the local neighborhood. This results in what has been referred to as a "self-pinning" effect. This cooperative relaxation may also result in the observed remanent domain structures seen in ferroelectric materials.

There are issues with respect to the dimensionality of the problem, but, for this work, we consider primarily polarization and conduction along a single principal axis at a time and ignore the tensor nature of the problem.

It has been shown that the "universal dielectric response" is expected to produce 1/f noise. [26]. It is important to note that the model of dynamic disorder described above fits extremely well with other models of 1/f noise production in that very carefully prepared pure materials generate the least noise, while the level of noise grows with increasing "ab initio," or "quenched," disorder.

Competition and Mixing

From the experimental data reported in the literature, it is likely that there will be several competing bound and mobile charge carrying processes going on within any

material. If we are lucky, these will have sufficiently different distributions of waiting times and the effects of each will be distinct. The composite model permittivity will then contain terms proportional to the electric field times a strength factor, ϵ_i and fractional frequency dependence $(i\omega)^{\alpha_i}$, where, in general, the exponent α_i depends on whether the process represents a bound or mobile charge response to the field. In addition, there will be a polarization relaxation term proportional to $(i\omega)^q$, where $q = 1 - \alpha$ from the Funke model to account for the relaxation upon removal of the external field. Each of these, in turn, will be interpreted as a Laplace transform of a fractional derivative operator of the form ${}_0D_t^q$ to be described in the next chapter.

An open question is whether or not the competition between and among processes can lead to mixing of exponents. One of the models to be derived in Chapter 5 treats the exponents as separate entities while another allows such mixing.

There is still no detailed microscopic description of polarization that produces the CPE behavior. There is still some ambiguity as to whether the low-frequency dispersion is due to interface effects between the electrodes and the dielectric or whether it originates within the bulk of the dielectric or both.

Distributions of Relaxation Times

While this chapter has concentrated on the statistical description of power-law dynamics, it should be noted that the theory of distributions of relaxation times has made complementary progress as well. Reference [10] provides a description

of multifractal functions of the distribution for Cole-Cole, Havriliak-Negami, and Davidson-Cole relaxation processes. Analysis of these functions as thermodynamic entities reveals the competition between processes with different time scales. The discovery of phase transitions in multifractal analysis is a new development and, as the authors of Reference [10] point out, there are many unanswered questions. It may turn out that further advances on both fronts will lead to development of more specific models. In both the fractional-time power-law and fractal-time distribution models, the creation of the exponents and the divergence of the distributions are due to the macroscopic sum of an enormous number of contributing microscopic activities.

A Plethora of Models?

Any of the forms in Table 2 may be used as a starting point for development of a spectral permittivity function, but the models proposed here abandon the assumption that the high and low frequency terms must necessarily be represented by purely real permittivity terms. The result of this is that any proposed equivalent circuit element, resistor or capacitor, should be replaced with an appropriate constant phase element (CPE) as described in Chapter 2. This process will be undertaken in Chapter 5 where two specific model forms are developed.

CHAPTER 4

THE FRACTIONAL CALCULUS

The fractional calculus is the natural mathematical language of power-law relations and has been proposed by a number of authors as being applicable to the problem of power-law relaxation dynamics. While frequency domain plots of dielectric response have been accurately fit with power-law equations, it has yet to be shown that the fits truly represent fractional differential equations capable of predicting time domain transients. This chapter introduces some basic concepts of the fractional calculus that will be required in later chapters.

The fractional calculus dates from very shortly after the classical calculus became known; Leibniz mentioned it in a letter to L'Hopital in 1695. Euler and Lagrange made significant contributions with the more systematic treatment credited to Liouville, Riemann and Holmgren in the mid-19th century. Somewhat different definitions exist today but translations are tabulated in texts and have to do mainly with composition rules and treatment of initial conditions. The two most useful texts, References [27] and [28], are unfortunately out of print. Also useful for analytic manipulation of fractional differential equations is Mathai and Saxena's text on the Fox function. [29] More recently Podlubny [30] discussed a number of techniques for attacking fractional differential equations including rudimentary numerical methods.

While the name "differentiation and integration to arbitrary order" may be more accurate, "fractional calculus" is the term that is generally used. Nonetheless, the order is arbitrary and not limited to the set of rational numbers.

The Definition of the Fractional Derivative

This section on the definition of the fractional derivative presents excerpts from Chapter 3 of Reference [27].

The fractional order derivative can be motivated via the standard integer order derivative, which can be defined via Cauchy's integral formula:

$$\frac{\mathrm{d^n}}{\mathrm{dz^n}} f\left(z\right) = \frac{n!}{2\pi i} \oint_C \frac{f(\zeta) d\zeta}{\left[\zeta - z\right]^{n+1}} \tag{4.1}$$

where C describes a closed contour in the complex plane surrounding the point z and enclosing a region of analyticity of the function f. When the positive integer n is replaced be a non-integer q, then $[\zeta - z]^{-q-1}$ no longer has a pole at $\zeta = z$ but a branch point. One is no longer free to deform the contour C surrounding z, since the integral will depend on the location of the point at which C crosses the branch line for $[\zeta - z]^{-q-1}$. The point of origin is chosen to be 0 and the branch line to be the straight line joining 0 and z and continuing indefinitely in the quadrant Re $(\zeta) \leq 0$, Im$(\zeta) \leq 0$. Then one simply defines, for q not an integer,

$$\frac{\mathrm{d^q}}{\mathrm{dz^q}} f\left(z\right) = \frac{\Gamma(q+1)}{2\pi i} \oint_C \frac{f(\zeta) d\zeta}{\left[\zeta - z\right]^{q+1}}, \tag{4.2}$$

where the contour C begins and ends at $\zeta = 0$ enclosing z once in the positive sense.

The Gamma function, $\Gamma()$, is the generalized factorial function described in Chapter 6 of Reference [31].

To uniquely specify the denominator of the integrand, one defines

$$[\zeta - z]^{q+1} = \exp\left([q+1]\ln(\zeta - z)\right), \tag{4.3}$$

where $\ln(\zeta - z)$ is real when $\zeta - z > 0$. Equation 4.2 can be simplified as

$$\begin{aligned} \frac{\Gamma(q+1)}{2\pi i}\oint_C \frac{f(\zeta)d\zeta}{[\zeta - z]^{q+1}} &= \frac{\Gamma(q+1)}{2\pi i}\left[1 - \exp(-2\pi i[q+1])\right]\int_0^z \frac{f(\zeta)d\zeta}{[\zeta - z]^{q+1}} \\ &= \frac{1}{\Gamma(-q)}\int_0^z \frac{f(\zeta)d\zeta}{[\zeta - z]^{q+1}}. \end{aligned} \tag{4.4}$$

This definition has been attributed to Nekrassov (1888).

The Riemann-Liouville definition is

$$\left[\frac{d^q f}{d(x-a)^q}\right] = \frac{1}{\Gamma(-q)}\int_a^x [x-y]^{-q-1} f(y)dy, \quad q < 0, \tag{4.5}$$

which extends the Nekrassov definition to a non-zero starting point. The Riemann-Liouville definition is of considerable interest in analytical methods but has notoriously bad numerical convergence.

A more useful definition for numerical application was first given by Grünwald (1867) and later extended by Post (1930). Derivatives (of positive order q) or integrals (of negative order q) can be defined by the formula

$$\frac{\mathrm{d^q}}{\mathrm{d(t-a)^q}} f(t) = \lim_{N\to\infty}\left\{\frac{\left[\frac{t-a}{N}\right]^{-q}}{\Gamma(-q)}\sum_{j=0}^{N-1}\frac{\Gamma(j-q)}{\Gamma(j+1)} f\left(t - j\left[\frac{t-a}{N}\right]\right)\right\}, \tag{4.6}$$

where q is arbitrary. Due to the fact that the definition is continuous in q, it is sometimes given the name "differintegral" to imply that it applies to both derivatives

and integrals in the classical sense. This definition exhibits excellent numerical convergence for finite N, thus allowing use in finite difference methods. The Grünwald definition, Equation 4.6, can be shown to be completely equivalent to the Riemann-Liouville definition, Equation 4.5.

A notable difficulty is that the fractional derivative is "non-local" as it is defined over a finite interval, between a and x, where $x > a$. Note that the differential step size, dt, is defined via $(t-a)/N$ just as it is in integer order calculus for integrals. Evaluation at the point $x = a$ is specifically excluded. In the limit of $q \to n$, n a positive integer, all but $n+1$ of the terms of the sum in Equation 4.6 go to zero. In this case, as $N \to \infty$, only the most immediate past is incorporated into the computation and the definition becomes "local." For non-integer q, the weighting factors, $\Gamma(j-q)/(\Gamma(-q)\Gamma(j+1))$, scale as a power-law in j for large j. This weights prior history, back to the beginning of the interval, with a power law in time. Only for integer q does the derivative have geometric meaning in the sense of slope or curvature "at a point."

A example of the weights involved in the fractional derivative, for $q = 0.5$, is shown in Figures 11 and 12. The fractional derivative is found by taking the sum of the products of the function value times the weight times dt^{-q}.

This power-law weighting of history is how the mathematics reflects the physics of power-law relaxation processes. The limit of q approaching an integer represents a process with a finite second moment of the waiting time distribution. When q is

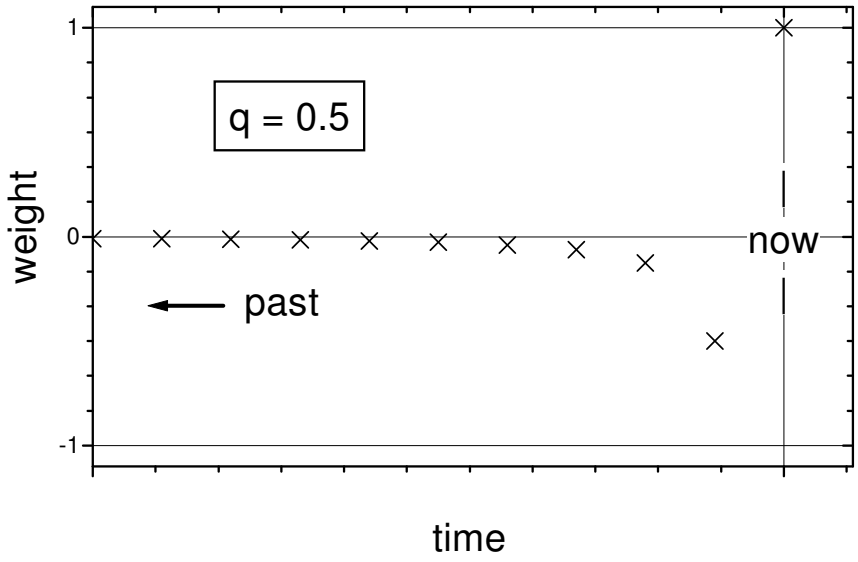

Figure 11. Linear plot of weights associated with the fractional derivative for $q = 0.5$.

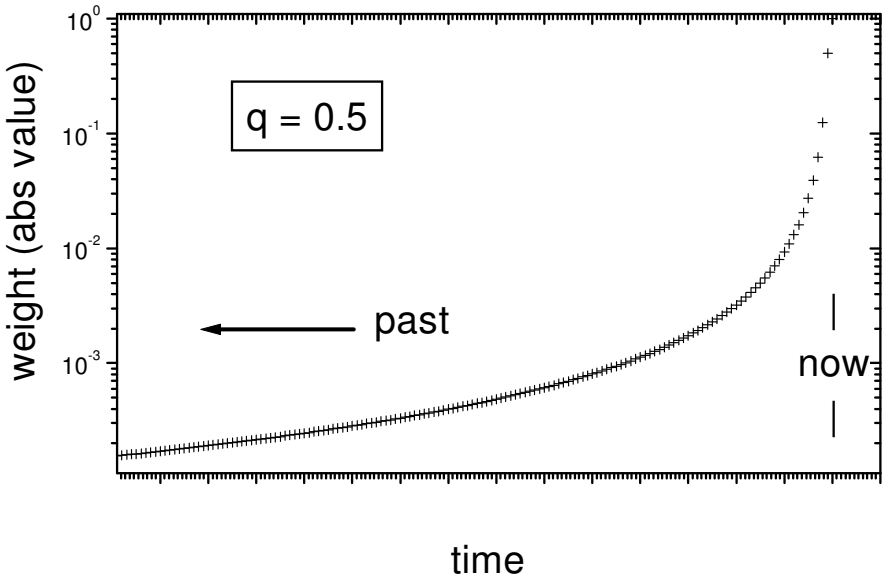

Figure 12. Logarithmic plot of the absolute value of the weights associated with the fractional derivative for $q = 0.5$. The time scale shown here is 15 times longer than that shown in Figure 11.

not an integer, an infinite amount of information is required to accurately produce the fractional derivative. The problem then fails to meet the criteria for a Markov process and we are faced with a fundamentally non-Markovian process. [32] While finite difference equations can be used for some purposes, as will be developed in subsequent chapters, we will always be losing information.

The notation used in fractional calculus has been adapted for the differintegral requiring specification of the interval for both positive and negative orders. In the older notation used by Oldham and Spanier in Reference [27], $\mathrm{d}^q/[\mathrm{d}(t-a)]^q$ indicates that the interval is from a to t. The modern notation, used by Miller and Ross [28], is ${}_aD_t^q$.

A second notable difficulty with the fractional order derivative is that the derivative of a nonzero constant is not zero. This is a direct consequence of the branch cut required in the definition. For example, the derivative of unity is:

$$\frac{\mathrm{d}^q[1]}{[\mathrm{d}(t-a)]^q} = {}_aD_t^q[1] = \lim_{N\to\infty}\left\{\left[\frac{N}{t-a}\right]^q \frac{\Gamma(N-q)}{\Gamma(1-q)\Gamma(N)}\right\} = \frac{[t-a]^{-q}}{\Gamma(1-q)} \tag{4.7}$$

The fractional differintegral is a linear operator. The Laplace transform applies to fractional real and reciprocal space variables continuously in all orders of q. The Mellin transform,

$$\mathcal{M}\{f(t);s\} = \int_0^\infty f(t)t^{s-1}dt, \tag{4.8}$$

finds extensive use in fractional analysis due to its power-law transform kernel. Green's function methods have also been developed for use with fractional calculus.

As with integer order calculus, care must be taken when forming compositions of operators. For example, the integral of a derivative of a function differs from the derivative of the integral of the function by the value of any terms taken to zero by the differentiation in the first case. With integer order calculus this problem is addressed through the addition of constants of integration. In the fractional case, the initial conditions result in the inclusion of terms such as Equation 4.7 for both derivatives and integrals. The rules get rather complicated and the reader is referred to texts such as [27] and [28] for the details.

Causality and Time Inversion

Since the fractional differintegral operates over the interval $(-\infty, t)$, it satisfies causality by construction. It is this property that guarantees that response functions based on fractional differintegrals will satisfy the Kramers-Kronig relations. The fractional differintegral operator is not symmetric with respect to time inversion, and so the dynamics are irreversible and will not generally conserve energy.

Fractional Derivative of a Sinusoid

Since much of what follows in the next two chapters involves *ac* responses, we will need the fractional derivative of a sinusoid, which is

$$\frac{\mathrm{d}^q}{\mathrm{d}t^q}\sin(\omega t) = {}_0D_t^q \sin(\omega t) = \omega^q \sin(\omega t + q\frac{\pi}{2}) + \ transient\ terms. \tag{4.9}$$

That the fractional derivative operator is linear means that superposition holds and no

additional frequency components are generated in a fractional process. The fractional derivative converges to the integer order result as the exponent approaches an integer value. Note that the phase angle is independent of frequency, i.e. a "constant phase element." The frequency independent loss factor discussed in Chapter 2 is seen as a direct result of the memory function.

The transient terms are complicated, but can generally be described as a combination of a power-law decaying bias plus a power-law decaying oscillation. In combination they can produce an apparent phase drift with the phase settling to $q\pi/2$ asymptotically. Since the phase accuracy is potentially in question, both the numerical simulations and experimental measurements will allow for long (in terms of τ) waiting periods after initiating an *ac* field.

Fractional Relaxation

The problem of non-exponential relaxation illustrates some of the methods of fractional calculus. It is often the case that fractional differential equations can be developed from generalizations of integer order systems.

Following Glöckle and Nonnenmacher [33], simple first order relaxation can be written

$$(1 + \tau\, {}_0D_t)\, \phi(t) = 0. \tag{4.10}$$

or:

$$\dot{\phi}(t) = -\frac{1}{\tau}\phi(t), \tag{4.11}$$

where $\phi(t)$ represents a physical variable such as electrical polarization or mechanical strain. The solution is

$$\phi(t) = \phi_0 - \frac{1}{\tau}\int_0^t \phi(t')\mathrm{dt}'. \tag{4.12}$$

We can generalize the system to allow non-exponential response by replacing the Riemann integral operator (the anti-derivative) $(1/\tau)\,{}_0D_t^{-1}$ with $(1/\tau)^q\,{}_0D_t^{-q}$, to obtain

$$\phi(t) - \phi_0 = -\frac{1}{\tau^q}\,{}_0D_t^{-q}\phi(t). \tag{4.13}$$

Applying $\tau^q{}_0D_t^q$ from the right and using the differential rule for a constant, ${}_0D_t^{-q}\phi_0 = \phi_0 t^{-q}/\Gamma(1-q)$, results in

$${}_0D_t^q\phi(t) - \phi_0\frac{t^{-q}}{\Gamma(1-q)} = -\tau^{-q}\phi(t). \tag{4.14}$$

From here, we apply the Laplace transform, leading to

$$\tilde{\phi}(s) = \phi_0\frac{s^{-1}}{1+(s\tau)^{-q}}. \tag{4.15}$$

Looking up this form in a reference (e.g. [29]), we find the series expansion

$$\phi(t) = \phi_0\sum_{k=0}^{\infty}\frac{(-1)^k}{\Gamma(1+qk)}\left(\frac{t}{\tau}\right)^{qk}, \tag{4.16}$$

from which we recover the exponential in the limit $q \to 1$.

Time domain plots of Equation 4.16 with various values of q are shown in Figure 13. Even for values of the exponent near unity, there is still a transition to power law behavior after some time. Note that the solution is, in fact, dominated by the initial condition at short times and can be fit quite well with a "stretched exponential" for $t \sim \tau$.

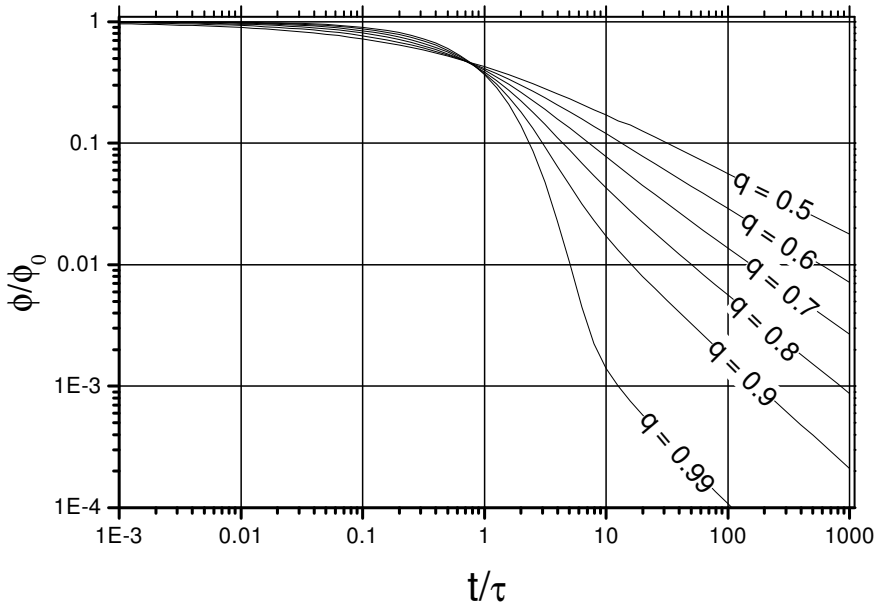

Figure 13. Time domain decay of polarization for various values of the exponent q.

The derivation above actually represents an overly idealized situation and can be misleading. The initial condition ignores the history of how the initial polarization or strain was achieved. For the fractional calculus to provide a meaningful model of dynamic behavior, the fractional derivative operator must include the entire history from the last moment that the field and response were both zero. Since this is not feasible with the analytical methods currently available, a major effort of this work was dedicated to the development of numerical methods to allow exploration of the effect of imposing a arbitrary field of finite duration. The results of this effort will be presented in Chapter 6.

CHAPTER 5

DERIVATION OF THE DIFFERENTIAL EQUATION

A major step in constructing a consistent model of polarization dynamics is the development of a time domain differential equation. This will be carried out by generalizing models of ideal circuit elements, e.g. the Debye behavior, and adding low frequency conductivity. As discussed in Chapter 3, any of the forms in Table 2 could be used as a starting point. Alternatively, an equivalent circuit could be proposed and selected resistors and/or capacitors could be replaced with CPE. One of each is developed here: one generalizing the Cole-Cole model directly and the other by generalizing the impedance function of a circuit model. Both dynamical models incorporate both a dielectric loss peak and low-frequency dispersion.

Other models can be proposed, each potentially suffering from the act of attempting to obtain the general case from an ideal equivalent circuit model. The thrust of future experimental work will be to attempt to eliminate incorrect models.

Much of the methodology used in this chapter was motivated by Reference [34] which suggests application of the fractional calculus to the problem of relaxation in mechanical systems. While the idea of applying the fractional calculus to the description of dielectric response is not new, the work presented here is unique in that it incorporates (almost) all of the dynamics of the dielectric response over an

extended range of frequencies and times. Additionally, the models developed as part of this research will allow comparison between *ac* and *dc* responses, which was an objective outlined in Chapter 1.

As will be seen, the caveat "almost" above applies to the fact that a piezoelectric resonance will be seen in the spectral response of PVDF that is not taken into account, as yet, in the models presented.

The Permittivity Equation

We can construct a form of the constitutive equation relating the polarization to the applied field, by starting with the electric displacement,

$$\mathbf{D}(t) = \epsilon_0 \mathbf{E}(t) + \epsilon_0 \int_{-\infty}^{\infty} f(\tau)\mathbf{E}(t-\tau)\mathrm{d}\tau, \quad \text{with } f(\tau) = 0 \text{ for } \tau < 0, \tag{5.1}$$

where $f(t)$ represents a memory function associated with the material properties of the dielectric. [35] This convolution in the time domain becomes a simple product of functions in the frequency domain. With $\mathbf{D}(\omega) = (1 + \chi_e(\omega))\epsilon_0\mathbf{E}(\omega)$ and $\mathbf{P}(\omega) = \chi_e(\omega)\epsilon_0\mathbf{E}(\omega)$, we see that

$$\chi_e(\omega) = \int_{-\infty}^{\infty} f(\tau)e^{i\omega\tau}\mathrm{d}\tau. \tag{5.2}$$

In words, $\chi_e(\omega)$ is just the Fourier transform of the memory function. Since χ_e is often on the order of 10 or greater for dielectric materials of interest, it is customary to equate $\epsilon(\omega)$ and $\chi_e(\omega)$. With this approximation, $\epsilon(\omega)$ can be interpreted as the limiting case, $s \to i\omega$, of the Laplace transfer function $\mathbf{P}(\mathrm{s})/\mathbf{E}(\mathrm{s})$.

It is important to note that the expectation should be that the polarization response depends on the entire past history of the the applied field.[36] Power law behavior is the simplest non-exponential response that incorporates the memory effect.

We can begin to see how to incorporate memory by viewing the Debye formula as the limiting case of a Laplace transfer function and inverting it to form a time domain differential equation:

$$\mathbf{P}(t) + \tau \frac{\partial}{\partial t}\mathbf{P}(t) = \epsilon_s \mathbf{E}(t) + \epsilon_\infty \tau \frac{\partial}{\partial t}\mathbf{E}(t). \tag{5.3}$$

Applying the Fractional Calculus to Non-exponential Processes

Interpretation of complex permittivity plots using power-law fitting dates back to Cole and Cole [3]. In terms of the complex conjugate of the permittivity $\epsilon^* = \epsilon' - i\epsilon''$, simple Debye relaxation would appear as a semicircle on a plot of ϵ'' versus ϵ'. [1] Written in traditional form:

$$\epsilon^* - \epsilon_\infty = \frac{\epsilon_s - \epsilon_\infty}{1 + i\omega\tau} \quad \text{(Debye)} \tag{5.4}$$

The use of the complex conjugate ϵ^* places the Cole-Cole plot in the first quadrant.

As stated above, the permittivity, sometimes referred to as the "dielectric constant," is the *relative* permittivity. However, it is often convenient to set the scaling constant ϵ_0 between $\mathbf{D}$ and $\mathbf{E}$ to unity when convenient for computational purposes as will be done here.

In general the data for real dielectrics seem to fit an arc of a circle with the center below the real axis over a range centered on the loss peak. The interpretation made by Cole and Cole was that the "resistive" part of the equivalent circuit should be replaced with a frequency dependent complex impedance, the CPE, that just happened to produce a loss factor that was nearly constant over a very wide range of frequencies.

$$\epsilon^* - \epsilon_\infty = \frac{\epsilon_s - \epsilon_\infty}{1 + (i\omega\tau)^{1-\alpha}} \quad \text{(Cole-Cole)} \tag{5.5}$$

Using a convenient form $e^* = (\epsilon^* - \epsilon_\infty)/(\epsilon_s - \epsilon_\infty)$, the Cole-Cole form, Equation 5.5, can be written

$$e^* = \left(1 + (i\omega\tau)^{1-\alpha}\right)^{-1}. \tag{5.6}$$

From Equation 5.6, other known forms can be developed, such as those listed in Table 2. Unfortunately, use of the spectral functions with their inherent assumptions about the high and low frequency behavior may limit the interpretation of the complex permittivity. As discussed in Chapter 2, while systems can be approximately capacitive at high frequencies, they virtually always exhibit some level of conductivity at low frequencies.

Development of a Differential Equation

Cole and Cole began the practice of describing the power-law in frequency as due to a distribution of exponential decays, i.e. a distribution of time domain functions, rather than as fundamentally power-law in time as well. Unfortunately, the spread of

time constants needed for this model can encompass seven or more decades. These time constants often overlap other processes, requiring models to be broken up into sections with arbitrary frequency and time scales.

Breaking with the tradition of writing the permittivity function as $\epsilon^*(\omega) - \epsilon_\infty$, the derivations developed in this work will be in terms of $\epsilon(\omega)$, or $\epsilon^*(\omega)$, directly. This is done for three reasons. First, $\epsilon(\omega)$ can be computed directly from impedance measurements using Table 1. Second, there is no requirement to make an accurate guess at the value of ϵ_∞, it becomes a minor fitting parameter to which the rest of the function is quite insensitive. Third, the possibility that the high frequency limit might have some residual loss factor is left open.

By rewriting Equation 5.5 to isolate $\epsilon^*(\omega)$, and letting $q = 1 - \alpha$,

$$\epsilon^*(\omega) = \frac{\epsilon_s + \epsilon_\infty (i\omega\tau)^q}{1 + (i\omega\tau)^q}, \tag{5.7}$$

we can identify the effects of the power law behavior associated with the exponent q.

A Fractional Form of the Constitutive Equation

Using the notation of fractional calculus, we can take the first step toward incorporating memory and power law behavior by likewise transforming the Cole-Cole form, Equation 5.7, to the time domain:

$$\left(1 + \tau^q \, {}_0D_t^q\right) \mathbf{P}(t) = \left(\epsilon_s + \epsilon_\infty \tau^q \, {}_0D_t^q\right) \mathbf{E}(t) \tag{5.8}$$

and noticing that fractional derivatives replace the integer order forms in the Debye

version. Here the scaling constant $\epsilon_0 = 1$ and we are using the more useful convention of calling the integrated current the polarization, $\mathbf{P}$.

The fractional units that show up in the time domain form disappear neatly in the frequency domain form. It is possible to rescale in the time domain as well, so that the resulting equation contains only dimensionless quantities.

There is no compelling reason to require that the exponent q appearing on the right hand side (RHS) and the one on left hand side (LHS) be the same. In fact, as noted in Chapter 3, for anomalous processes the exponent associated with relaxation under no-field conditions can differ from that associated with drift in the presence of a symmetry breaking field.

It is also expected that the material should be conductive at low frequencies/long times and that more than one mechanism may be responsible for the conductivity. This additional generalization assumes that even the low frequency conductivity is governed by a power law, i.e. $\epsilon_s \rightarrow \epsilon_s(i\omega\tau)^\delta$. In order to account of anomalous low frequency dispersion, an additional low frequency term is proposed, i.e. $\epsilon_c(i\omega\tau)^\beta$. These terms transform to the time domain as $\epsilon_s(i\omega\tau)^\delta \rightarrow \epsilon_s\tau^\delta\, {}_0D_t^\delta$ and equivalently for the ϵ_c term to give

$$\left(1 + \tau^q\, {}_0D_t^q\right)\mathbf{P}(t) = \left(\epsilon_s\tau^\delta\, {}_0D_t^\delta + \epsilon_\infty\tau^\mu\, {}_0D_t^\mu + \epsilon_c\tau^\beta\, {}_0D_t^\beta\right)\mathbf{E}(t). \tag{5.9}$$

On the LHS, there is a term proportional to $\mathbf{P}$ and a term proportional to a generalized "velocity" of $\mathbf{P}$, a "friction with memory" term. On the RHS, the ϵ_∞ term is the high frequency response with $\mu \approx q$. The ϵ_s term represents a low

frequency response to a field with δ negative and typically small, accounting for the low frequency dispersion; i.e. Equation 2.13 with $\delta = n - 1$. The extra term proportional to ϵ_c accounts for an additional, qualitatively different, conductivity at very low frequencies with $-1 < \beta < 0$. There is only one time constant, τ, and all underlying processes exhibit memory effects through the various exponents.

In this model, there are three terms on the RHS. Each term represents a process with an exponent. The derivation follows the general procedure outlined by Cole and Cole in Reference [3] of direct geometric interpretation of the Cole-Cole plot. In this case there are three distinct regions; a high frequency region above (in frequency) the loss peak, one just below the loss peak, and a third distinguished by the low frequency anomaly. There is no mixing of exponents; the competition among the processes is accounted for only in their relative strengths at any given frequency.

The form of the constitutive equation represented by $\epsilon^*(\omega)$ is not just an academic issue. It implies that the power law behavior will also show up in the time domain as a long time decay transient response as demanded by the fractional calculus. In this interpretation, the time constant τ is established by the polarization relaxation and is approximately equal to the reciprocal frequency of the main loss peak. The coefficients, ϵ_k, and the exponents, δ, μ, and β, represent the interaction of the electric field with the material. In effect, τ represents a scaling of time and frequency space rather than a traditional time constant in the exponential decay interpretation.

Transforming back to the frequency domain, Equation 5.9 becomes

$$\epsilon^*(\omega) = \frac{\epsilon_s (i\tau\omega)^{\delta} + \epsilon_\infty (i\tau\omega)^{\mu} + \epsilon_c (i\tau\omega)^{\beta}}{1 + (i\tau\omega)^{q}}. \tag{5.10}$$

Figure 14 shows a typical "textbook" Cole-Cole plot fit using Equation 5.10 and data extracted from reference [37]. No attempt was made to optimize the parameters since there were no error bars indicated in the original figure. This example was chosen due to the fact that a large section of the loss peak and the anomalous tail were available. Obtaining data this complete is not always possible.

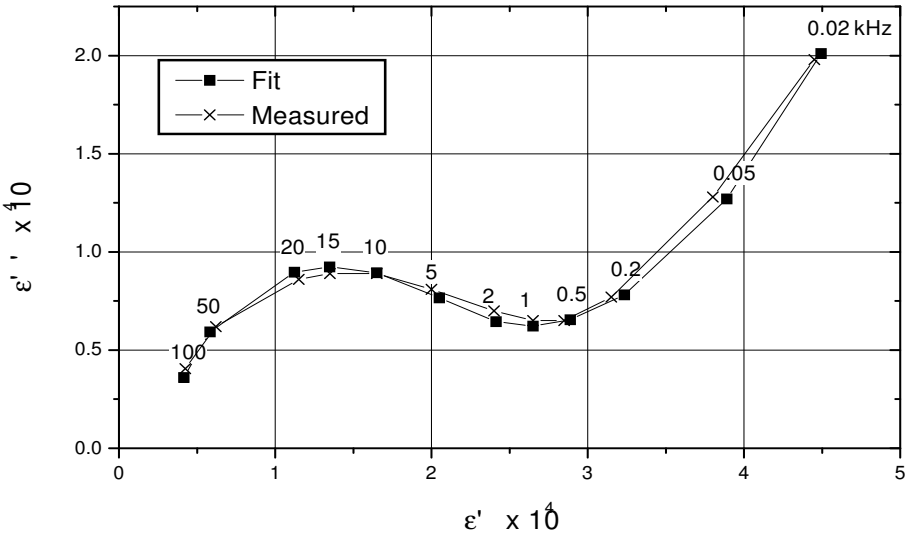

Figure 14. Nb-doped (1 at. %) Remeika ($BaTiO_3$) single crystal. Fit to Equation 5.10 with parameters: $\epsilon_s = 19.4 \times 10^3$, $\delta = -0.11$, $\epsilon_\infty = 6 \times 10^3$, $\mu = 0.79$, $\epsilon_c = 60$, $\beta = -0.795$, $q = 0.977$, $\tau = 8.8\mu\,\mathrm{sec}$. Data point labels are in kHz. Solid lines drawn as aids to the eye.

It was noted in Chapter 3 that the low-frequency dispersion, the "universal dielectric response," should generate a 1/f-like noise spectrum. This is demonstrated through the use of a standard technique for predicting noise spectra as shown in

Figure 15.[38] The technique makes the assumption that the "resistive" part of the dielectric constant produces thermal noise proportional to ϵ'' at each frequency.

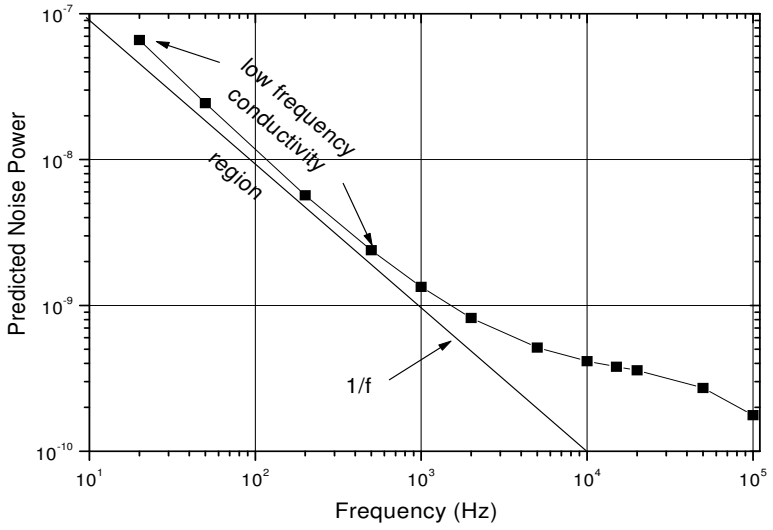

Figure 15. The noise power spectrum predicted from Figure 14. A line with 1/f shape is drawn to demonstrate how close the predicted noise spectrum is to 1/f behavior in the anomalous conduction region. Solid line drawn as an aid to the eye.

A Second Fractional Form of the Constitutive Equation

The differential equation described above was obtained by direct generalization of the ideal non-conductive case by adding a conductivity term. The derivation was based on direct appeal to the geometry of the Cole-Cole plot. Another candidate form of the differential equation may be obtained by starting with an ideal equivalent circuit for a system with *dc* conductivity as shown in Figure 16.

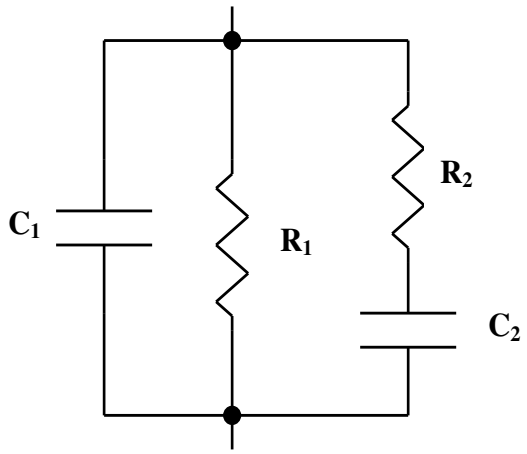

Figure 16. An ideal element RC circuit incorporating conductivity.

The impedance for the circuit is

$$Z = \frac{1}{i\omega \mathrm{C}_1 + \frac{1}{\mathrm{R}_1} + \frac{1}{\mathrm{R}_2 + \frac{1}{i\omega \mathrm{C}_2}}} \tag{5.11}$$

which can be transformed using Table 1 to

$$\epsilon = \frac{\frac{\mathrm{C}_1+\mathrm{C}_2}{\mathrm{C}_\mathrm{c}} + \frac{\tau}{\mathrm{R}_1\mathrm{C}_\mathrm{c}} + \frac{\mathrm{C}_1}{\mathrm{C}_\mathrm{c}}(i\omega\tau) + \frac{\mathrm{R}_2}{\mathrm{R}_1}\frac{\mathrm{C}_2}{\mathrm{C}_\mathrm{c}}(i\omega\tau)^{-1}}{1 + i\omega\tau} \tag{5.12}$$

where $\tau = \mathrm{R}_2\mathrm{C}_2$.

By replacing the resistive elements with constant phase elements (CPE):

$$\mathrm{R}_1 \to \mathrm{R}_1(\mathrm{i}\omega\tau)^{-\gamma}, \quad \mathrm{R}_2 \to \mathrm{R}_2(\mathrm{i}\omega\tau)^{-\alpha},$$

one obtains

$$\epsilon^*(\omega) = \frac{\epsilon_s + \epsilon_\infty(i\omega\tau)^q + \epsilon_c(i\omega\tau)^\beta + \epsilon_c(i\omega\tau)^\nu}{1 + (i\omega\tau)^q}, \tag{5.13}$$

where

$$\tau = \mathrm{R}_2\mathrm{C}_2, \quad \epsilon_s = \frac{\mathrm{C}_1 + \mathrm{C}_2}{\mathrm{C}_\mathrm{c}}, \quad \epsilon_\infty = \frac{\mathrm{C}_1}{\mathrm{C}_\mathrm{c}}, \quad \epsilon_c = \frac{\tau}{\mathrm{R}_1\mathrm{C}_\mathrm{c}},$$

$$q = 1 - \alpha, \quad \beta = -1 + \gamma, \quad \nu = \gamma - \alpha.$$

To be true to the spirit of Chapter 3, we should also replace capacitor C_1 with a CPE. However, for simplicity, we will assume that the high frequency effects are fast enough to be insignificant for our current purposes.

As in the first model, the parameter τ represents a scaling of the time and frequency space and is determined by the relaxation term. To keep the units of the constant phase elements in ohms, the values of R_1 and R_2 are numerically adjusted by τ^γ and τ^α, respectively.

It is clear that the element $R_1(i\omega\tau)^{-\gamma}$ no longer represents a pure conduction process. The CPE also includes a phase shift producing an imaginary contribution to the impedance and a real part to the permittivity. We can refer to this effect as "phase shifted conductivity." Physically, this appears to represent flow of charge carriers along a chain of defects or along the backbone of polymer. A much higher barrier is encountered at the end of the chain resulting in a trapping site with the kind of relaxation discussed in Chapter 3.

In this model, the physical model exponents α and γ mix to form ν in the dynamical equation. This mixing allows the model to produce asymmetries of the forms noted in Table 2. This allows an additional venue of competition among processes and no longer links the number of terms on the RHS to the number of competing processes as in the previous model.

This model contains two fewer fitting parameters than the preceding version. Just

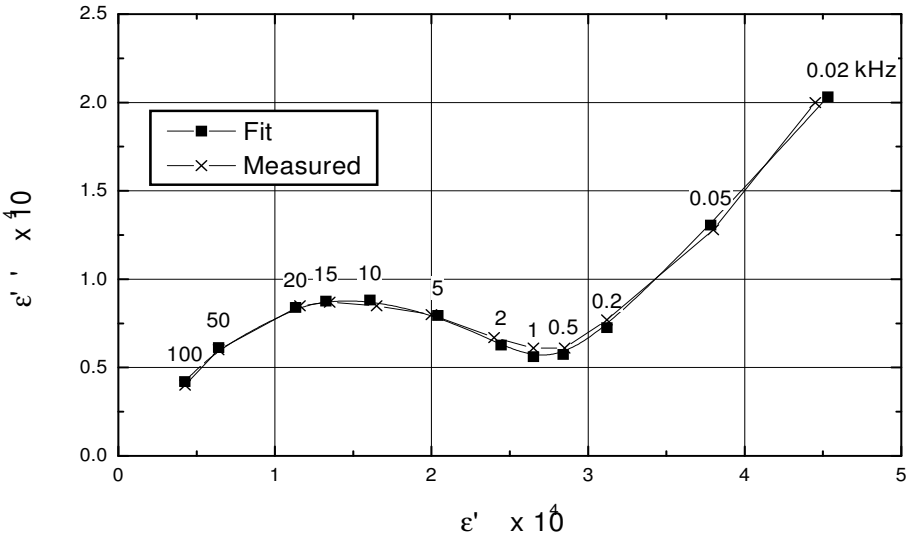

Figure 17. Nb-doped (1 at. %) Remeika ($BaTiO_3$) single crystal. Fit to Equation 5.13 with parameters: $\epsilon_s = 25.2 \times 10^3$, $\epsilon_\infty = 1.5 \times 10^3$, $\epsilon_c = 1.1 \times 10^3$, $q = 0.76$, $\beta = -0.5$, $\nu = 0.26$, $\tau = 12.06 \mu\,\mathrm{sec}$. Data point labels are in kHz. Solid lines drawn as aids to the eye. Note that the values of parameters vary from those in Figure 14.

as with equivalent circuit models in linear electronics, there may not be a limit to the possible CPE models. As is seen here, even parameters with equivalent meaning may not be the same among different models. Some of the difference between the relaxation exponents q in the two models may stem from the fact that the loss peak represents a rather broad and not necessarily symmetric distribution. The two models predict slightly different symmetries in the form of the dispersion peak.

Fitting six, or eight, parameters with only twenty four data points (twelve complex values) can be a questionable undertaking and there is as yet no compelling reason to choose one model over another at this point. Much more comparison with real data from many different materials will be required to allow judgement.

An Alternative View of the Models

There is some ambiguity in the interpretation of τ and the coefficients ϵ_k. It is possible to rescale any of the coefficients by $\tau_k^{-q_k}$ while incorporating the time constant in the $(i\omega\tau_k)^{q_k}$ term accordingly. This leads to an alternative view of the models derived above. Since the various processes all involve the same set of charge carriers, one may think of a single strength coefficient with the competition being among the rates of the various processes. Even in a hydrogen-bonded crystal such as KH_2PO_4 (KDP), where the mobile carriers are protons but the bound charge contributing to polarization is primarily the potassium ion, vacancies in the H-bonds must affect the ability of the associated K^+ ions to react to the field. Thus, the processes are not completely independent.

In the second model, or example, Equation 5.13 becomes

$$\epsilon^*(\omega) = \frac{\epsilon_s(1 + (i\omega\tau_\infty)^q + (i\omega\tau_\beta)^\beta + (i\omega\tau_\nu)^\nu)}{1 + (i\omega\tau_q)^q}. \tag{5.14}$$

In this view, the static coefficient, ϵ_s, represents the strength factor while τ_∞, τ_β, and τ_ν, along with their exponents, represent the time scales and distributions of the various processes.

The ambiguity raised here may be equivalent to the question of whether the electrostatic energy is contained in the field or the charge distribution.

Assumption Regarding Initial Conditions

A fractional differential equation deduced from the steady state *ac* response necessarily assumes that phase and amplitude measurements were made long after the polarization and electric field transients had become insignificant, that is the differential equation has no terms accounting for initial conditions. A time domain equation (e.g. Equation 5.9) can be used in this form if the polarization and field are zero for $t < 0$. The superposition property ensures that the fractional derivative of zero is always zero. In this case, composition rules become simpler and are straightforward to apply.

From an experimental perspective, this means that the samples need to have the electrode layers applied and the electrodes shorted together for a long time prior to initiating any measurements. Because the exponents are temperature sensitive, the material needs to held at the temperature of interest for some time, typically 30 minutes, before applying a field.

Disclaimer

The derived equations cover a wide range of behaviors, but there is no implied or intended claim that Equations 5.10 or 5.13 are complete descriptions of all possible

polarization responses. Rather, they represent initial suggestions for development of a more consistent model exhibiting the observed experimental response. In fact, any of the forms of Table 2 may be used as a starting point for a derivation such as has been done above.

CHAPTER 6

COMPUTATIONAL METHOD

The objective of this chapter will be to develop the capability to make time domain predictions based on dynamical models developed in Chapters 3 and 5 using the mathematics of Chapter 4.

There have been several references to the possibility that the fractional calculus should be used to describe polarization response in ferroelectrics, see e.g. [20, 39, 40]. These workers discuss steady state *ac* response. To demonstrate that the fractional calculus is applicable requires that it be used to predict the response to arbitrary external fields. In particular, it should predict the transient responses. A few analytical solutions of fraction differential equations exist, mostly in the form of Fox functions, but these are limited to steady state conditions or response to a given initial condition. As discussed in Chapter 4, these fail to fully account for the prior history of how the polarization came to be.

While the interest in the application of the fractional calculus to physical problems is growing, see e.g. [41, 42, 43, 44, 45], only one, by Podlubny [46], was found covering the mechanics of carrying out numerical integration of fractional difference equations. Podlubny's technique apparently suffers from poor convergence and slow operation. For this reason, a major effort was expended to develop methods applicable to the

problem outlined in the Chapters 2 and 5. While the methods presented here are restricted to order unity or less in the relaxation exponent q, this method applies to a large percentage of cases observed.

In attempting numerical integration of fractional differential equations, three major obstacles are encountered. First, the computation of derivatives requires $\mathcal{O}(N)$ calculations at the N^{th} step. As N gets large, the cumulative number of calculations grows as N^2. This requires the use of efficient computation schemes as outlined in the next section. The second major obstacle is that due to the non-Markovian nature of power-law relations, fractional differential equations cannot be reduced to a finite set of first order equations. It is the ability to deal with non-Markovian history dependence that makes fractional calculus potentially so useful. Third, power-law behavior inherently exhibits dynamics on all time scales. This forces the use of techniques similar to those used to numerically integrate "stiff" equations (see e.g. [47]). The fact that there will be dynamic activity on all time scales is what will end up costing us loss of information. We will necessarily have to jump over some short time dynamical effects.

Our program will be to predict the value of the polarization at equally spaced intervals of time, $\mathbf{P}(t = Ndt)$, from the previous $N-1$ values of $\mathbf{P}$ and the assumed known values of the applied electric field $\mathbf{E}$. We will then simulate measurement of the amplitude and phase of the predicted polarization response to a sinusoidal field over a range of frequencies to estimate the dielectric function $\epsilon^*(\omega)$. The response

to a short duration square wave pulse, or sequence of pulses, will be simulated as well to investigate the effect of past history on the polarization relaxation. The currents resulting from application and removal of a polarizing field will be investigated for clarification of the low-frequency dispersion and "universal dielectric response" discussed in Chapter 2.

Development of a Numerical Integration Scheme

Oldham and Spanier [27] presented a number of algorithms for approximating $\mathrm{d}^q/\mathrm{dt}^q$ for arbitrary q when the value of $f(t)$ is known at $N+1$ evenly spaced points in the range 0 to t of the independent variable. (Not all of the algorithms use exactly $N+1$ values of f. In fact, the $G1$-algorithm defined below uses only N points.) They adopted the nomenclature

$$\begin{aligned} f_N &\equiv f(0), \\ f_{N-1} &\equiv f\left(\frac{t}{N}\right), \\ &\vdots \\ f_j &\equiv f\left(t - \frac{jt}{N}\right), \\ &\vdots \\ f_0 &\equiv f(t). \end{aligned}$$

Note that an increasing value of the subscript refers to the value at a point *further in the past.*

Grünwald Algorithm

Probably the simplest algorithm is generated from the Grünwald definition of differintegration (Equation 4.6)

$$\frac{\mathrm{d^q}}{\mathrm{d(t-a)^q}} f(t) = \lim_{N\to\infty} \left\{ \frac{\left[\frac{t-a}{N}\right]^{-q}}{\Gamma(-q)} \sum_{j=0}^{N-1} \frac{\Gamma(j-q)}{\Gamma(j+1)} f\left(t - j\left[\frac{t-a}{N}\right]\right)\right\}, \tag{6.1}$$

by omitting the $N \to \infty$ operation. Setting $a = 0$,

$$\frac{\mathrm{d^q}}{\mathrm{d(t)^q}} f(t) \approx \left(\frac{\mathrm{d^q}}{\mathrm{d(t)^q}} f(t)\right)_{G1} = \frac{\left[\frac{t}{N}\right]^{-q}}{\Gamma(-q)} \sum_{j=0}^{N-1} \frac{\Gamma(j-q)}{\Gamma(j+1)} f\left(t - \frac{jt}{N}\right) \tag{6.2}$$

$$= \frac{t^{-q} N^q}{\Gamma(-q)} \sum_{j=0}^{N-1} \frac{\Gamma(j-q)}{\Gamma(j+1)} f_j. \tag{6.3}$$

This is the approximation formula termed the "$G1$-algorithm." Because of the recursion

$$\frac{\Gamma(j-q)}{\Gamma(j+1)} = \frac{j-1-q}{j} \frac{\Gamma(j-1-q)}{\Gamma(j)}, \tag{6.4}$$

the $G1$-algorithm may be implemented by the convenient multiplication-addition-multiplication $\cdots$ multiplication-addition scheme,

$$\left(\frac{\mathrm{d}^q f}{\mathrm{dt}^q}\right)_{G1} = \frac{N^q}{t^q}\left[\left[\left[\cdots\left[\left[f_{N-1}\left\{\frac{N-q-2}{N-1}\right\} + f_{N-2}\right]\left\{\frac{N-q-3}{N-2}\right\} + f_{N-3}\right]\cdots\right]\left\{\frac{1-q}{2}\right\} + f_1\right]\left\{\frac{-q}{1}\right\} + f_0\right], \tag{6.5}$$

which avoids the explicit use of gamma functions and which lends itself to ease of programming. Other algorithms with improved convergence have been developed but suffer from increased complexity due to the need to interpolate between known points.

In applying Equation 6.5 to a numerical integration scheme, we note that N increases by one each time step. Using equal size time steps of length dt, $t = N\,dt$

permits the replacement $dt = t/N$. In what follows, we will normally require $f[0] = 0$ in order to avoid the difficulties imposed by operator composition rules. This requirement is also imposed by the physical interpretation of the fractional differintegral as a memory function.

Translating the Grünwald indexing scheme into that used in a programming language such as C/C++, $f_j \rightarrow f[n]$, where $n = N - j$, and using the modern notation for the differintegral,

$$\begin{aligned}({}_0D_t^q f)_{G1} &= dt^{-q}\Bigg[\Bigg[\Bigg[\cdots\Bigg[\Bigg[f[1]\left\{\frac{N-q-2}{N-1}\right\}+f[2]\Bigg]\left\{\frac{N-q-3}{N-2}\right\} \\ &\quad + f[3]\Bigg]\cdots\Bigg]\left\{\frac{1-q}{2}\right\}+f[N-1]\Bigg]\left\{\frac{-q}{1}\right\}+f[N]\Bigg]. \end{aligned} \tag{6.6}$$

Coding of the fractional derivative is deceptively simple:

```
double FracDeriv(double f[ ], int N, double q, double dt)
{
      double Numerator = N-q-1;
      double Denominator = N;
      double PartialSum = f[1];
      for(int i=1; i<(N-1); i++) PartialSum = f[i+1]
            + PartialSum*(Numerator-i)/(Denominator-i);
      return pow(dt, (-q)) * PartialSum;
}
```

It is worth repeating that Equation 6.6 is, in general, not the derivative evaluated at the point t. It is the derivative evaluated over the interval $(0, t)$. This distinction is the primary impetus for the modern notation which explicitly includes the interval. For a fractional differential equation to make physical sense, all the derivative terms in the equation need to be evaluated over the same interval.

It will be convenient to define another operator over the interval $(0,t)$

$$\begin{aligned}({}_0S_t^q f)_{G1} &= dt^{-q}\Bigg[\Bigg[\Bigg[\cdots\Bigg[\Bigg[f[1]\left\{\frac{N-q-2}{N-1}\right\}+f[2]\Bigg]\left\{\frac{N-q-3}{N-2}\right\}\\ &\quad +f[3]\Bigg]\cdots\Bigg]\left\{\frac{1-q}{2}\right\}+f[N-1]\Bigg]\left\{\frac{-q}{1}\right\}\Bigg],\end{aligned} \tag{6.7}$$

which just leaves out adding $f[N]$ at the last step. Then

$$({}_0D_t^q f)_{G1} = f[N]\,dt^{-q} + ({}_0S_t^q f)_{G1}\,. \tag{6.8}$$

From here on, the subscript $G1$ will be dropped. The use of the index notation of brackets, e.g. $f[n]$, versus function notation of parentheses, e.g. $f(t)$, will distinguish between the function value at discrete points and the function evaluated at arbitrary time t. The function name alone, e.g. f, will refer to the entire history of the function over the interval $(0,t)$, or to the complete set of values of the array $\{f[0],\ldots,f[N]\}$, depending on context.

Direct Integration

Starting with Equation 5.9,

$$\mathbf{P}(t) + \tau^q\,{}_0D_t^q\mathbf{P} = \left(\epsilon_s\tau^\delta\,{}_0D_t^\delta + \epsilon_\infty\tau^\mu\,{}_0D_t^\mu + \epsilon_c\tau^\beta\,{}_0D_t^\beta\right)\mathbf{E}, \tag{6.9}$$

and following the approach outlined in the discussion of fractional relaxation in Chapter 4,

$$\tau^q\,{}_0D_t^q\mathbf{P} = -\mathbf{P}(t) + \left(\epsilon_s\tau^\delta\,{}_0D_t^\delta + \epsilon_\infty\tau^\mu\,{}_0D_t^\mu + \epsilon_c\tau^\beta\,{}_0D_t^\beta\right)\mathbf{E}. \tag{6.10}$$

Applying the operator $\tau^{-q}\,{}_0D_t^{-q}$ to both sides

$$\begin{aligned}\mathbf{P}(t)-\mathbf{P}(0) &= -\tau^{-q}\,{}_0D_t^{-q}\mathbf{P} \\ &\quad +\left(\epsilon_s\tau^{\delta-q}\,{}_0D_t^{\delta-q}+\epsilon_\infty\tau^{\mu-q}\,{}_0D_t^{\mu-q}+\epsilon_c\tau^{\beta-q}\,{}_0D_t^{\beta-q}\right)\mathbf{E}. \quad (6.11)\end{aligned}$$

Using Equation 6.8 to isolate $\mathbf{P}[N]$ in terms of the previous $N-1$ values of $\mathbf{P}$,

$$\begin{aligned}\mathbf{P}[N] &= \mathbf{P}[\mathbf{0}]-\left(\frac{dt}{\tau}\right)^q\mathbf{P}[N]-\tau^{-q}\,{}_0S_t^{-q}\mathbf{P} \\ &\quad +\left(\epsilon_s\tau^{\delta-q}\,{}_0D_t^{\delta-q}+\epsilon_\infty\tau^{\mu-q}\,{}_0D_t^{\mu-q}+\epsilon_c\tau^{\beta-q}\,{}_0D_t^{\beta-q}\right)\mathbf{E}, \quad (6.12)\end{aligned}$$

or

$$\begin{aligned}\mathbf{P}[N] &= \left(1+\left(\frac{dt}{\tau}\right)^q\right)^{-1}\Bigg\{\mathbf{P}[\mathbf{0}]-\tau^{-q}\,{}_0S_t^{-q}\mathbf{P} \\ &+ \left(\epsilon_s\tau^{\delta-q}\,{}_0D_t^{\delta-q}+\epsilon_\infty\tau^{\mu-q}\,{}_0D_t^{\mu-q}+\epsilon_c\tau^{\beta-q}\,{}_0D_t^{\beta-q}\right)\mathbf{E}\Bigg\}. \quad (6.13)\end{aligned}$$

Inclusion of the initial condition $\mathbf{P}[0]$ is required for comparison with Equation 4.16 and is used for testing purposes only. In fact, for the initial condition case, i.e. $\mathbf{P}[0]\neq 0$ and $\mathbf{E}\equiv 0$, the numerical method of Equation 6.13 produces a much more stable result over a longer simulated time. Equation 4.16 exhibits serious numerical stability problems for $t\gtrsim 30\tau$, and requires stitching together asymptotic solutions. The stability of the integration scheme up to $10^{10}\tau$ has been demonstrated.

The method is inherently stable as it uses a generalized Euler method of numerical integration at each step, i.e. it is an end-point method. The alternative algorithms alluded to above represent other generalized integration methods, analogous to the mid-point and trapezoid rules of traditional numerical methods. The algorithm potentially suffers from loss of accuracy for the same reasons as the Euler method, but

the results of testing shows that it retains high accuracy even with time steps several orders of magnitude greater than the time constant τ. Until it is possible to compare the results of the simpler algorithm to measured results, the extra development expense does not seem justified.

Example *ac* Reconstruction

Figure 18 shows a typical simulation run using the parameters of Figure 14, the Nb-doped $BaTiO_3$ single crystal, with a 10 kHz sinusoidal driving field turned on at $t = 0$. Note the bias induced at early times. The simulation package allows measurements of ϵ' and ϵ'' to be estimated after a selected decay time. The phase shift over time affects the ratio of ϵ' to ϵ'' as shown in Table 3.

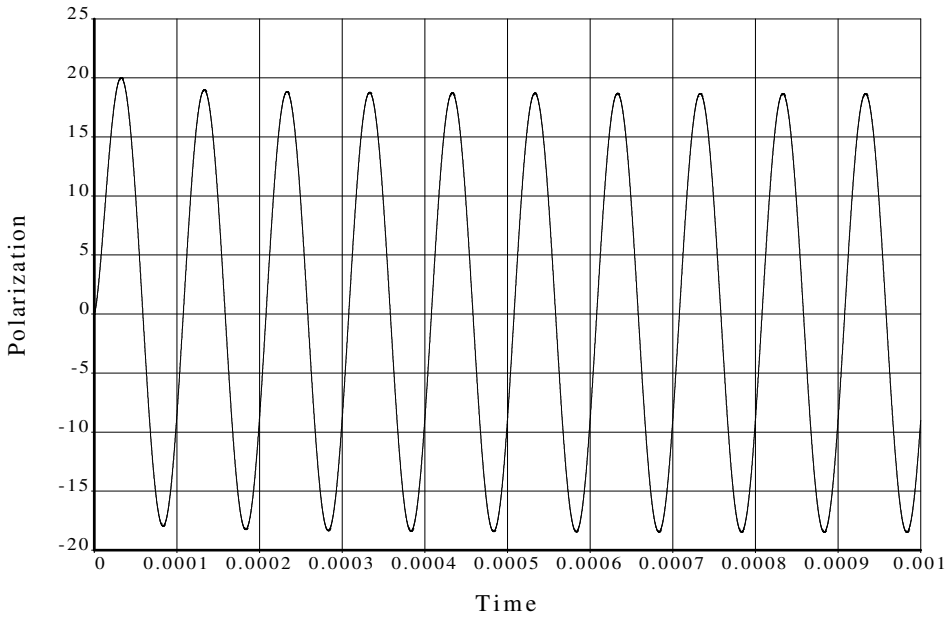

Figure 18. A time domain simulation reconstructing the response to a 10.0 kHz field using the parameters of Figure 14.

Table 3. Simulated measurements of complex permittivity at 10 kHz for varying delay times.

Delay Time	ϵ'	ϵ''
0.0	17.25	7.96
0.0001	16.26	9.09
0.0003	16.20	9.10
0.0005	16.19	9.10
0.0009	16.19	9.10

Measurements of ϵ' and ϵ'' were simulated at the same set of frequencies used in Figure 14 and the results are shown in Figure 19. From Table 3, the permittivity measurements stabilized after about 50 to 60 τ, so delay times of 60 τ or greater were used. At this point, we have shown that the numerical integration of the time domain equation does indeed reproduce the frequency domain picture of Equation 5.10 as required by the Laplace transform. We have not yet shown that the equation truly represents the transient dynamics of the dielectric response.

Spectrum of Response and Noise Masking

The power-law decay of transients results in a low frequency anomaly in the predicted power spectrum, as shown in Figure 20. This low frequency anomaly is not produced by noise but will add to any 1/f-like noise in the total system.

The effect of even very small amounts of noise in the applied signal is dramatic. Figure 21 shows the resulting spectrum with 0.1% rms white noise applied to the electric field. The time domain display showed no difference from Figure 18. In this case the low frequency anomaly is almost completely masked. Given the stability and

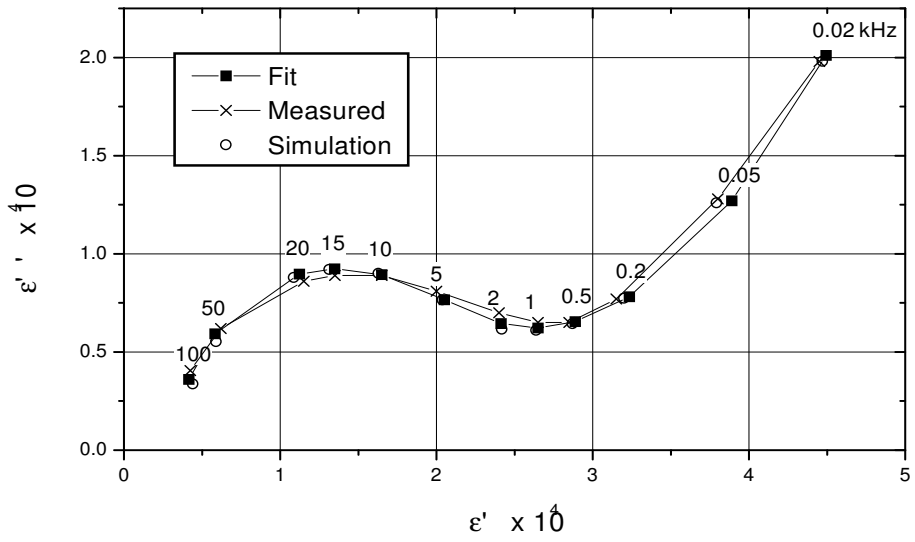

Figure 19. Figure 14 with ϵ^* values computed from simulation by numerical integration of Equation 6.13.

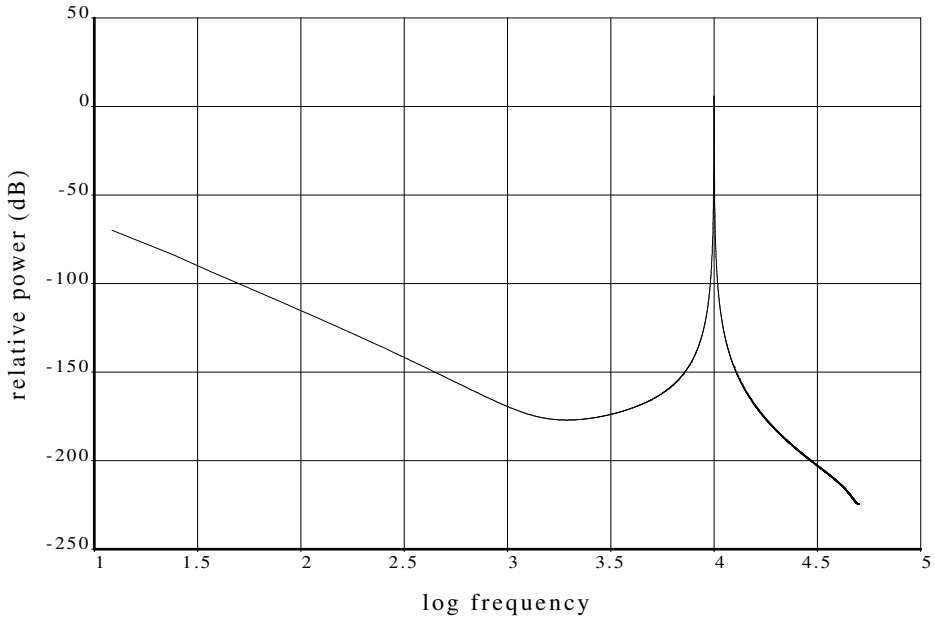

Figure 20. The computed power spectrum of Figure 18 with no noise.

accuracy of function generators and measurement devices, it is unlikely that a physical experiment will reveal the true nature of the low frequency spectrum anomaly. This is quite disappointing as the spectral response would provide very convincing evidence of power-law transient behavior.

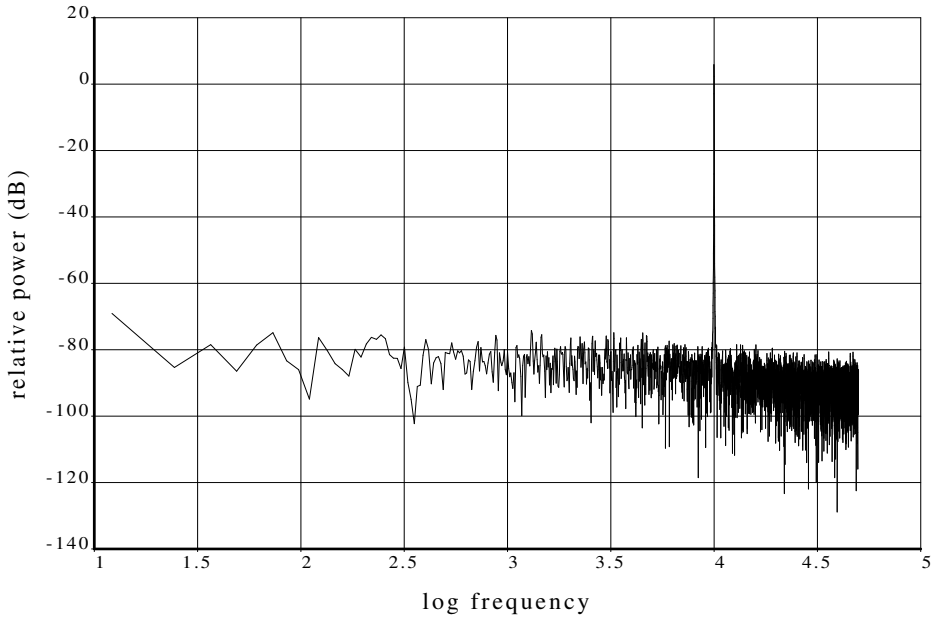

Figure 21. The computed power spectrum of Figure 18 with 0.1% rms noise applied to the electric field.

Example Pulsed *dc* Reconstruction

In order to look at the long term history effect, it is necessary to use a system with minimal low frequency conductivity. For the purposes of this section, we will start with a toy problem simulating a "classical" Cole-Cole permittivity function

$$\epsilon^* = \frac{\epsilon_s + \epsilon_\infty (i\omega\tau)^q}{1 + (i\omega\tau)^q}, \tag{6.14}$$

with $q = 0.9$, $\tau = 0.1$, $\epsilon_s = 10$, and $\epsilon_\infty = 1.0$. The external field was turned on at $t = 0$ and turned off after a specified time. The simulation recorded the polarization response. The decay response after pulses of 40, 120 and 600 τ are compared in Figure 22.

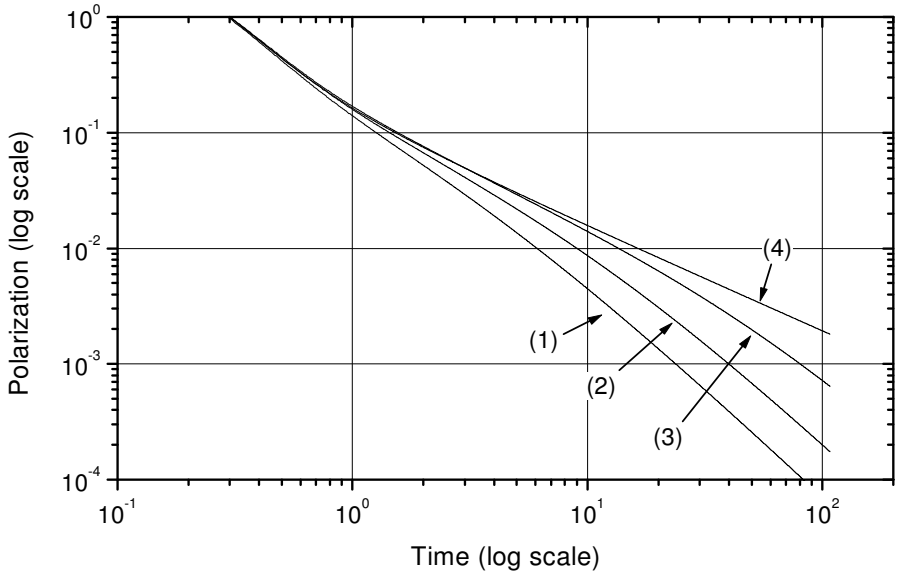

Figure 22. Polarization decay curves resulting from pulses of varying duration. The toy system has a time constant $\tau = 0.1sec$. Curve (1) is decay after pulse of 40 τ, curve (2) after pulse of 120 τ, curve (3) after pulse of 600 τ. Curve (4) is the fractional relaxation curve predicted by Equation 4.16.

The history dependence is quite apparent. Note that as the duration of the application of the polarizing field gets longer, the decay curve follows the theoretical initial condition curve for a longer time. This suggests that the meaning of the "initial conditions" is not that a measurement was made at $t = 0$, but that the system was held in an equilibrium state of polarization for an "infinite" time. The constraint of knowledge of all past history remains.

No physical condensed matter system can remain in an equilibrium state of polarization under an applied field for an arbitrary length of time. There is always some degree of conductivity in dielectrics. The same can be said of mechanical systems under strain; there is always some degree of creep. This almost certainly voids the use of initial conditions in these calculations except as an ideal approximation.

For a second toy system, we will include the "universal dielectric response" as suggested by the observation of the residual current a long time after application of a field. For this system, the permittivity function includes a low frequency dispersion as given in Equation 2.13.

$$\epsilon^* = \frac{\epsilon_s(i\omega\tau)^\delta + \epsilon_\infty(i\omega\tau)^q}{1 + (i\omega\tau)^q}. \tag{6.15}$$

From the literature the relaxation current in the presence of an applied field is best fit with a functional form $i_d(t) \sim t^{-n}$. A value of $n \approx 0.9$, with $\delta = n - 1 = -0.1$, appears to be typical. For this simulation, the external polarizing field was turned on for 200 seconds (2000 τ) and then turned off. The polarization history is shown in Figure 23. Note that the net polarization does not return to zero at the same rate as it responded to the onset of the field. The magnitude of current during the field-on condition is compared with the current in the field-off condition in Figure 24. The long term behavior of the current under the applied field follows a -0.9 slope on the log-log plot, while the relaxation current after removal of the field decays much more rapidly than t^{-1}.

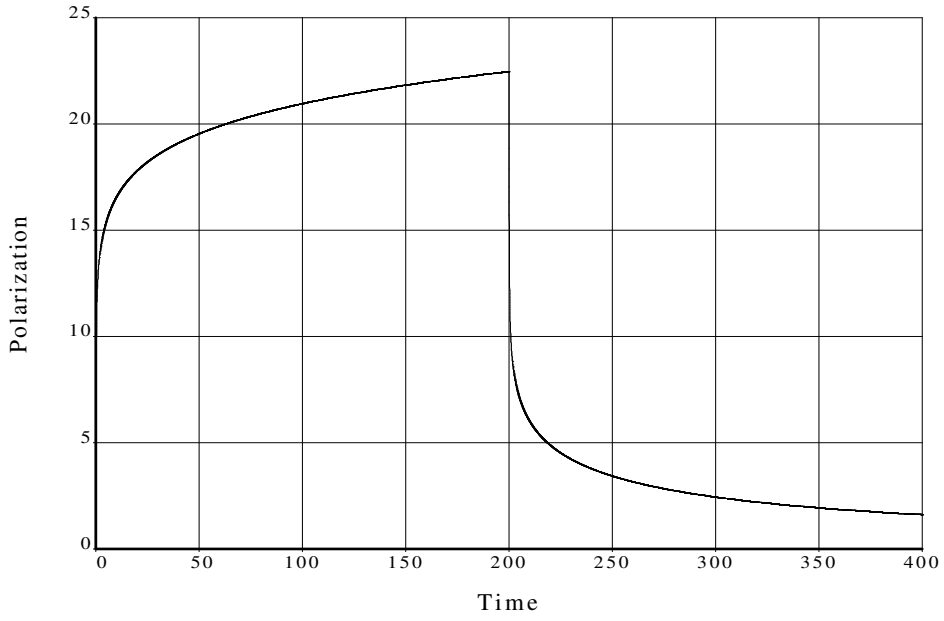

Figure 23. A time domain simulation reconstructing the response of the second toy system to a pulse 200 seconds (2000 τ) in duration. The exponent $\delta = -0.1$ for this case.

This is a major result in this research. The fractional calculus predicts that the polarization and current responses depend on the electrical field history as well as the polarization history. As mentioned in the introduction to this chapter, the analytical solutions may have limited physical applicability. The predicted response due to an external field of finite duration, is neither pure power-law nor fractional power ("stretched") exponential over all time. The simulation exhibits the different asymptotic behaviors of the charging and discharging current as predicted by Jonscher, outlined in Chapter 2, while filling in the details of the cross-over. This will addressed further in the experimental work described in Chapter 7 where we will predicting the transient currents using the parameters obtained in *ac* fitting.

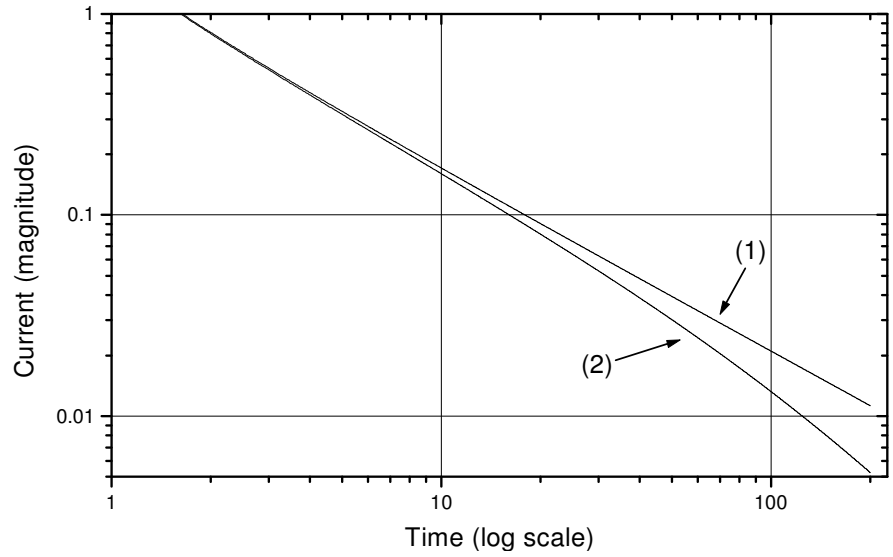

Figure 24. Comparison of relaxation currents in the second toy system; (1) during application of an external field and (2) after it is removed.

Stepwise Integration

The direct integration mode introduced above requires that all of the prior history be included at every step, resulting in a growth in the computation load of $\mathcal{O}(N^2)$ as N gets large. A second method for integrating fractional differential equations was produced in order to investigate the possibility of whether the memory could be truncated after some time, say M steps or a fixed length of time, thus allowing simulation over extended times while keeping the computational load constant.

In the program for stiff sets of equations outlined in section 16.6 of Reference [47], we try to rewrite the problem in the form

$$\mathbf{y}' = \mathbf{f}(\mathbf{y}) \tag{6.16}$$

and apply implicit differencing to get

$$\mathbf{y}_{n+1} = \mathbf{y}_n + h\mathbf{f}(\mathbf{y}_{n+1}), \tag{6.17}$$

where h is the time step. Implicit differencing is required here to achieve absolute stability when h is larger than the fastest underlying relaxation time of the dynamical system.

Upon linearizing the equations, we get

$$\mathbf{y}_{n+1} = \mathbf{y}_n + h\left[\mathbf{f}(\mathbf{y}_n) + \left.\frac{\partial \mathbf{f}}{\partial \mathbf{y}}\right|_{\mathbf{y}_n} \cdot (\mathbf{y}_{n+1} - \mathbf{y}_n)\right] \tag{6.18}$$

where $\partial\mathbf{f}/\partial\mathbf{y}$ is the Jacobian matrix of the right hand side. Rearranging, we get

$$\mathbf{y}_{n+1} = \mathbf{y}_n + h\left[\mathbf{1} - h\left.\frac{\partial \mathbf{f}}{\partial \mathbf{y}}\right|_{\mathbf{y}_n}\right]^{-1} \cdot \mathbf{f}(\mathbf{y}_n). \tag{6.19}$$

Following operator manipulation similar to the previous sections, we find the normal first derivative of $\mathbf{P}$

$$\begin{aligned} \frac{d\mathbf{P}}{dt} &= -\tau^{-q}\,{}_0D_t^{1-q}\mathbf{P} \\ &\quad + \underbrace{\left(\epsilon_\infty \tau^{\mu-q}\,{}_0D_t^{1-q+\mu} + \epsilon_s \tau^{\delta-q}\,{}_0D_t^{1-q+\delta} + \epsilon_c \tau^{\beta-q}\,{}_0D_t^{1-q+\beta}\right)\mathbf{E}}_{RHS(t)}, \end{aligned} \tag{6.20}$$

where $RHS(t)$ refers to the time series resulting from all of the operations on $\mathbf{E}$. In this context $RHS(t)$ appears as a forcing function. For this method, just as with the direct integration method, the initial conditions for the field are explicitly assumed to be zero. We will again carry along an initial value of $\mathbf{P}$ for comparison with analytic results, but it will not have any physical meaning. Because the forcing function

depends explicitly on time, the method requires that the time variable be evolved alongside the polarization, that is

$$\mathbf{y} = \left\{ \begin{array}{c} \mathbf{P} \\ t \end{array} \right\} \tag{6.21}$$

in the formulae outlined above.

Applying the implicit differencing method described above, we are faced with interpreting an operation of the form

$$\mathbf{J}_{11} = \frac{\partial}{\partial \mathbf{P}} \left(\frac{d\mathbf{P}}{dt} \right) \Bigg|_{\mathbf{P}[N]} \tag{6.22}$$

in the calculation of the Jacobian matrix. We will take this as the variation in the term $-\tau^{-q}\, {}_0D^{1-q}_{t[N]}\mathbf{P}$ resulting from varying $\mathbf{P}[N]$ in the $G1$ algorithm. This results in

$$\mathbf{J}_{11} = -\tau^{-q} \left(\frac{1}{dt} \right)^{1-q}. \tag{6.23}$$

The rest of the process is straightforward and, completing the algebra, we get

$$\begin{aligned} \mathbf{P}[N+1] \;=\; & \frac{dt}{\left(1 + \left(\frac{\tau}{dt}\right)^{-q}\right)} \Bigg[\mathbf{P}[N] - \left(\frac{\tau}{dt}\right)^{-q} {}_0D^{1-q}_{t[N]}\mathbf{P} \\ & + RHS[N] + \frac{dt}{2} \left\{ RHS[N+1] - RHS[N-1] \right\} \Bigg]. \end{aligned} \tag{6.24}$$

This form is inherently stable but suffers from accuracy decay as the step size grows. There is no immediate advantage in using this form over the direct integration approach since the computational loads are equivalent if all of the prior history is taken into account according to the theory of fractional calculus.

Limiting the computational load becomes crucial in applying the fractional calculus to practical control systems. The simplest method for achieving this is to truncate

the memory after some amount of time. [48] This revises the fractional differintegral operator according to

$$ {}_0D_t^q \rightarrow {}_{t-L}D_t^q, \tag{6.25} $$

where L represents the duration of the effective memory. In this case, memory older than L falls off exponentially. The result is a non-physical kink in the decay curve. An interesting effect of this "forgetting" process is that echoes can be produced. For the toy problem, $L = 30$ seconds was simulated for an applied pulse of ~ 5.5 seconds. The response curve is shown in Figure 25 with the time around $t = 30$ seconds expanded in Figure 26.

Macdonald [4] provides a description of a CPE in terms of a distributed element transmission line. It appears that truncation of the memory is analogous to the truncation of a transmission line. Improperly terminated, open or shorted, the line produces echoes. What is needed is a more appropriate termination of the memory function than just truncation. The issue of termination of the memory effect will be discussed in more detail in Chapter 8.

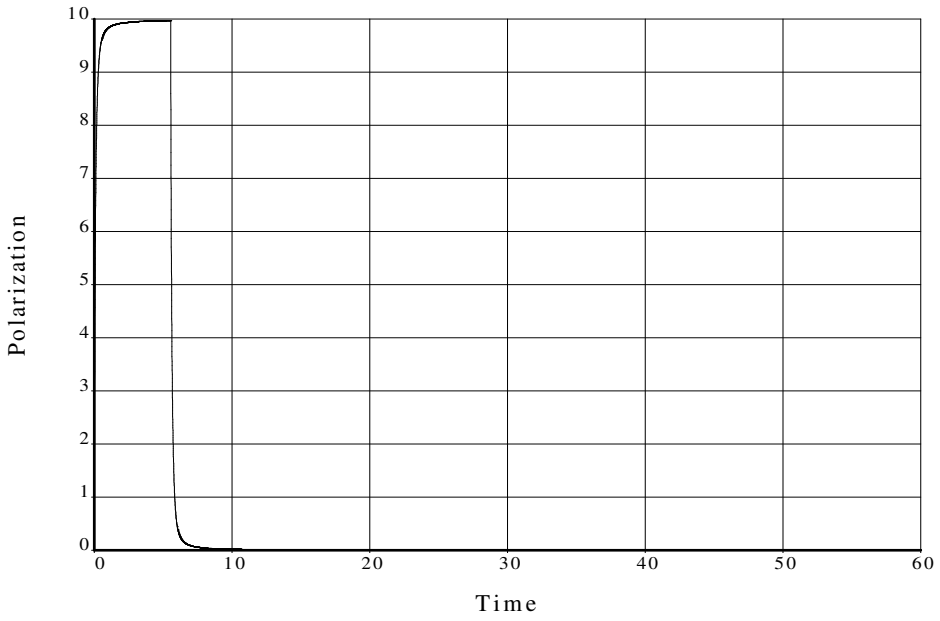

Figure 25. A time domain simulation reconstructing the response of the first toy system to a pulse of ~ 5.5 sec. Memory retention limited to 30 seconds.

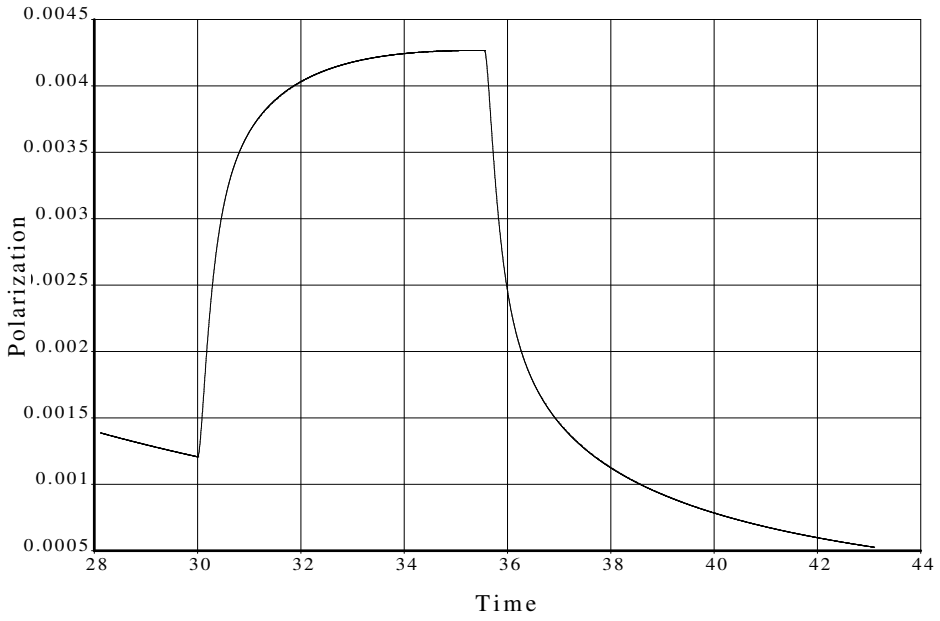

Figure 26. An enlargement of the response around the $t = 30$ second time-frame from Figure 25 above showing the pulse echo resulting from truncating the memory. Duration of memory is 30 seconds in this simulation.

CHAPTER 7

EXPERIMENTAL METHODS AND RESULTS

No attempt will be made to reproduce the wealth of measurements published by Jonscher, Ngai, Westerlund and many others who have probed the power-law behavior of dielectric materials. What is not covered in the literature is a discussion of both the frequency and time response of a given material over relevant frequencies and time scales. The primary objective of the measurements performed as part of this work is to demonstrate whether a complete steady state *ac* and transient *dc* response can be fit with a composite model based on the fractional calculus as stated in the hypothesis.

Since the hypothesis states that the behaviors are universal, any dielectric crystal or polymer will suffice for this purpose. Given the supporting laboratory's interest in piezoelectric materials, the polymer PVDF will be investigated. As noted in Chapter 1, we would like to find an accurate relation between charge and voltage across the material to allow more efficient use of the material as an actuator.

Material Studied

The material being studied was 28 μm thick poly(vinylidine fluoride) (PVDF) film with a silver electrode layer. Square samples with electroded areas of 1 cm, 4.7

cm, and 9.6 cm on a side were available from stocks obtained for a vibration isolation project. The rated relative permittivity is 12 at 10 kHz, according to Measurement Specialties, Inc. (formerly known as AMP, Inc.). [49]

PVDF is notoriously ill characterized. In the preparation of Reference [15], we found that parameters such as the Young's modulus along any given direction could vary by a factor of three in published data. As a result, we had to measure every significant parameter directly for each batch of material delivered. There were significant differences between batches, but there was a high degree of consistency within a given batch.

The PVDF samples had been poled during manufacturing to produce a piezoelectric property. This may be responsible for the thermally enhanced resonance which typically shows up in the permittivity above 10 kHz.

Equipment

A Wayne-Kerr 6425 impedance meter was used for the *ac* measurements. A Lakeshore temperature controller was used to maintain temperature to within ± 0.1 K. For measurements of transient response at room temperature, a Faraday cage was devised to hold samples too large to fit in the cryogenic sample holder. A Keithley 642 electrometer was used for transient current measurements. The larger samples were required to achieve the current level necessary for detection by the electrometer in transient response testing.

Sample Holder for Varying Temperature

The sample holder and cryogenic chamber used for *ac* measurements between 20 Hz and 300 kHz are shown in Figure 27. A silicon diode thermistor was attached near the sample to obtain accurate measurement of the sample actual sample temperature. A thermocouple attached to the outer wall of the sample chamber provided for temperature control. Due to the nature of the control algorithm in the Lakeshore, there was a difference between the set temperature and the sample temperature. This difference could be held constant, however, and the sample temperature could be held to within the desired $\pm$ 0.1 K for the duration of the measurements. A funnel and feed tube routed liquid nitrogen past the sample holder so that refilling the liquid nitrogen can be done during a measurement run without affecting the temperature of the sample.

The sample holder also allowed operation above room temperature up to approximately 400 K. This was due to the use of Nylon as the primary material in the dewar and the extended range of the temperature sensors.

Faraday Cage for Low Frequency Measurements

For low frequency and long time measurements, a Faraday cage arrangement was devised to hold various sizes of PVDF film. Care was taken to ensure that the material was maintained in the zero external stress condition to avoid confusion with piezoelectric induced fields.

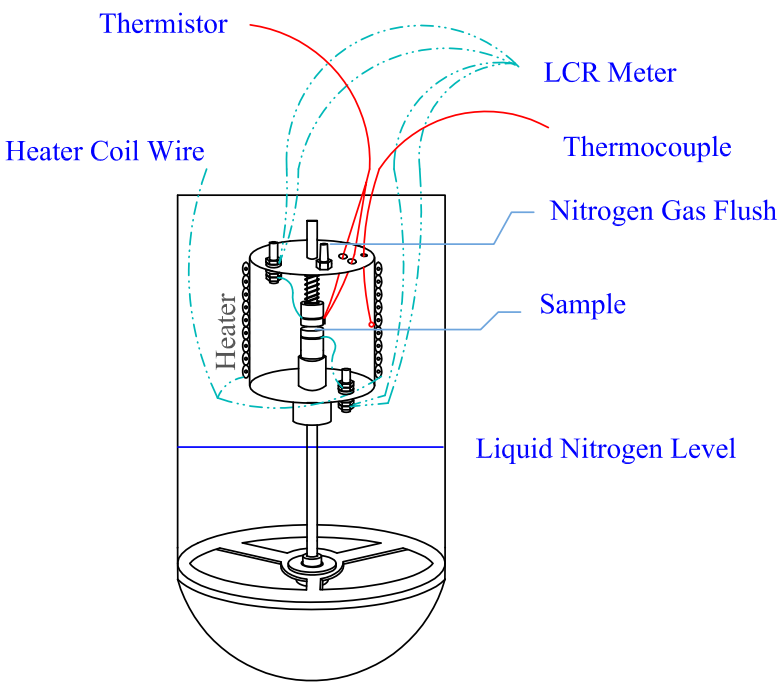

Figure 27. The sample holder and LN2 cryogenic chamber.

ac Measurements

A schematic of the *ac* measurement apparatus is shown in Figure 28. The Wayne-Kerr Impedance Meter operates over the range of 20 Hz to 300 kHz. In these measurements, the magnitude of the impedance, |Z|, and the phase angle, $\angle^{\circ}$, were measured. These measured values were then converted to permittivity using Table 1.

Transient Response Measurement

A schematic of the transient response measurement setup is shown in Figure 29. The bypass switch, Switch 2, is required to protect the electrometer from the initial current pulse occurring immediately after the change in the position of Switch 1. Although this arrangement can be implemented with electronic switching units, the

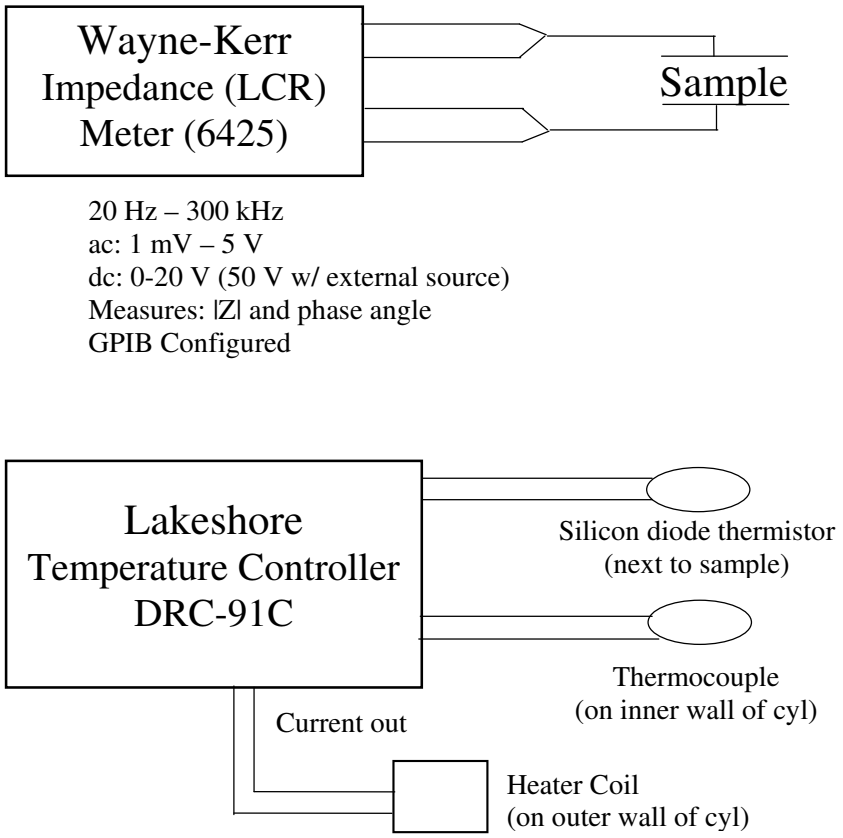

Figure 28. A schematic of the experimental setup for measuring *ac* permittivity.

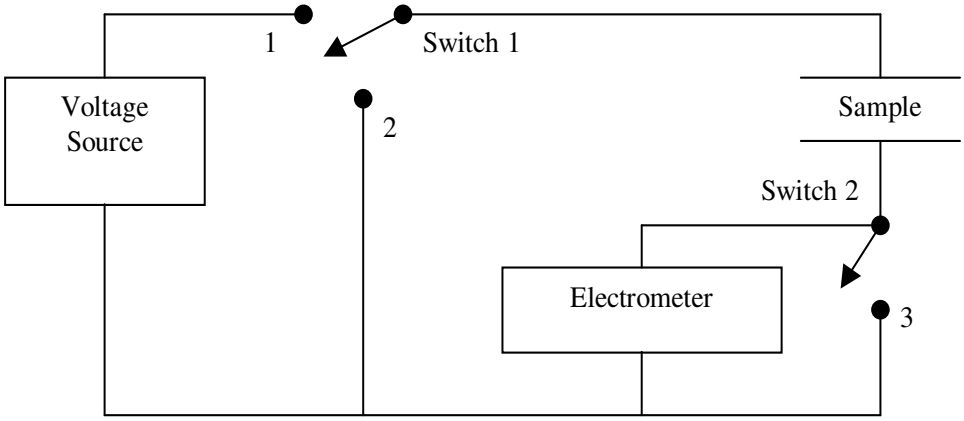

Figure 29. A schematic of the experimental setup for measuring transient response.

time scales of the problem of interest are slow enough that switching by hand using a stop watch are quite adequate.

Because of the fluctuating currents due to noise in the high voltage supply (the HV supply "ripple"), the charging current was estimated using the technique described by Jonscher [8]. In this procedure, the voltage is applied for ten times longer than the desired measurement of relaxation current. Then the voltage is switched off and the current measured. This discharging current is very nearly equal to the negative of the charging current within the time frame of about one-tenth the on-time of the applied voltage. To within the noise limit of the currents measured with the voltage on, this technique appeared to be valid.

During initial trials of measuring charging and discharging currents, it was evident that the noise level registered by the electrometer was far greater than that which could be attributed to the electrometer or the Faraday cage setup. The noise was isolated to the piezoelectric response of the piezo film moving in response to the air currents in the room and vibrations of the experiment table. The Faraday cage was placed on several layers of cloth and foam for isolation from the table and then wrapped in several layers of cloth towels to eliminate air currents across the sample. This reduced the current noise to approximately $\pm 2 \times 10^{-11}$ amps. This restricted the range of data collected for the discharge currents but the differences between the charging and discharging cycles should be evident.

Data Analysis

Temperature dependence measurements of the permittivity of the 1 cm square sample (sample #1) are shown in Figures 30 through 33. The sequence started at room temperature with the sample electrodes shorted for 12 hours prior to beginning the measurements. The Wayne-Kerr LCR meter was set to slow measurement mode and the impedance readout delayed for at least one minute after changing frequencies. Temperatures were changed slowly and the data collection commenced only after one hour after the temperature had settled to $\pm$ 0.1 K drift. After the measurements at 325 K, the sample was allowed to cool to 305 K for the fourth set of measurements, Figure 33. This was done to confirm that the resonance was, in fact, thermally enhanced and reversible. Since the depolarizing transition for PVDF is above 375 K, the material piezoelectric properties were not compromised.

The slight "glitch" around 50 kHz at 295 K, Figure 30, is seen to grow into a resonance loop at 315 K, which expands at 325 K. Upon return to 305 K, the resonance loop is almost completely gone. Since our interest is mainly below 1 kHz and room temperature for the example problem outlined at the beginning of Chapter 2, this resonance has little effect and will be ignored in what follows. The resonance problem was addressed in terms of the fractional calculus in Reference [40].

The permittivity of the 4.7 cm square sample (sample #2) was obtained using the Faraday cage. Figure 34 displays the results. Since this sample was obtained from

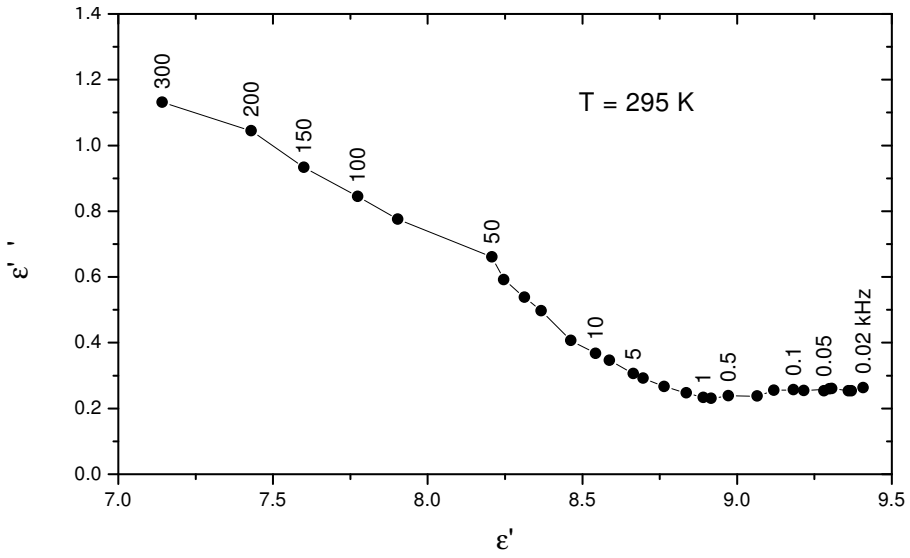

Figure 30. Cole-Cole plot for PVDF sample #1 at 295 K. Note the slight offset of the data point at 50 kHz.

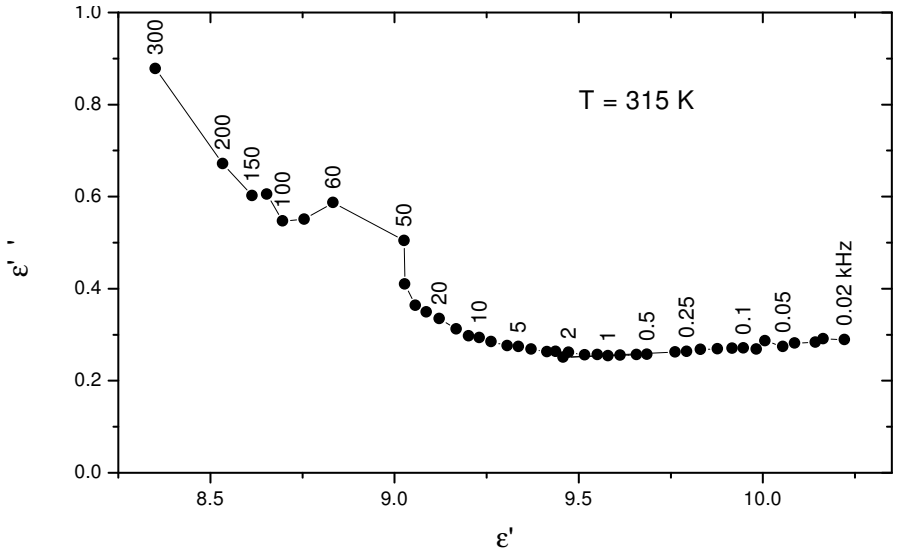

Figure 31. Cole-Cole plot for PVDF sample #1 at 315 K. The resonance loop at 50 - 60 kHz is well developed.

a different batch than sample #1, it is not surprising that there are differences in the relative permittivity, i.e. the plot appears shifted along the real axis. Also note

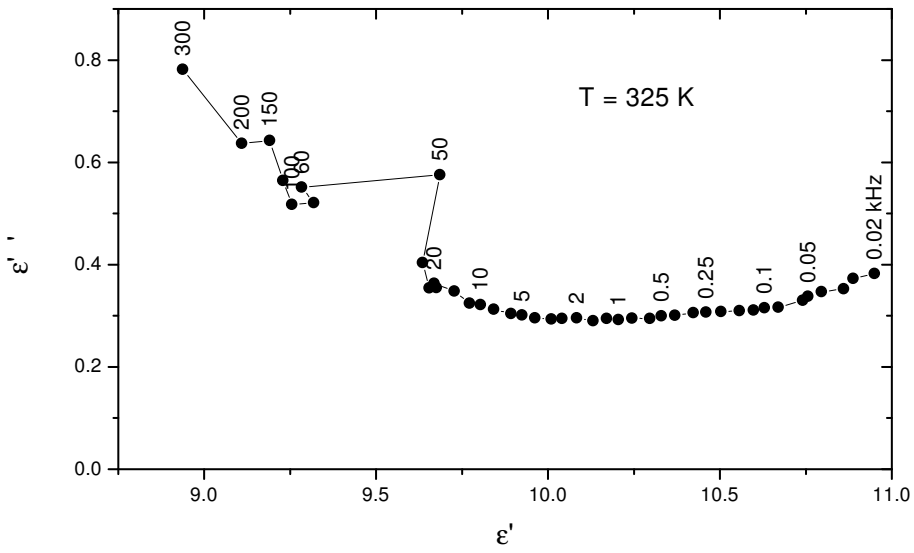

Figure 32. Cole-Cole plot for PVDF sample#1 at 325 K. The resonance loop is even more developed.

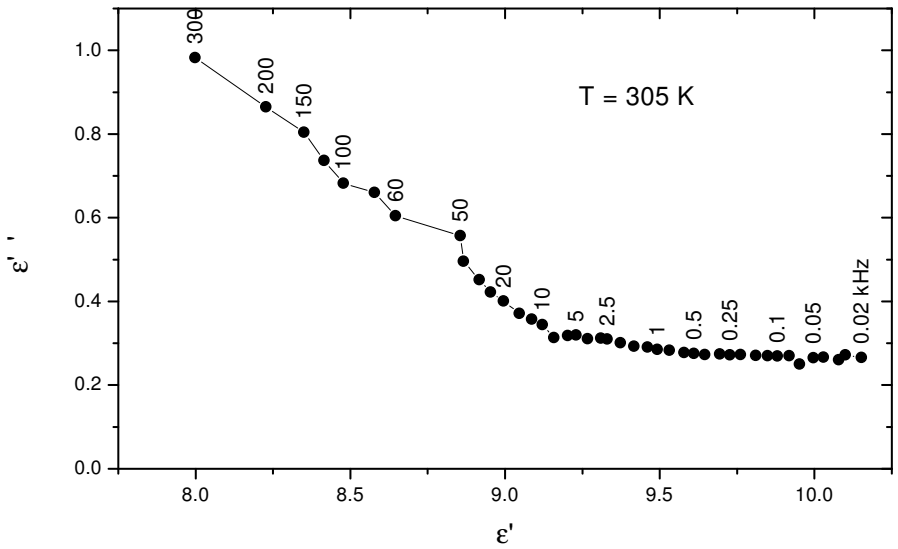

Figure 33. Cole-Cole plot for PVDF at 305 K. After cooling from 325 K, the resonance loop has been suppressed.

that the "glitch" point is now at 20 kHz, indicating that the resonance is probably offset somewhat from that of sample #1. This resonance is still high enough and

suppressed enough to be ignored of our purposes. In curve fitting, we will give much less weight to the 20 kHz data point.

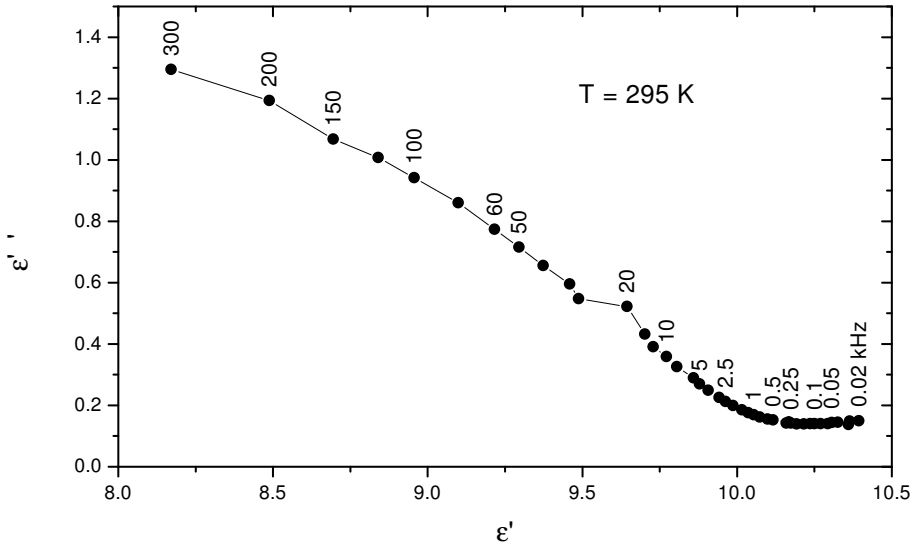

Figure 34. Cole-Cole plot for PVDF sample #2 (4.7 cm ×4.7 cm) at room temperature.

The data of Figure 34 were fit to the second model of Chapter 5, Equation 5.13. Equation 5.13 was chosen due to the simpler task of fitting six, rather than eight, parameters. The time constant is $\tau = 173$ ns, the exponents $q = 0.603$ and $\nu = 0.524$ and the coefficients $\epsilon_\infty = 3.75, \epsilon_s = 9.32, \epsilon_c = 0.465$. The underlying exponents of the model are $\alpha = 0.397$ and $\gamma = 0.921$. The results of the fit are shown in Figure 35. The model predictions extrapolated to much lower frequencies are shown as well. The available impedance measuring equipment does not have the sensitivity to make these measurements. However, the effects of the very low frequency end will show up in the time domain simulation predicting the charging and discharging currents.

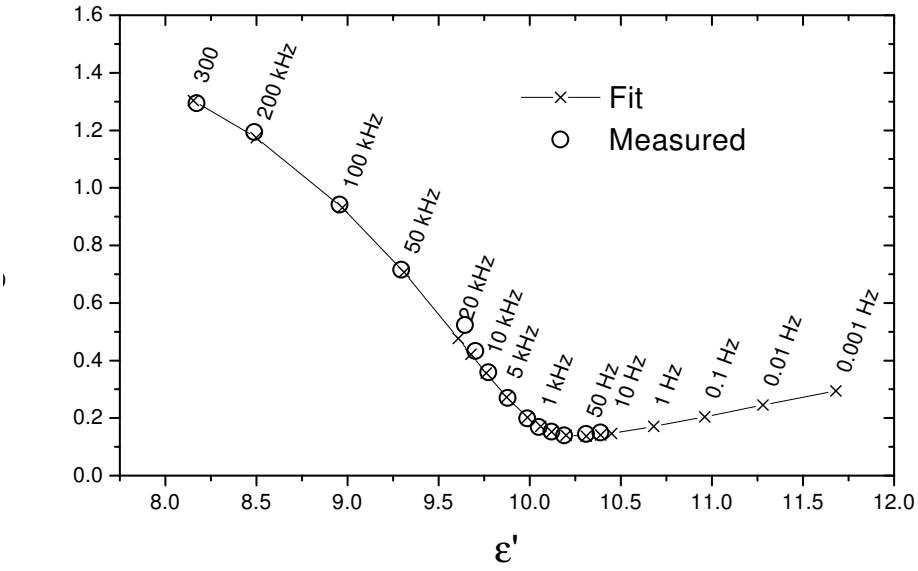

Figure 35. Parameter fit for PVDF sample #2 at room temperature. The time constant is $\tau = 173$ ns, the exponents $q = 0.603$ and $\nu = 0.524$ and the coefficients $\epsilon_\infty = 3.75, \epsilon_s = 9.32, \epsilon_c = 0.465$. The underlying exponents of the model are $\alpha = 0.397$ and $\gamma = 0.921$. The model has been extrapolated to very low frequency.

The data and parameter fit for PVDF match the literature value for the "universal dielectric response" exponent of PVDF as listed in Reference [17]. To exhibit this exponent, one plots $\epsilon'(\omega) - \epsilon_\infty$ versus frequency on a log-log scale. This is shown in Figure 36 with the extracted exponent $1 + \lambda = 0.9777$. Westerlund reported this exponent to be 0.9773. The note that accompanies the listing of exponents for various dielectric polymers states that the relative permittivity will vary considerably between production batches of material, but the exponents are highly consistent. The exponent persists in our samples, which have been stretched and poled at elevated temperature to achieve the bulk piezoelectric response. Although the universal dielectric response exponent, here called $1+\lambda$, is a favorite of some researchers, it is just

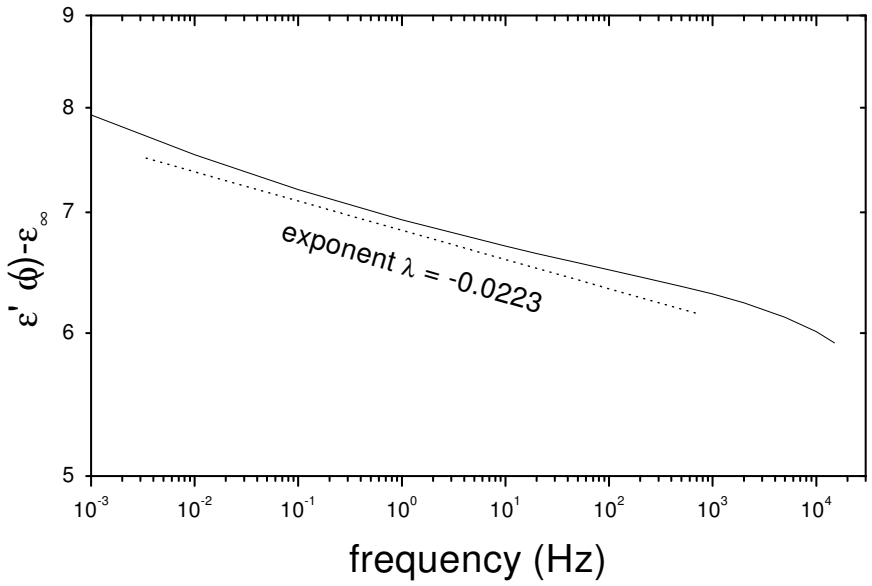

Figure 36. Universal dielectric response display for PVDF. The exponent derived from this plot is $1 + \lambda = 0.9777$.

an artifact from the point of view of the models presented here. Isnin and Jonscher noted the ambiguity in this exponent due to the uncertainty in the value of ϵ_∞ that needs to be subtracted out. [21]

Interpretation of the results of the data fitting to the model of Equation 5.13 leads to a somewhat surprising result. The value of the exponent γ in the CPE replacing R_1 in Figure 16 is 0.921, nearly unity. If it were unity, then R_1 would have been replaced by a capacitor. Exponents less than 0.5 would be more "resistor-like." As it is, this CPE is primarily a charge storage element. The exponent α is in the typical range reported for polymers.

The parameter values were then used in a numerical simulation of Equation 5.13. The charging and discharging currents predicted for a 100 second pulse are shown in

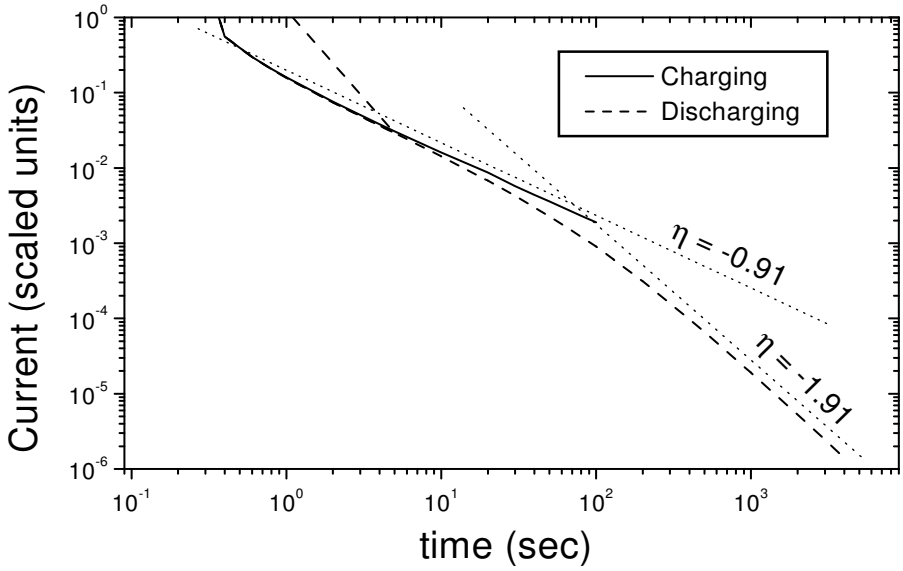

Figure 37. Predicted charging and discharging currents for PVDF sample #2 at room temperature using Equation 5.13 and the parameters from Figure 35. The two asymptotic exponents are also shown. Current in amps is found by multiplying the displayed value by $C_c\times$ Voltage.

Figure 37. The model clearly predicts that the discharging current matches the charging current for a short period, then drops off with an exponent one larger than that of the charging current. This is consistent with the predictions made in Equations 2.15 and 2.16.

The simulation indicates that virtually all of the charge transferred during the charging cycle is recovered during discharge. A net 0.054% of the "polarization" remained after 4000 seconds. To within the accuracy of the available data, integrating the current from the 4000 second mark to infinity is exactly that remaining polarization. With this, we can say that PVDF is a perfect insulator in that all of the charge

applied across it is recovered (after an infinite time). The extrapolated *dc* conductivity is zero. This does not mean that there is no energy loss. In fact, compared with polystyrene, PVDF is quite lossy in this regard. The energy loss is due to the phase shift in the CPE.

Permittivity measurements of several samples from different manufacturing batches of the electroded PVDF material were obtained. While the values of the coefficients ϵ_i, the time constant τ, and the exponent q varied slightly, the exponent most responsible for the long-time transient response, β, did not change from batch to batch, nor did it vary by size of the sample tested. The resonance was more pronounced at room temperature in some of the material, but it was above 5 kHz in all cases. The resonance for sample #8 is well defined as shown in Figure 38. Sample #8 was constructed by gluing two layers of electroded PVDF film together to reduce noise and enhance the current signal as described below. The lamination process did not change the permittivity or resonance characteristics in any measurable way from that of single sheets.

The actual predicted current is obtained by multiplying the scaled current of Figure 37 by $C_c \times$Voltage, where $C_c = \epsilon_0 \times Area/d$ is the cell capacitance. We realized that the available electrometer would probably not have the sensitivity to confirm the predicted roll-off of the discharging current using sample #2. For this reason, a larger Faraday cage was constructed to hold larger samples of 9.6 cm $\times$ 9.6 cm. After several attempts, we found that sandwiching two layers of the larger material together with

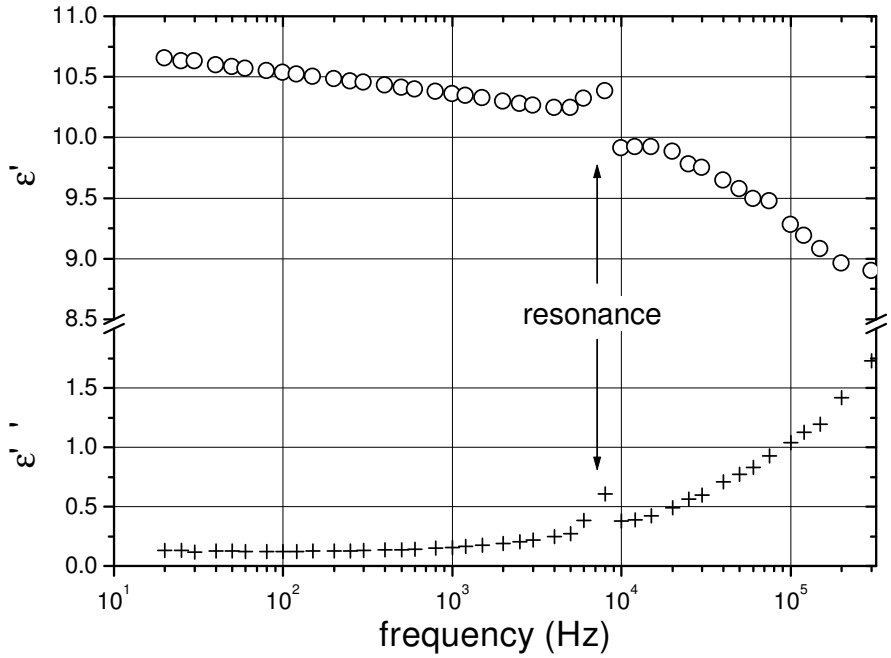

Figure 38. Real and imaginary parts of measured permittivity of sample #8 at room temperature showing the resonance between 5 and 12 kHz.

a thin layer of adhesive would reduce the low frequency piezoelectric response and increase the current signal to the level necessary to distinguish the separation of charging histories. With the high voltage sides placed to the inside of the sandwich, the chance for external atmosphere charge contamination was reduced. The predicted current for this sample is shown in Figure 39.

Figure 40 shows the results of three tests. In each case, the electrodes were shorted together for several hours prior to application of the voltage to ensure the zero initial condition required by the model. In the first, a discharging curve after applying 100 volts for an hour was obtained. The results are plotted as circles on the figure. In the second test, a pulse of 100 volts for 100 seconds was applied and the discharge current

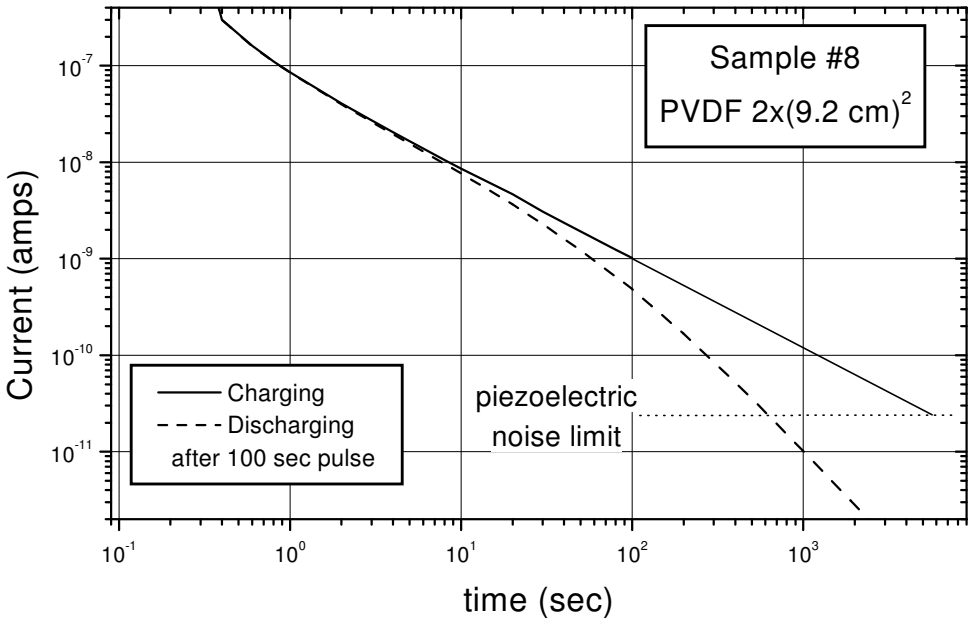

Figure 39. Predicted charging and discharging currents for PVDF sample #8, 2 × (9.6 cm × 9.6 cm), at room temperature. From Figure 37.

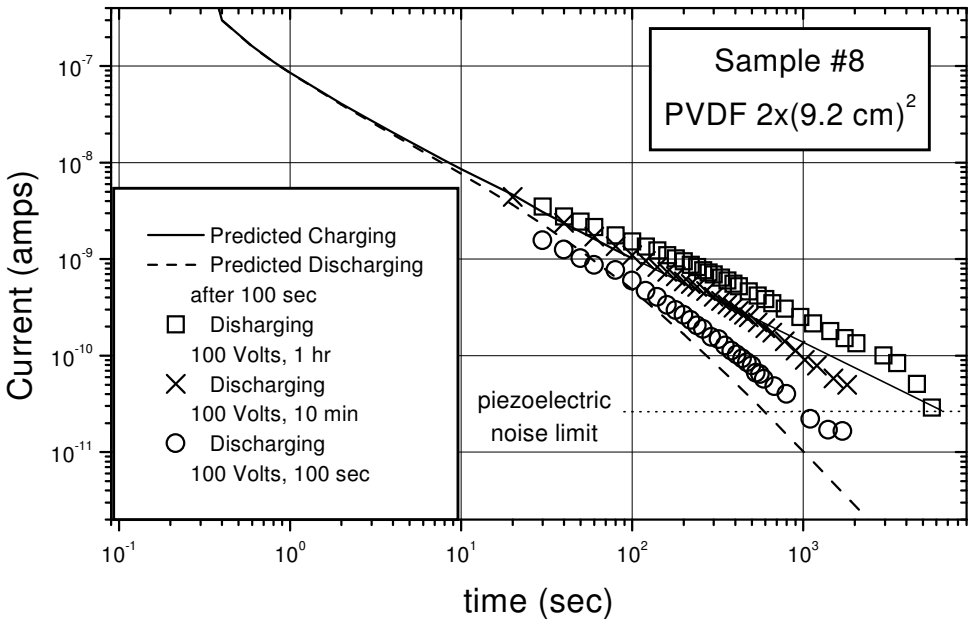

Figure 40. Measured discharging currents for PVDF sample #8, 2 × (9.6 cm × 9.6 cm), at room temperature. Solid and dashed lines are predicted values, symbols are measured data.

was then recorded. The squares on the figure show the results of this measurement. The third test applied a pulse of intermediate length, 10 minutes. The crosses on the figure record this test. Note that the longer the charging time, the longer time the discharging current follows the charging curve slope.

The deviation of the measured results from the predicted values in Figure 40 are greatly distorted due to the log-log plot. The currents predicted by the numerical simulation, and those measured experimentally, exhibit the separation of time histories predicted by Jonscher [8].

To place these results in perspective, the initial *ac* measurements were made over the range of 20 Hz to 300 kHz. All of these measurements represent dynamics in the fraction-of-a-second time scale. The permittivity curve was fit to this limited data and then extrapolated by five decades in frequency. These parameters were input to a numerical simulation that used a 0.2 second time step. This numerical time step is over one million times larger than the underlying time constant τ. In all this, we ignored the effects of the resonance and made no overt effort to account for the now sizable piezoelectric response from application of 100 volts in the current testing versus 0.5 to 1.0 volts used in the *ac* testing. There was no accounting for any nonlinearity and no accounting of the effects of using hand thrown switches. Clearly, automating the data collection process would produce more accurate data by removing the potential biases of human observation.

One of the reasons we were able to do this at all was that the resonance was

isolated and well above the low frequency dispersion. Undoubtedly there were other interesting fast dynamics occurring on the application and removal of the field. The simulation was able to skip over these, at some loss of accuracy, to produce a quantitative prediction of the long-time transient response.

Part of the difference between the predicted curves and the measured may well be the loss of accuracy in the time scale of the numerical calculation. With a time step of over a million times the underlying time constant, there is very likely a decay in the accuracy of the time evolution. It is anticipated that further comparison with experiment will provide feedback to the development of improved numerical schemes. Some ideas for such improvements are outlined in Chapter 8.

It is by no means assured that all of the differences between the predicted and measured currents are the fault of the computational model. There may well be some additional ultra-slow process that was not discovered in the *ac* testing between 20 Hz and 300 kHz. Such an ultra-slow response is found in KH_2PO_4 (KDP), for example. [50] Nonetheless, any such additional processes must be minimal in order to achieve the degree of accuracy demonstrated here.

CHAPTER 8

OTHER APPLICATIONS AND FUTURE QUESTIONS

The work presented up to this point is just the start of a potentially vast array of investigations. In many ways it represents a very elementary phenomenological treatment. There is as yet no way to derive the exponents from first principles. Even the interpretation of the models is left open in many ways, e.g. should we view the strength coefficients or the time scales as more fundamental? Nonetheless, there is reason to speculate that the models and methods presented here might focus future research into these questions. This chapter outlines some of the areas of research that might shed more light on the subject while extending the range of the tools for characterizing power-law behavior.

Extending the Dynamic Range

Tests of the time domain calculations using one-tenth the step size did not appreciably change the predicted response curves. This is a strong indicator that the limit of accuracy with the present scheme has been reached. Attempting to increase the number of steps in the time interval, N, will most likely result in decreased accuracy due to the number of additions and multiplications required per time step. Instead, a revised scheme will have to be developed. In all of the time domain calculations

included here, we used the $G1$ algorithm of Grünwald. Other algorithms are available that represent mid-point calculation schemes and could improve accuracy somewhat.

A variable time step procedure is more likely to produce a much more dramatic improvement in dynamic range. This is not as straightforward a task as in integer order numerical integration. The relation between the step size and the weights discussed in Chapter 4 is fundamental to the definition of the fractional derivative. In order to implement a variable time step algorithm, we need to find a way to maintain the connection between the weights and the time index into the past. This is possible, but could not be considered as a useful project until the hypothesis was validated and a picture such as Figure 40 obtained.

NMR Relaxation Times

If exponential relaxation really is the exception rather than the rule, then the relaxation dynamics probed by NMR and NQR would be expected to violate the Debye model as well. There is ample evidence that this is the case, see e.g. References [51] and [2]. Reference [52] includes a discussion of how specialized NMR measurement techniques have been used to verify nonexponential relaxation as the result of a hierarchy of relaxation mechanisms operating over varying spatial and temporal ranges, at least for the materials studied. Our NMR equipment is being upgraded as of this writing to apply these techniques to materials of interest.

Domain Wall Relaxation and Self-Pinning

A shortcoming of the dynamical model of domain wall motion in KDP, reported in Reference [53], is that it assumed a fixed set of energy levels for the configurations of the protons in the H-bonds of the KDP lattice. If the fixed set of exponential relaxation times were replaced with a Lévy distribution, would the domain walls exhibit self-pinning as seen in actual experiments? It may be possible to incorporate both intrinsic and extrinsic defects effects. Additional investigation into the dynamics of remanent domain wall structures, e.g. with a polarizing microscope, will have to be conducted in order to guide the development of such a model.

Where is the Charge?

The phase shifted conductivity models all have a common characteristic: they all allow motion of charge along a chain of random but low barriers, much longer than a single unit cell, until reaching a very high barrier. This would imply that the charge distributed on the surface of a dielectric actually penetrates into the bulk of the material but does not "flow" all the way through. What is the charge distribution?

A question left over from Chapter 2 is: what happens to a dielectric, such as PVDF, under open-circuit conditions? If, as we have seen, there is a continuous, but not constant, current flow under fixed voltage conditions, then, if we open the circuit after transferring a given amount of charge, we should expect the voltage across the

dielectric to sag. Is this a relaxation or a current flow? If we later short-circuit the dielectric back through an electrometer, do we recover the charge in the discharge current? What role does the electrode play in all this? The reference manual for the PVDF we have been using actually suggests using the actuator as a capacitor of the driving power supply, so this issue would seem to apply to a wide range of applications.

As a related issue, we are planning a series of experiments with the PVDF actuators to measure the mechanical relaxation under open-circuit versus closed-circuit conditions to determine if the piezoelectric response is due more to the voltage or the charge applied, i.e. which is more linear $\Delta l(V)$ or $\Delta l(Q)$, where Δl is the change in actuator displacement? This will help guide further studies into development of efficient control of actuators.

Application to Mechanical Systems

Nonnenmacher and Glöckle [34] developed a fractional model much like Equation 5.10 for mechanical stress relaxation. The rheological constitutive equation they derived is

$$G^*(\omega) = \frac{G_0 + G_e(i\omega\tau_0)^{-\mu}}{1 + (i\omega\tau_0)^{-q}}, \tag{8.1}$$

where $\tau_0 = \eta_m/G_m$ is the relaxation time of Maxwell element with spring constant G_m, η_m is the viscosity, G_e is the constant of a spring parallel to the Maxwell element, and $G_0 = G_m + G_e$. All of the methods of computation and analysis could be applied

directly to analysis of their model, which they handled with the Fox function formalism. We can now use numerical techniques to extend the test options to virtually any time varying excitation.

Since both dielectric and mechanical problems can be handled with fractional constitutive equations, the obvious question is: can we combine the two problems to produce a common description of the piezoelectric effect?

In reference [54] the expansion of actuators constructed of PVDF material is discussed. Under a constant 200 V applied field, the actuators continued to expand with a power-law relation at long times (2000 - 8000 sec). The exponent of displacement increase under constant voltage is close to the exponent of polarization increase under the same conditions. Given the nature of the coupling between mechanical and electrical responses in piezoelectric materials, it is very unlikely that this similarity in exponents is a coincidence. In particular, can we confirm the suspicion that the charge creep and displacement creep exponents are actually related?

Along this line, a first attempt at eliminating the polarization and piezoelectric creep effects was recently reported in Reference [55]. The authors modified the applied voltage curve to match the natural voltage relaxation of the piezoelectric under open-circuit conditions. The result was that the hysteresis typical of piezoelectric actuators was removed. It remains to be confirmed that they actually eliminated the decay currents in the process, i.e. creating the open circuit described in the previous section.

$PI^{\lambda}D^{\mu}$ Control Systems

Proportional plus Integral plus Derivative (PID) control systems are used extensively in feedback control loops to provide stable and linear operation of a device or system that otherwise would not be useful. In these systems, having a very accurate dynamical model of the response function is critical to successful operation. Podlubny [48] has suggested the use of a fractional control model $PI^{\lambda}D^{\mu}$ to better account for the memory in many types of systems. The major challenge is the development of a scheme to limit the computational load associated with the calculation of fractional derivatives. What needs to be developed, it appears, is a damage control procedure to avoid the echo effect of truncation as described at the end of Chapter 6.

Since a CPE can be described in terms of a distributed element transmission line and mathematically described by an infinite continued fraction, it may be possible to use some of the ideas of Reference [56], which addresses the issue of terminating the continued fraction after a finite number of steps. If such a terminator could be derived, then we might have the equivalent of the the proper termination of the transmission line and avoid the echo effect. We would still be faced with the problem that the amount of memory required would be dictated by the values of the exponents and coefficients in each case. Generating rules for use of such control systems may prove to be challenging. This work will probably have to be carried out incrementally in conjunction with testing of a variety of mechanical systems as described above.

Boundaries and Barriers

The effect of a blocking electrode layer has been discussed, but is it really as independent an effect as some would suggest? The electrode interface can produce substantial nonexponential, CPE-like behavior and nonlinear responses which can be confused with the response of the bulk material. On the other hand, internal barriers can produce the "phase shifted conductivity" indicative of a CPE. The role of the electrode-electrolyte interface in polarization dynamics is very much an open question. Electrode interface affects are of significant interest in the bio-medical community as well, see e.g. References [57] and [58].

Tests are being designed to begin investigating this question by coating a a variety of dielectrics with different electrodes and using varying *ac* voltage levels with *dc* biases. Some potential electrode materials such as palladium will allow limited transport of hydrogen and so would not be a blocking layer for protonic conduction as would some other metals. We are also designing comparison tests in which blocking layers of polymers are deposited prior to application of an electrode layer.

Many Body Dynamics

The idea of a "phase shifted conductivity" is not new. One such model was described in Reference [59]. The key point made in that article was that a random set of barriers can produce an effect very much like that attributed to the CPE. The

open question is: can we take this to a more precise level? Could we apply many body dynamics theory, such as that outlined in Reference [56], to develop such a theory?

Relation to Generalized Thermodynamics

Tsallis and others have developed a theory of generalized statistical mechanics, which accounts for the failure of the Gibbs-Boltzmann statistics when processes are not adequately independent. [60]. The theory leads to power-law statistics very similar to that seen in the fractional calculus and deal with both sub- and super-diffusive processes. As yet, there is no connection between the fractional calculus and the generalized statistical mechanics. Is there one?

One of the effects that can result in failure of the G-B statistics is long-range dipolar interactions. It would seem that such exist in ferroelectric materials since it is the bulk polarization energy from interacting dipoles that forces the formation of domains. Domains typically have dimensions on the order of microns compared to the unit cell size on the order of nanometers, which would imply a relatively long-range interaction. Is the effect just too small to be noticed in this regard?

Fractional versus Fractal

The spatial distribution of charge trapping defects producing the power-law behavior has not been discussed in this treatment. It would be interesting to investigate this spatial distribution from the point of view of interaction between and among

trapping sites. To what extent does one defect affect the relaxation dynamics of a neighboring defect? Reference [52] suggests that the nonexponential relaxation might be due to cooperative relaxation over a hierarchy of spatial scales. Would it be possible to analyze such a hierarchy of scales in a lattice structure using Density Functional Theory (DFT) to predict the coupled relaxation dynamics from first principles? What size of super-cell would be required in DFT to reproduce the fractal structure implied in this question? Experimentally, it may be possible to create mesoscopic structures, such as ultra-thin films to test for the possibility that a critical size, or number of contributing elements, might be required for the generalized central limit theorem to apply.

Is there some cross-over phenomenon that could be used to distinguish between "quenched" disorder effects and dynamic "annealed" disorder, as described in Chapter 3? Are the roles of the different classes of disorder distinguishable in their effect on the dynamics?

Another open question is whether the multifractal distribution of relaxation times approach discussed at the end of Chapter 3 can be applied to the low-frequency dispersion as well as the loss peak. There is reason to suspect that the roughness of the electrode interface may affect the exponents. How does this relate to the thermodynamic phase transitions discussed in Reference [10]? Is there some "critical roughness" for the interface to become fractal?

Quantum Mechanical Treatment

All of the treatment here has been from a classical perspective. A more complete treatment would include quantum mechanical aspects that must show up when dealing with the fermion nature of non-superconducting charge carriers. It is particularly intriguing that the 1/f noise phenomenon in dielectrics has been discussed in the literature as an infrared divergence in quantum electrodynamics. [61] Which is the cause and which the effect? Is it the infrared divergence or the memory that produces the 1/f noise and the universal dielectric response? This question relates to the ability of theoretical condensed matter methods such as DFT to handle dynamical interactions among highly perturbed wavefunctions describing trapping sites and defects.

1/f Noise in Resistors

The relationship between the universal dielectric constant in "insulating" dielectrics and 1/f noise was discussed in Chapter 5. Since the CPE model also appears to apply to resistive elements, is there an equivalent connection between 1/f noise and the low frequency response in conductors? Since the 1/f noise phenomenon is so universal to conductors, it is likely that the result is again due to a statistical limit as it was with dielectrics.

CHAPTER 9

SUMMARY AND SIGNIFICANCE

Subsequent to completion of the bulk of the work reported here, two new texts have become available. Reference [30], by I. Podlubny, includes a discussion of a method for numerical integration of fractional differential equations although the method is noted to have stability and accuracy problems. The methods developed here do not exhibit stability problems, but may benefit from efforts to improve accuracy.

Reference [51] is a compendium of articles covering both the theory and practical applications of fractional calculus in physics. In this text, the fractional calculus is developed as a consequence of the irreversibility of most phenomena seen in nature. Extensive discussion of anomalous (fractional) diffusion is included, but polarization dynamics are not.

Lesson Learned

The major lesson learned in this research is that it we need to relax assumptions about nature that may seem obvious but may not be supported in observation of physical systems.

The first assumption is that a material contains a fixed set of defects at a given temperature. It is more reasonable to assume that the defect structure is dynamically

changing in time. There may be some additional defect structure due to dopants or other sources, but there must also be a dynamic nature to the defects.

Second, there is no reason to assume, *a priori*, that the waiting time distribution associated with charge carrier trapping at defect sites need have a distribution with convergent second moment.

After we abandon these assumptions, there comes the possibility that the waiting time distribution violates the canonical Central Limit Theorem (CLT), and Lévy statistics percolate to the macroscopic level producing power-law behavior. The power-law dynamics are then governed by the fractional calculus. We are faced with non-Markovian processes which are the nemesis of theoretical statistical mechanics and stochastic analysis. The degree to which fractional models truly negate the methods of stochastic analysis such as in References [32] and [62], is not known.

Given the ubiquity of power-law behavior in dielectrics, it seems we need to improve our description of these materials to include the "anomalous" characteristics. After all, with the power-law decay of the current exhibited by PVDF, the true *dc* conductivity is, indeed, zero. This statement is all but meaningless, however, given the eternity one must wait to get to the zero current state; and by then the charge accumulation would be infinite. Clearly, we need to augment our language to include the memory effects in real materials. We need to correct the confusion involved with terms such as "universal anomaly."

Conclusion

The hypothesis stated in Chapter 2, that the fractional calculus can be used to describe polarization dynamics, cannot be rejected. In fact, it has withstood a very challenging test by allowing model extrapolation by five decades in time scale. The connection between the steady state *ac* response and the transient response has been rather dramatically demonstrated via the fractional calculus. There is much more to do, but the generation of new questions is the ultimate joy of almost any researcher.

APPENDICES

APPENDIX A

α-STABLE DISTRIBUTIONS

This appendix provides some additional detail on the nature of Lévy, or α-stable, distributions and their relation to Gaussian distributions.

The Law of Large Numbers and the Central Limit Theorem

Consider a set of random variables $\{X_1, X_2, \ldots, X_n\}$ where the X_i are mutually independent with an arbitrary but common distribution. We want to investigate the properties of the sum $S_n = X_1 + \cdots + X_n$. The law of large numbers states that if the expectation $\mu = E(X_i)$ exists, then for every $\epsilon > 0$ as $n \to \infty$

$$\text{Prob}\left\{\left|\frac{X_1 + \cdots + X_n}{n} - \mu\right| > \epsilon\right\} \to 0. \tag{A.1}$$

That is, the probability that the average S_n/n will differ from the expectation by less than an arbitrary prescribed ϵ tends to unity. It is not necessary that the variance $\text{Var}(X_i)$ also be finite for the law of large numbers to hold.

Now suppose that $\mu = E(X_i)$ and $\sigma^2 = \text{Var}(X_i)$ exist and, as before, $S_n = X_1 + \cdots + X_n$, then the central limit theorem states that for every fixed β

$$\text{Prob}\left\{\frac{S_n - n\mu}{\sigma n^{\frac{1}{2}}} < \beta\right\} \to \Phi(\beta), \tag{A.2}$$

where $\Phi(\beta)$ is the normal, or Gaussian, distribution function,

$$\Phi(x) = \frac{1}{(2\pi)^{\frac{1}{2}}} \int_{-\infty}^{x} \exp(-\frac{1}{2}y^2)dy. \tag{A.3}$$

See Reference [63] for proofs and further details.

Note that the CLT is built on the assumption that at least the first two moments of the underlying random variable distribution converge, i.e. the distribution of X_i is

not too broad. There is extensive evidence that these statistical moments often do not converge. Additionally, the CLT fails if the individual random variables show "long-range correlations," i.e they are not independent. In the discussion of anomalous dielectric responses, the model calls for only the first of these failure criteria to be in effect, e.g. broad waiting time distributions.

Lévy Distributions

The central limit theorem discussed above is only a special case of a much more general theorem which applies whether or not the second moment, or variance, exists. For "adequately" independent distributions, i.e. no long-range correlations, the generalized CLT states that the sum of random variables will converge to a Lévy, or α-stable, distribution. Proofs and additional discussion may be found in References [64] and [65].

There is, unfortunately, no closed analytical form for the α-stable distributions. They contain a Gaussian core plus power-law tails. The parameter α denotes the exponent of the decay of the tails of the distribution. The tails have the form $x^{-1-\alpha}$, with $0 < \alpha < 2$. For individual distributions with tails decaying like $\alpha \geq 2$, the second moment of the distribution will exist and the canonical CLT will apply. It must be noted that the distribution of contributing variables, the X_i, need not be power law. For non-Gaussian statistics, the distribution need only fall off slower that x^{-3}. It is the sum distribution that converges to power law.

The Gaussian core may confuse matters since the power-law tails may be treated as statistical "outliers" by those convinced that the Gaussian distribution must be the true representation of the underlying statistics. Texts on handling random data often include data rejection techniques based on this Gaussian assumption.

While there is currently no general closed form for representing the probability density function (pdf), $p(x)$, for α-stable distributions, the characteristic function does have a closed form. The characteristic function is defined by

$$\phi(\theta) = \int dx\ p(x) \exp(i\theta x). \tag{A.4}$$

so that, by Fouier inversion

$$p(x) = \frac{1}{2\pi} \int d\theta\ \phi(\theta) \exp(-i\theta x). \tag{A.5}$$

The characteristic function for the α-stable distribution is given by

$$\log \phi(\theta) = -\sigma^{\alpha} |\theta|^{\alpha} \{1 - i\beta \mathrm{sgn}(\theta) tan(\alpha\pi/2)\} + i\mu\theta, \tag{A.6}$$

where α is the index of stability, $\beta \in [-1, 1]$ is the skewness parameter, σ is the scale parameter and μ is the shift. The parameter σ is referred to as the "scale parameter" since the variance does not exist except for the limiting case $\alpha = 2.0$. For some combinations of α and β, even the mean does not exist, therefore the term "shift" is given to the parameter μ. When $\mu = \beta = 0$, the distribution is referred to as symmetric α-stable.

Estimates of the $p(x)$ curve can be generated through numerical integration of the Fourier transform of Equation A.6. Additionally, pseudo-random number generators

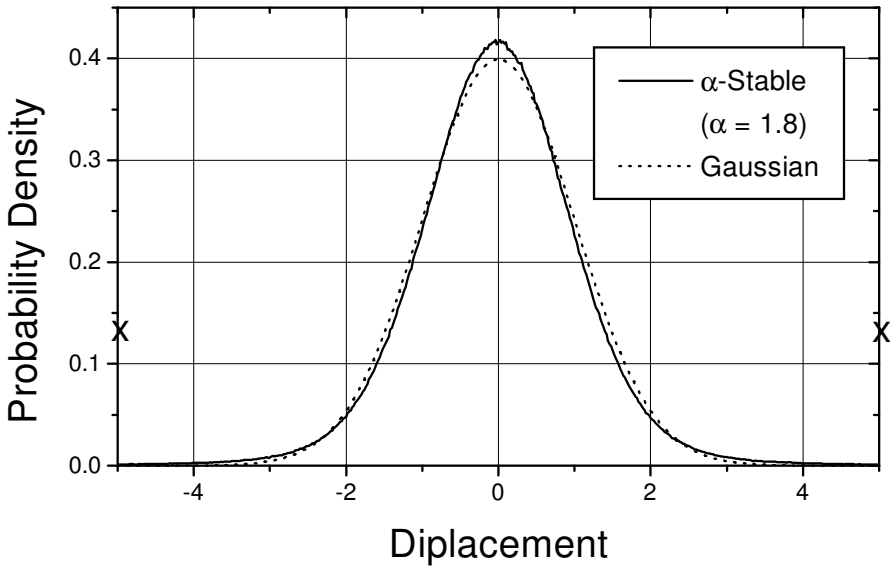

Figure 41. Comparison of an α-stable distribution of $\alpha = 1.8$ with a Gaussian. Both have $\sigma = 1.0$. Note the slightly greater emphasis at the center of the distribution. The X marks on the graph indicate the relative number of events outside ± 5 σ for the $\alpha = 1.8$ case.

for α-stable distributions exist. [66] It is possible to estimate the pdf by sampling and creating a histogram display. This is shown in Figure 41 with 10^7 trials recorded. The figure provides a comparison of a Gaussian distribution with an α-stable distribution with $\alpha = 1.8$. In perspective, the Gaussian is an α-stable distribution with $\alpha = 2.0$. The X marks on the figure represent the relative number of events that fell outside the ± 5 σ range. For comparison, out of 10^7 trials for each of the Gaussian and the $\alpha = 1.8$ cases, 12 events fell outside the ± 5 σ range for the Gaussian, while 28,768 fell outside for the $\alpha = 1.8$ case. As α gets smaller, the distribution becomes more peaked at the origin and greater weight is given to the tails of the distribution.

Although events at large values (compared to σ) are possible in Gaussian distributions, they become vanishingly rare. In α-stable statistics, those "possible" events become more probable. In many physical systems there is some limit, such as a limiting velocity, that requires the distribution to be truncated. For distributions of spatial jumps, there is a need to avoid very long jumps by particles that would imply travel faster than the speed of light, for example. In the case of divergent waiting time distributions, however, there is no such limit; the charge carrier can "sit forever" in a trapping site. In this case, the motion of the charge carriers gets slowed to the point of being sub-diffusive.

In the language of random walks, if the distribution of jump distances diverges one gets a super-diffusive response, $\left\langle (x(t))^2 \right\rangle \propto t^{\delta}$, where $\delta > 1$. If the distribution of waiting time between jumps diverges one gets a sub-diffusive response, $\delta < 1$. It now appears that super-diffusion results from long-range interactions, or correlations, while sub-diffusion results from local dynamic relaxation, although there is still some contention over how broadly this statement can be applied. The relation between diffusion and drift will be discussed in the next section.

It has been noted that the α-stable distributions represent limit distributions. There is the possibility that individual distributions involved in the sum are not exactly the same as the limit distribution. Tsallis has derived a set of individual "jump" distributions, based on the "q-calculus" of generalized entropy. [60] Sums

of these distributions converge to either Gaussian or α-stable depending on the parameter q. What role these distributions might play in the study of waiting time distributions is not known. In general, the interpretation of sub-diffusive dynamics within the generalized thermodynamics is an open question.

Diffusion and Drift

We now look at the random variable X_i as a sample from the evolving dynamics of the motion of a particle $x(t)$. The sum $S_n(t)$ will become time dependent. This section summarizes Reference [67].

For unbiased process, the mean and mean square displacement (assuming these exist) of a particle interacting with a thermal bath can behave like

$$\left\langle x^2(t)\right\rangle_0 \sim t^\delta \quad \text{and} \quad \left\langle x(t)\right\rangle_0 = 0. \tag{A.7}$$

The subscript zero denotes the case when there is no external driving force. When $\delta \neq 1$ the diffusion is anomalous. The case $\delta < 1$ is referred to as slow diffusion or sub-diffusion and the case $\delta > 1$ is referred to as enhanced diffusion or super-diffusion.

When a force F is applied the symmetry is broken and then

$$\left\langle x(t)\right\rangle_F \sim t^{\delta_F}. \tag{A.8}$$

A process in which $\delta_F = \delta = 1$ is referred to as a normal process. Normal processes are usually Gaussian while anomalous processes are typically non-Gaussian.

If the system is close to thermal equilibrium at a temperature T, the generalized Einstein equation relates the fluctuations of the particle position in the absence of an

external field to its behavior under the influence of a constant force field F, according to

$$\left\langle \left(x_{\parallel}(t)\right)^2 \right\rangle_0 = 2\frac{k_B T}{F} \left\langle x_{\parallel}(t) \right\rangle_F , \tag{A.9}$$

where $x_{\parallel}$ is the component of x along F. Equation A.9 is only valid in the linear response regime where $F \to 0$. For anomalous diffusion the generalized Einstein equation is not expected to hold. In particular, if δ_F depends weakly on the field, then $\delta_F \neq \delta$. In the anomalous process case, we would expect the response to the field to differ from the relaxation in the absence of the field.

The subject of anomalous diffusion has been extensively studied, see for example References [25, 68, 69]. What can be taken away from these, and many other studies, is that anomalous processes, both slow and enhanced, occur quite often in nature. For our current purposes, we note that the relaxation currents measured after application and removal of an external field represent *subdiffusive* processes. This will provide some insight into the nature of the anomalous processes involved in dielectric dynamics.

APPENDIX B

ANOMALOUS DIFFUSION

This appendix investigates a different but related use of the fractional calculus. As noted in the main text, models involving polarization or conduction deal with coarse-grained models. These represent statistical sums of individual responses, so called "limit distributions." At the other extreme is the reconstruction of individual sample trajectories of particles through some kind of phase space. This latter program is the domain of the stochastic calculus. In this case, we investigate the random actions of the sample particles and look at ensembles of these particles to make estimates of the statistical properties of the ensemble.

Properties of Normal and Anomalous Diffusion

Normal, or Fickian, diffusion follows a statistical evolution of the form

$$\frac{\mathrm{d}\rho(x,t)}{\mathrm{dt}} = -D\nabla^2\rho(x,t) \tag{B.1}$$

where $\rho(x,t)$ is the local particle density and D is the diffusion coefficient, which depend on the mass of the particles, the viscosity, and temperature. The common geometric interpretation is that the greatest time rate of change of the density is in regions of high spatial curvature of the density function. The individual particles follow a stochastic equation of the form

$$\mathrm{d}X_t = a(X_t) + b(X_t)\mathrm{d}W_t \tag{B.2}$$

where $a(X_t)$ represents a drift, $b(X_t)$ represents a diffusion, and W_t represents a Wiener process. [70] Note that $a(X_t)$ and $b(X_t)$ may also be functions of an applied

field, but the field is considered to be held constant for this model. A Wiener process is a mathematical construction of the physical Brownian motion. In practice, a Wiener process is produced from a Gaussian random variable. The result of the combination of essentially independent random trajectories of the ensemble of X_t's, is the Gaussian distribution spreading out over time. The fact of random collision interactions is imbedded in the random jump simulated by the Wiener process. The Gaussian nature of the process is a result of the short range of the interactions.

If there are "long-range" interactions, then there are spatial correlations which destroy the independence of the individual random processes. In this case, the generalized central limit theorem demands convergence to a Lévy, or α-stable distribution, but the result is super-diffusive motion. That is, $\langle (X_t)^2 \rangle \sim t^\alpha$ with $\alpha > 1$. The motion is sometimes referred to as a "Lévy flight."

Initially, the intent of the time-of-flight secondary ion mass spectrometer (TofSIMS) imaging study of cocaine was to determine if it could be detected in the presence of contaminants such as polydimethylsiloxane (PDMS), even with the two materials diffusing across the same substrate. The answer was affirmative, but the results were much more profound than that. It was discovered that by taking images repetitively over time TofSIMS could register diffusion quite nicely and that cocaine showed significantly enhanced surface diffusion.

Surface Diffusion of PDMS

In this experiment, a TofSIMS imaging system was used to monitor the diffusion of PDMS over a gold-coated silicon substrate. The surface of the substrate was thoroughly cleaned and a drop of PDMS was placed at the edge of the scanned area with an extremely sharp steel needle. The first column of Figure 42 shows the images taken after 12, 27, and 88 minutes. The second column displays the detection counts for a range of distance from the edge of the scanned area. Note the smoothing of the edges of the distribution of the PDMS over time as the curve takes on the normal "bell" shape.

In the third and fourth columns are the results of a two-dimensional simulation of Equation B.2 in which 10,000 simulated particles are distributed randomly across an initial deposition area according to a uniform distribution. They are then allowed to jump according to the following rules: (1) the length of the jump is obtained from a Gaussian pseudo-random number generator and (2) the direction of the jump is taken from a uniform distribution $[0, 2\pi]$. If the jump causes the particle to fall outside the "scanned substrate area," it is placed back in the lay-down area according to the uniform distribution. This creates a conservation of particles and simulates a thick initial lay down of material. The simulation results were recorded after 6, 48, and 234 jumps per particle. Again, the smoothing of the curvature is evident.

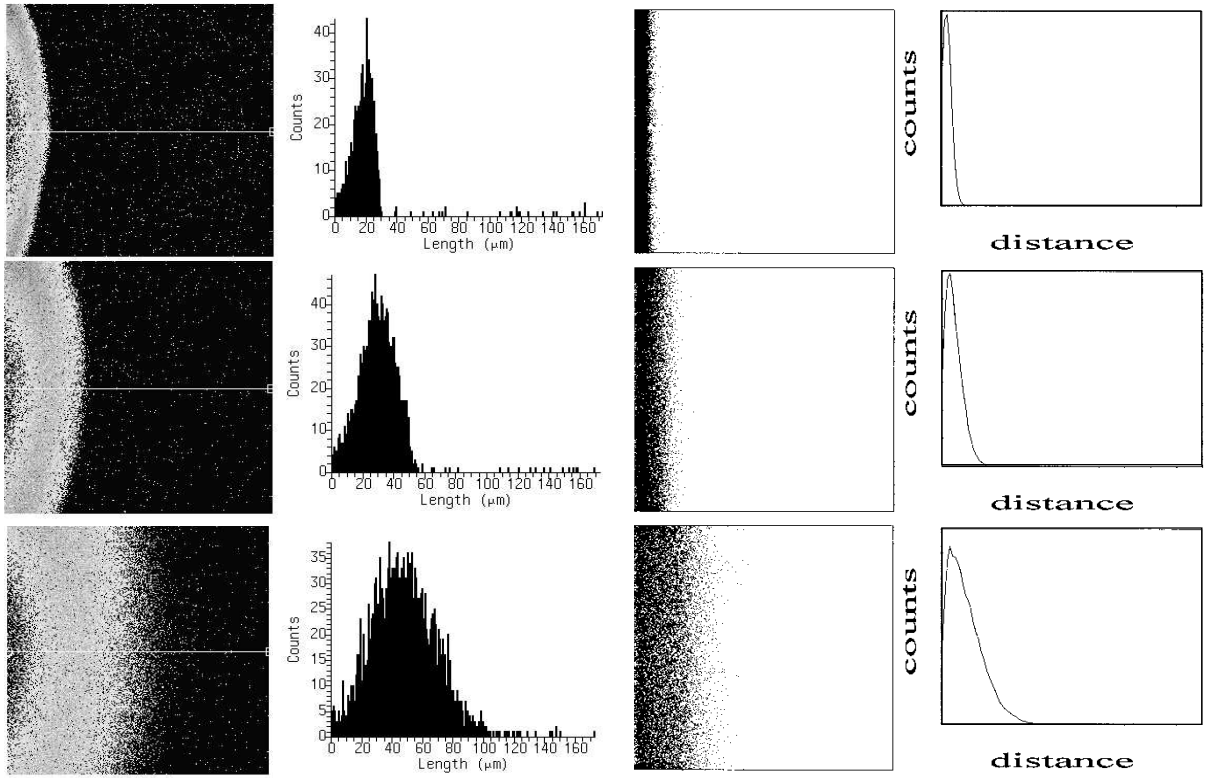

(a) Measured (b) Simulated

Figure 42. Measured and simulated diffusion of PDMS. In (a), from top, the images were recorded at 12, 27 and 88 minutes. In (b), from top, the simulation results were recorded after 6, 48, and 234 jumps.

Surface Diffusion of Cocaine

In this experiment, a nylon fiber contaminated with cocaine was pressed against a cleaned substrate of gold-coated silicon. The image area was oriented so that the cocaine deposition was on the edge of the image. TofSIMS images were then obtained at 2, 28, and 52 minutes. These are displayed in the first column of Figure 43. The corresponding density graphs are displayed in the second column. Note that the sharp curvature does not soften. There is dispersion of cocaine across the surface, but the density curve follows almost a straight line.

To model this dynamic, the Wiener process in Equation B.2 was replaced with an α-stable process and a corresponding Lévy, or α-stable pseudo-random number generator was used. [66] This simulation is based on a diffusion model of the form

$$\frac{\mathrm{d}\rho(x,t)}{\mathrm{dt}} = -D\nabla^{\alpha}\rho(x,t) \tag{B.3}$$

where $0 < \alpha \leq 2$, with $\alpha = 2$ representing Brownian motion. The diffusion coefficient D now has fractional dimension units.

Typical super-diffusion is modeled with $\alpha = 1.6 \sim 1.8$. A value of $\alpha = 1$ represents ballistic diffusion with a broad distribution of velocities. In the cocaine diffusion case, the best fit is $\alpha = 0.01$. This is hyper-diffusive behavior, indicative of accelerated motion. Model results at 4, 12, and 64 jumps per particle are shown in the third and fourth columns of Figure 43. It is most amazing that the fractal clustering typical of both Gaussian and most "typical" α-stable distributions is absent in this case. It is as if there were a "condensed" phase and a gas-like phase.

Since the TofSIMS can detect only the surface layer, it is likely that the actual material density is more like that shown in the "counts" column of Figure 43b than in the "counts" column of 43a. The bulk of the material stays in the "condensed phase," while the particles that do break loose fly off to form what appears to be a very low density two-dimensional gas. The density comparison shows that there is an almost imperceptible amount of material distributed into the open area of the substrate.

The statistical interpretation for this apparent phase separation can be seen in Figure 44. The tails of the Gaussian distribution go to zero very strongly outside of three to four sigma. The α-stable distribution with $\alpha = 0.01$ has approximately half its distribution contained in a Dirac delta-distribution like spike at the origin and very long, flat tails. In the α-stable case, the particle either stays where it is (the condensed phase) or executes a jump of arbitrary distance.

This interpretation should not be viewed as a violation of special relativity. In the time it takes to complete a scan using the TofSIMS, the particles could get to any location in the ultra-high vacuum chamber at the speed of sound on the various chamber surfaces. The evidence indicates that this is exactly what happens. The cocaine contaminates the entire inner surface of the TofSIMS chamber within the course of any given experiment and the entire chamber needs to be thoroughly cleaned prior to any subsequent measurements or the cocaine returns to contaminate the new samples. Several additional experiments were run to confirm that the diffusion is only on the surfaces, not via flight through the vacuum, even at elevated temperatures.

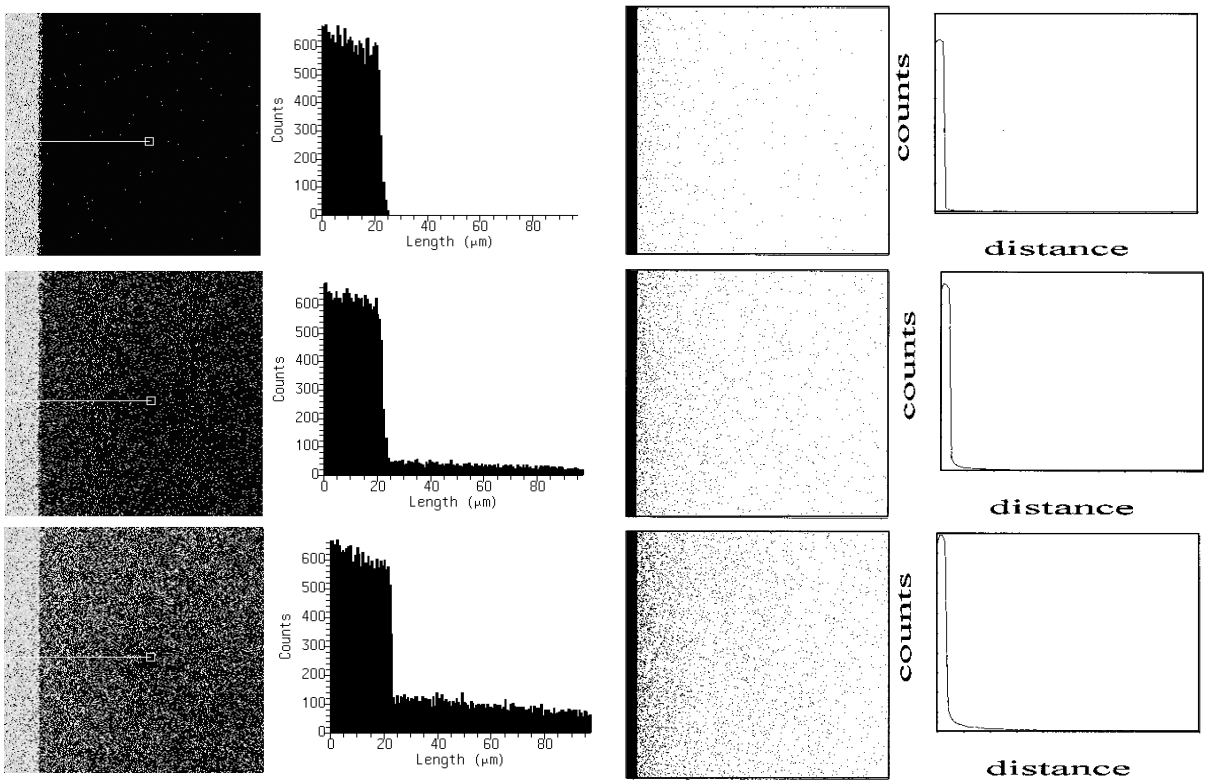

(a) Measured (b) Simulated

Figure 43. Measured and simulated diffusion of cocaine. Note that the sharp edges remain in both the measurements and simulation. Due to the ability of the TofSIMS to detect the surface layer only, the actual density differences between the lay down region and the open surface are more likely to be that shown in the fourth column. The density in the open substrate area is almost imperceptible compared to the amount retained in the original deposition region.

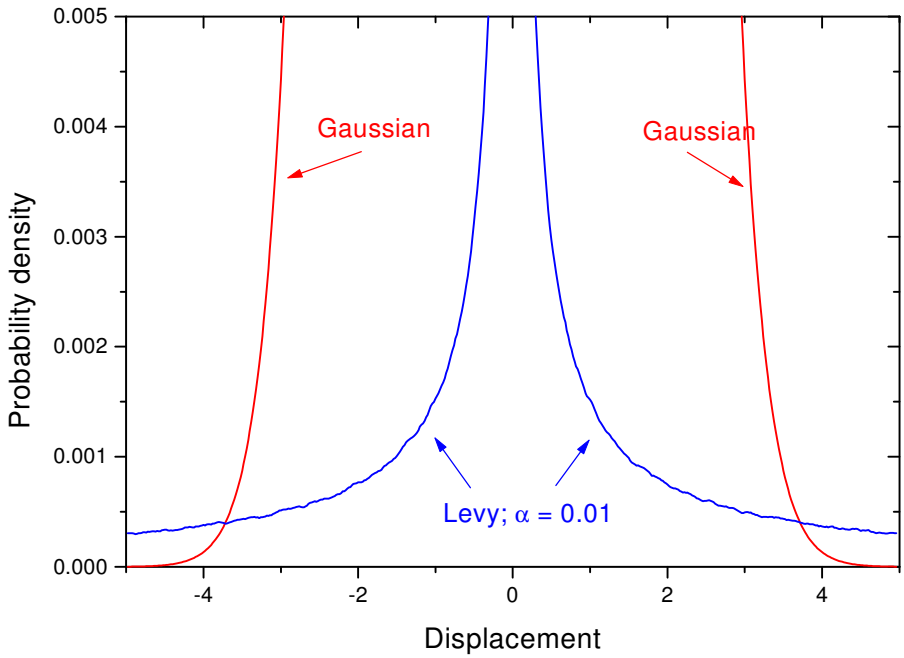

Figure 44. Comparison of the Lévy, or α-stable, ($\alpha = 0.01$) and Gaussian distributions in the cross-over regime.

Statistical Implications

The physical manifestations of the two potential violations of the canonical central limit theorem appear to be quite distinct. In the case of divergent waiting time distributions, the result was a sub-diffusive response. In the case of long-range correlations the result is a super-diffusive response. The implication is that long-range spatial correlations are not important in the case of the dielectric permittivity function. The trapping sites may interact with nearest neighbors, but it now seems unlikely that long-range interactions play a significant role in the dynamical properties discussed in this dissertation.

This statement is still quite speculative, as there are many unanswered questions concerning super-diffusive processes in general. But, if long-range dipolar interactions were significant, then a logarithmic divergence would exist that would result in a violation of Gibbs-Boltzmann statistical mechanics. [60] The fact that G-B statistics do so well for describing the thermodynamical properties of dielectrics mitigates against this being the case.

REFERENCES CITED

[1] P. Debye, *Polar Molecules*, Chemical Catalogue Company, New York, 1929.

[2] K. L. Ngai, "Evidences for universal behavior of condensed matter at low frequencies/long times," in *Non-Debye Relaxation in Condensed Matter: Proceedings of a Discussion Meeting, Bangalore*, T. Ramakrishnan and M. R. Lakshmi, eds., pp. 23–191, World Scientific Publishing Co. Pte. Ltd., 1987.

[3] S. Cole and R. Cole, "Dispersion and absorption in dielectrics," *J. Chem. Phys.* **9**, pp. 341–351, 1941.

[4] J. R. Macdonald, *Impedance Spectroscopy*, John Wiley & Sons, New York, 1987.

[5] A. K. Jonscher, "Physical basis of dielectric loss," *Nature* **253**, pp. 717–719, 1975.

[6] A. K. Jonscher, "The interpretation of non-ideal dielectric admittance and impedance diagrams," *Phys. Stat. Sol. (a)* **32**, pp. 665–676, 1975.

[7] A. K. Jonscher, "The "universal" dielectric response," *Nature* **267**, pp. 673–679, 1977.

[8] A. Jonscher, *Dielectric Relaxation in Solids*, Chelsea Dielectric Press, London, 1983.

[9] G. D. Esposti and D. Tommasini, "A model for the simulation of relaxation phenomena in dielectrics," *IEEE Trans. Electrical Insulation* **25**, pp. 617–621, 1990.

[10] A. Leyderman and S.-X. Qu, "Multifractal phase transitions in the non-Debye relaxation processes," *Phys. Rev. E* **62**, pp. 3293–3298, 2000.

[11] R. M. Hill and A. K. Jonscher, "The dielectric behavior of condensed matter and its many-body interpretation," *Contemporary Physics* **24**, pp. 75–110, 1983.

[12] K. Funke, "Debye-Hückel-Type relaxation processes in solid ionic conductors: The model," *Solid State Ionics* **18&19**, pp. 183–190, 1986.

[13] V. H. Schmidt, J. Conant, G. Bohannan, J. Eckberg, S. Halko, J. Hallenberg, C. Nelson, N. Peterson, C. Smith, C. Thrasher, and B. Tikalsky, "Piezoelectric polymer actuators for vibration suppression," *Proc. SPIE* **3669**, pp. 162–170, 1999.

[14] G. Bohannan, V. H. Schmidt, D. Brandt, and M. Mooibroek, "Piezoelectric polymer actuators for active vibration isolation in space applications," *Ferroelectrics* **224**, pp. 211–217, 1999.

[15] G. W. Bohannan, V. H. Schmidt, R. J. Conant, J. Hallenberg, C. Nelson, A. Childs, C. Lukes, J. Ballensky, J. Wehri, B. Tikalsky, and E. McKenzie, "Piezoelectric polymer actuators in a vibration isolation application," *Proc. SPIE* **3987**, pp. 331–342, 2000.

[16] T. Ikeda, *Fundamentals of Piezoelectricity*, Oxford Univ. Press, 1990.

[17] S. Westerlund and L. Ekstam, "Capacitor theory," *IEEE Trans. Dielectrics and Electrical Insulation* **1**, 1994.

[18] K. Uchino, "High electromechanical coupling piezoelectrics: relaxor and normal ferroelectric solid solutions," *Solid State Ionics* **108**, pp. 43–52, 1998.

[19] S. Westerlund, "Dead matter has memory," *Physica Scripta* **43**, pp. 174–179, 1991.

[20] N. Galiyarova and S. Gorin, "Fractal features of dielectric response of ferroelectrics with domains and clusters," *Ferroelectrics* **222**, pp. 373–379, 1999.

[21] A. Isnin and A. K. Jonscher, "Dielectric response of some ferroelectrics at "low" frequencies I," *Ferroelectrics* **210**, pp. 47–65, 1998.

[22] A. K. Jonscher and A. Isnin, "Dielectric response of some ferroelectrics at "low" frequencies II," *Ferroelectrics* **210**, pp. 67–81, 1998.

[23] N. Kumar, "Mechanisms for non-Debye relaxation in condensed matter and possiblity of universal dielectric response," in *Non-Debye Relaxation in Condensed Matter: Proceedings of a Discussion Meeting, Bangalore*, T. Ramakrishnan and M. R. Lakshmi, eds., pp. 11–22, World Scientific Publishing Co. Pte. Ltd., 1987.

[24] K. L. Ngai and A. K. Rajagopal, "A theory of non-Debye relaxation in condensed matter," in *Non-Debye Relaxation in Condensed Matter: Proceedings of a Discussion Meeting, Bangalore*, T. Ramakrishnan and M. R. Lakshmi, eds., pp. 387–401, World Scientific Publishing Co. Pte. Ltd., 1987.

[25] J.-P. Bouchaud and A. Georges, "Anomalous diffusion in disordered media: Statistical mechanisms, models and physical applications," *Physics Reports* **195**, pp. 127–293, 1990.

[26] V. M. Agfonov and A. Y. Antonin, "1/f noise from the "universal" dielectric response," in *AIP Conf. Proc. 285: Noise in Physical Systems and 1/f Fluctuations,* St. Louis, MO., P. H. Handel and A. Chung, eds., pp. 155–157, 1993.

[27] K. Oldham and J. Spanier, *The Fractional Calculus*, Academic Press, New York, 1974.

[28] K. S. Miller and B. Ross, *An Introduction to the Fractional Calculus and Fractional Differential Equations*, John Wiley & Sons, New York, 1993.

[29] A. Mathai and R. Saxena, *The H-Function with Applications in Statistics and Other Disciplines*, Wiley Eastern Limited, New Delhi, 1978.

[30] I. Podlubny, *Fractional Differential Equations: An Introduction to Fractional Derivatives, Fractional Differential Equations, to Methods of their Solution and some of their Applications*, vol. 198 of *Mathematics in Science and Engineering*, Academic Press, San Diego, CA, 1999.

[31] M. Abramowitz and I. A. Stegun, eds., *Handbook of Mathematical Functions*, Dover Publications, Inc., New York, 1965.

[32] N. G. Van Kampen, *Stochastic Processes in Physics and Chemistry*, North-Holland, Amsterdam, 1981.

[33] W. Glöckle and T. Nonnenmacher, "Fox function representation of non-Debye relaxation processes," *J. Stat. Phys.* **71**, pp. 741–757, 1993.

[34] T. Nonnenmacher and W. Glöckle, "A fractional model for mechanical stress relaxation," *Phil. Mag. Lett.* **64**, pp. 89–93, 1991.

[35] L. Landau and E. Lifshitz, *Electrodynamics of Continuous Media, A Course in Theoretical Physics*, vol. 8, Pergamon Press, Oxford, 1960.

[36] P. Grigolini, A. Rocco, and B. J. West, "Fractional calculus as a macroscopic manifestation of randomness," *Phys. Rev. E* **59**, pp. 2603–2613, 1999.

[37] Y. Xu, *Ferroelectric Materials and Their Applications*, North-Holland, Amsterdam, 1991.

[38] M. Buckingham, *Noise in Electronic Devices and Systems*, Halsted Press, New York, 1983.

[39] N. Galiyarova, "Fractal dielectric response of multidomain ferroelectrics from the irreversible thermodynamics standpoint," *Ferroelectrics* **222**, pp. 381–387, 1999.

[40] N. Galiyarova and Y. Korchmaryuk, "Response of some fractal nonlinear systems," *Ferroelectrics* **222**, pp. 389–395, 1999.

[41] F. Mainardi and P. Paradisi, "A model of diffusive waves in viscoelasticity based on fractional calculus," in *Proc. 36th Conf. on Decision & Control,* San Diego, CA., December 1997, pp. 4961–4966, 1997.

[42] B. M. Vinagre, V. Feliú, and J. J. Feliú, "Frequency domain identification of a flexible structure with piezoelectric actuators using irrational transfer functions models," in *Proc. 37th IEEE Conf. on Decision & Control,* Tampa, FL, December 1998, pp. 1278–1280, 1998.

[43] M. D. Ortigueira, "Introduction to fractional linear systems. Part 1: Continuous-time case," *IEE Proc. - Visual, Image and Signal Processing* **147**, pp. 62–70, 2000.

[44] M. D. Ortigueira, "Introduction to fractional linear systems. Part 2: Discrete-time case," *IEE Proc. - Visual, Image and Signal Processing* **147**, pp. 71–78, 2000.

[45] M. Seredyńska and A. Hanyga, "Nonlinear Hamiltonian equations with fractional damping," *J. Math. Phys.* **41**, pp. 2135–2156, 2000.

[46] I. Podlubny, "Numerical solution of ordinary fractional differential equations by the fractional difference method," in *Advances in Difference Equations: Proceedings of the Second International Conference on Difference Equations* Veszprém, Hungary, August 7-11, 1995, S. Elyadi, I. Győri, and G. Ladas, eds., pp. 507–515, Gordon and Breach Science Publishers, 1997.

[47] W. H. Press, S. A. Teukolsky, W. T. Vetterling, and B. P. Flattery, *Numerical Recipes in C: The art of Scientific Computing*, Cambridge University Press, second ed., 1992.

[48] I. Polubny, L. Dorcak, and I. Kostial, "On fractional derivatives, fractional-order dynamic systems and $PI^{\lambda}D^{\mu}$ controllers," in *Proc. 36th Conf. on Decision & Control,* San Diego, CA., December 1997, pp. 4985–4990, 1997.

[49] AMP, Inc., *Piezo Film Sensors Technical Manual*, 1993.

[50] K. Okada, H. Sugié, and K. Kan'no, "Extremely slow response of the polarization to the external field in KH_2PO_4," *Phys. Lett.* **44A**, pp. 59–60, 1973.

[51] R. Hilfer, ed., *Applications of Fractional Calculus in Physics*, World Scientific, Singapore, 2000.

[52] R. V. Chamberlin, "Nonexponential relaxation of condensed matter," in *35 Years of Condensed Matter and Related Physics: Proceedings of the Raymond L. Orbach Symposium Univ. of California, Riverside, USA, March 18, 1995*, pp. 66–79, World-Scientific, 1995.

[53] V. H. Schmidt, G. Bohannan, D. Arbogast, and G. Tuthill, "Domain wall freezing in KDP-type ferroelectrics," *J. Phys. Chem. Solids* **61**, pp. 283–289, 2000.

[54] M. Mooibroek, "Vibration control by piezoelectric actuators," tech. rep., Utrecht University and Montana State University, 1998.

[55] H. Jung, J. Y. Shim, and D. Gweon, "New open loop actuating method of piezoelectric actuators for removing hysteresis and creep," *Rev. Sci. Instr.* **71**, pp. 3436–3440, 2000.

[56] V. S. Viswanath and G. Müller, *The Recursion Method: Application to Many-Body Dynamics*, Springer-Verlag, Berlin, 1994.

[57] L. A. Geddes, "Historical evolution of circuit models for the electrode-electrolyte interface," *Ann. Bio. Eng.* **25**, pp. 1–14, 1997.

[58] E. T. McAdams and J. Jossinet, "Nonlinear transient response of electrode-electrolyte interfaces," *Med. Biol. Eng. Comput.* **38**, pp. 427–432, 2000.

[59] V. H. Schmidt, G. F. Tuthill, C.-S. Tu, T. Schogoleva, and S. Meschia, "Conductivity across random barrier distribution as origin of large low-frequency dielectric peak in perovskite crystals and ceramics," *J. Phys. Chem. Solids* **57**, pp. 1493–1497, 1996.

[60] C. Tsallis, "Nonextensive statistics: Theoretical, experimental and computational evidences and connections," *Brazilian J. Phys.* **29**, pp. 1–35, 1999.

[61] P. H. Handel, "The nature of fundamental 1/f noise," in *AIP Conf. Proc. 285: Noise in Physical Systems and 1/f Fluctuations,* St. Louis, MO., P. H. Handel and A. Chung, eds., pp. 162–171, 1993.

[62] C. W. Gardiner, *Handbook of Stochastic Methods for Physics, Chemistry and the Natural Sciences*, Springer, Berlin, second ed., 1985.

[63] W. Feller, *An Introduction to Probability Theory and Its Applications*, vol. I, John Wiley & Sons, New York, second ed., 1962.

[64] B. V. Gnedenko and A. N. Kolmogrov, *Limit Distributions for Sums of Independent Random Variables*, Addison-Wesley, Cambridge, MA, 1954.

[65] W. Feller, *An Introduction to Probability Theory and Its Applications*, vol. II, John Wiley & Sons, New York, 1966.

[66] A. Janicki and A. Weron, *Simulation and Chaotic Behavior of α-Stable Stochastic Processes*, Dekker, New York, 1994.

[67] E. Barkai and V. N. Fleurov, "Generalized Einstein relation: A stochastic modeling approach," *Phys. Rev. E* **58**, pp. 1296–1310, 1998.

[68] G. Trefán, E. Floriani, B. J. West, and P. Grigolini, "Dynamical approach to anomalous diffusion: Response of Lévy processes to a perturbation," *Phys. Rev. E* **50**, pp. 2564–2579, 1994.

[69] M. Vendruscolo and M. Marsili, "Diffusion in disordered media as a process with memory," *Phys. Rev. E* **54**, pp. R1021–R1024, 1996.

[70] P. E. Kloeden and E. Platen, *Numerical Simulation of Stochastic Differential Equations*, Springer, New York, 1995.